FLOW OBSTRUCTIONS IN VALLEY GLACIERS

RAVEN CARUSO
Bachelor of Science, University of Lethbridge, 2004

A Thesis
Submitted to the School of Graduate Studies
of the University of Lethbridge in Partial Fulfilment of the
Requirements for the Degree

MASTERS OF SCIENCE

Department of Geography
University of Lethbridge
LETHBRIDGE, ALBERTA, CANADA

For Murphy

Abstract

Valley glaciers often occur within complex dendritic systems where tributary glaciers contribute ice mass and blocking potential to the trunk glacier. Analysis of glacier inventories and maps in the regions of Svalbard, East Greenland, Yukon Territory and the Thompson Glacier system indicates that trunk - tributary intersections commonly occur at angles between 45° and 90°. An analogue material with flow properties similar to creep in pure ice has been used to simulate flow in a model valley glacier. The model and a series of blockages were constructed based on dimensions derived from the inventory and map analysis. The angled blockage indicates lower overall velocity rates and appears to have a funnelling rather than blocking affect on the analogue material. The perpendicular obstruction that blocked half the width of the model valley caused a piling up of analogue material prior to a release into the unobstructed side of the valley.

Acknowledgments

Financial support for this project came from the University of Lethbridge Graduate Assistantship, a Research Assistantship funded by a NSERC Discovery Grant to Dr. Hester Jiskoot, and The Alberta Advanced Education Graduate Student Scholarship.

First and foremost I would like to thank my supervisor, Dr. Hester Jiskoot. I wouldn't have put up with me. Thanks.

I'd also like to thank the rest of my committee, Dr. Robert Rogerson and Dr. Steve Patitsas, for their support and assistance over the course of this project.

The construction of the model glacial valley and all the blockages was carried out by Frank Klassen in the Arts and Science Tech Services department at the University of Lethbridge.

Thanks also go to Dr. Craig Coburn – thanks for the use of 'The White Bucket of Science', um…you might not want it back.

Dr. Shawn Bubel and Sue Lapp for their assistance and observations during the digitization process as well as Guy Duke and Kate Forbes for their help with ArcMap.

Thanks to all my friends and fellow grad students who listened to me rant about 'the albatross' over sushi and lattes. A special thanks to those who let me crash at their houses during revisions, you know who you are.

Thanks to my family and Sara and Mark, who are like family, for their words of encouragement and support. Thanks for helping me keep it together.

Table of Contents

List of Tables

List of Figures

Chapter 1 – Introduction

The continued decline of alpine glaciers as well as the marked reduction in the volume of large ice-sheets is fast becoming a major global concern. This diminution will be detrimental to regions that rely on them as a source of fresh water for drinking, irrigation and industry as well as recreation and tourism (IPCC, 2001; NRCan, 2002; Scott and Jones, 2005). Current water availability estimates may be overstating the amount of water that these glaciers are able to provide as they decline in size. An incomplete assessment of flow dynamics, including those related to the poorly understood effect of tributaries as flow blocking mechanisms in a glacier system increases the likelihood that current estimates are inaccurate (e.g. Hansen, 2007).

Very little research has been done in an attempt to elucidate the roll of confluent systems in glacial flow dynamics (Collins, 1970; Anderton, 1973; Gudmundsson *et al*., 1997; Jiskoot *et al*., 2001; Kargel *et al*., 2005). It has been hypothesised that the convergence of a tributary and a trunk glacier may influence the flow dynamics of a dendritic glacier system (Jiskoot *et al*., 2001; Jiskoot, 2003). The detachment of a tributary from its trunk glacier could potentially result in changes to the flow dynamics and mass balances of both glaciers (Jiskoot, 2003; Kargel *et al*., 2005). In the event of tributary detachment, the tributary will no longer feed ice into the trunk glacier and may accelerate recession of both the trunk and tributary glaciers (Jiskoot, 2003).

Studies of the interactions between tributary and trunk glaciers have been limited to few regions. The Kaskawulsh Glacier, Yukon Territory (Anderton, 1973) has been extensively studied, as has Unteraargletcher, Swiss Alps (Gudmundsson *et al*., 1997) and some work has been done on Berendon Glacier (Eyles and Rogerson, 1977). This thesis

focuses on tributary-trunk interactions through 1) experimentation with an analogue model; and, 2) statistical analysis of the morphometric relations of tributary-affected glacier systems in the regions of Yukon Territory, East Greenland, Svalbard and Arctic Canada. Pre-existing studies of glacial confluences are limited and because of this a large portion of this work is based on publications by Dr. Hester Jiskoot (Jiskoot et al., 2000; Jiskoot *et al.*, 2001; Jiskoot *et al*., 2003; Jiskoot, 2003; Jiskoot in Kargel *et al*., 2005) as well as an unpublished Ph.D dissertation (Anderton, 1973).

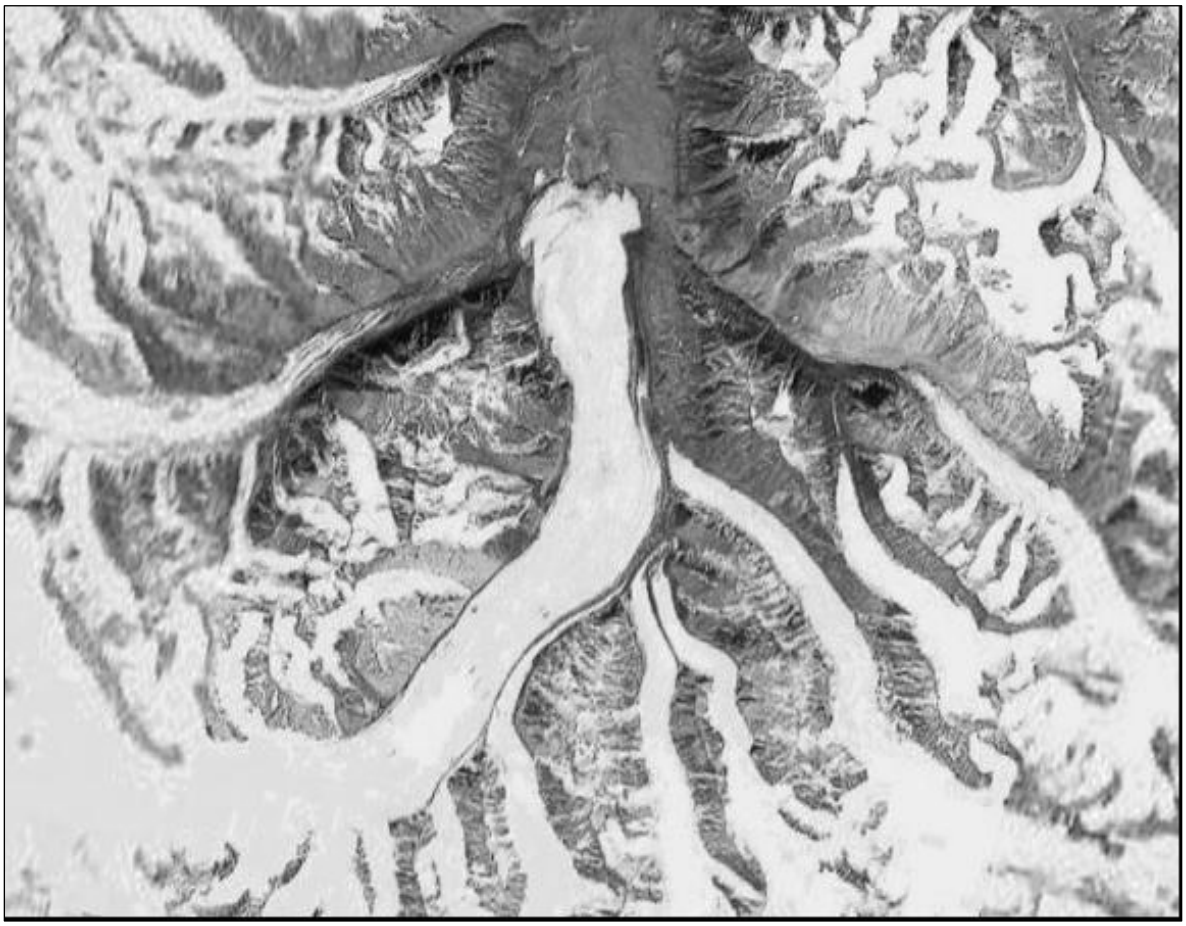

Fig 1.1 – Kluane Glacier, Yukon Territory, Canada. A dendritic glacier confluence system with some structural control by local fault systems. Glaciers in this region have experienced continuous recession and disintegration of confluent flow systems in recent history. 1:150000 Image modified from Google Earth, 2006-03-30.

1.1 - Hypotheses

Within this thesis two hypotheses were tested. These were tested through experimentation with an analogue model that was designed to simulate a valley glacier flowing both down an unblocked valley and down a valley with blockages of various sizes, each representing a constriction in the valley. A statistical analysis of tributary-trunk systems in existing and developed glacier inventories provided insight into the general characteristics of these systems and aided in the development of a realistic analogue model.

1.1.1 – Flow Constrictions in an Analogue Model Glacier

The first hypothesis pertains to the presence of localised compressive stress at or up-ice from a significant blockage in the flow of a trunk glacier, either as a result of tributary ice flow or a resistant geological obstruction such as a bedrock sill. This compressive stress is reflected in the surface deformation and an increase in velocity downstream of the constriction (Sugden and John, 1985). The extent of deformation and the magnitude of the velocity increase are suggested by this thesis to be relative to the size of the blockage. An analogue model was constructed and subjected to flow trials using blockages of differing sizes. The experiment is composed of a series of blockages that are affixed to the wall of the model trunk glacier, perpendicular to the trunk flow. Each blockage represents a different size, depth or type of constriction in the flow of the main trunk. The blockages used in this experiment are described in greater detail in Chapter 3. Results of these experiments are given in Chapter 4 and discussed in Chapter 5.

1.1.2 – Angled Flow Constrictions in an Analogue Model Glacier

A second hypothesis was tested through the addition of an angled blockage to the above mentioned analogue model experiments. Information such as tributary / trunk width ratios and confluence angles are used to provide comparison by regions and to provide correlations between the various geometries of the glaciers and their attributed confluence angles.

Two assumptions are made: 1) A large angle of tributary flow entrance is associated with high levels of compressive deformation (Eyles and Rogerson, 1977); and 2) A reduction in the angle of flow blockage from 90° to 45° will result in a reduction in compressive stress associated with the blockages. Details of this model are described in Chapter 3 and results from the model experiments in Chapter 4.

Chapter 2 - Literature Review

Publications of analogue model experiments displaying fluvial and geological processes (e.g. McCay and Dooley, 1995; Acocella *et al.*, 2001; Regard *et al.*, 2005) are quite common. Though they are useful tools for experimenting with various structures and systems, analogue model experiments are rarely used in glaciological studies. The basis for this literature review is an examination of several fundamental papers on glacial flow as well as publications that specifically deal with tributary – trunk interactions and those that discuss previous analogue models.

2.1 – Basic Principles of Polycrystalline Ice Flow

Ice has been shown to be a material similar in flow properties to some metals and rocks (Price and Cosgrove, 1994). It is often difficult to assign one simple flow law to a natural material because the behaviour of a natural material such as ice or rock often varies significantly from the behaviour of an idealised material (Price and Cosgrove, 1994). However, the flow law that is most often used for simple creep in glaciers is Glen's Flow Law (Glen, 1952) modified by Nye (1952) for use in defining flow in temperate, polycrystalline ice (Glen, 1955; Paterson, 1994).

It is easiest to explain the strain rate of ice by comparing it to the strain response of other materials. At one end of the spectrum there is a perfectly plastic material, at the other a perfectly viscous material. Each responds to stress in a different and distinct manner (Price and Cosgrove, 1994). In a Newtonian viscous material, a liquid, there is a linear relationship between stress and strain rates. In this instance the strain rate is directly proportional to the stress (n=1). In a perfectly plastic material the resistance to deformation is continuous until the yield stress is met and rapid deformation begins

(Paterson, 1994). Ice, and the analogue material used in the experiments presented in this thesis, will respond elastically to low levels of stress and can recover until the critical value is met at which point it will fracture (Nye, 1952). This behaviour in relation to the ice analogue material is discussed in greater detail later on.

Glen's Flow Law when applied to a non-linear viscous material such as ice states that the shear strain ($\dot{\varepsilon}$) is a function of shear stress (τ) and the ice temperature dependent constant, *A* (Paterson, 1994). Glen's flow law is defined by the following equation:

[Eq. 2.1] $$\dot{\varepsilon} = \mathrm{A}\tau^{n}$$

In this equation *n* is considered constant and has an approximate value of 3 but can vary from 1.5 – 4.2 over a range of stresses (50 – 200 kPa) relevant to glacier flow (Paterson, 1994). *A* is a mainly temperature dependent variable though it is also related to hydro-static pressure and other ice properties and has been shown to have a range from 10^{-14} to 10^{-17} $s^{-1}kPa^{-3}$ (Paterson, 1994). Shear stress (τ) is defined by the equation:

[Eq. 2.2] $$\tau = \rho g H \sin\alpha$$

In the above equation ρ is the density of ice which is an average of 900 kg m^{-3}, α is the surface slope angle, *g* is the gravitational acceleration (9.8 ms^{-2}) and H is the distance between the ice surface and bed, or the depth of the glacier (Paterson, 1994).

There has been some debate regarding the relative simplicity of Glen's Flow Law. Goldsby and Kohlstedt (2001) suggest that it may underestimate the creep rates for temperate glaciers because it excludes the effect of basal debris. However, it has been shown to successfully approximate creep rates in laboratory experiments (Nye, 1952) and is an appropriate flow law for use in the experiments discussed in Chapter 3.

2.1.1 – Flow in a Half Cylinder

The model used in this thesis is based on a half cylinder. Although the half cylinder hypothetical glacial valley does not fit the model of the traditional U-shaped valley that is associated with glacial erosion (Harbor, 1992), it provides an ideal generalised model for use in a lab setting.

Nye (1952) introduced a model of flow within a half cylinder as a theoretical intermediate between flow in a narrow, infinitely deep valley and flow within a wide and infinitely deep valley (Fig 2.1). In the half cylinder model the surfaces of maximum shear are all parallel to the bed and the shear stress at the bed (τ) still varies linearly with depth, however, it does so at a rate of half that of a wide valley (Nye, 1952). This relationship is represented by the expression:

[Eq 2.3]

$$\tau = \frac{1}{2}\rho g r \sin\alpha$$

where r is the radius, α is the surface slope, ρ is the density of ice (900 kg m^{-3}), and g is the gravitational acceleration (9.8 m s^{-2}) (Paterson, 1994).

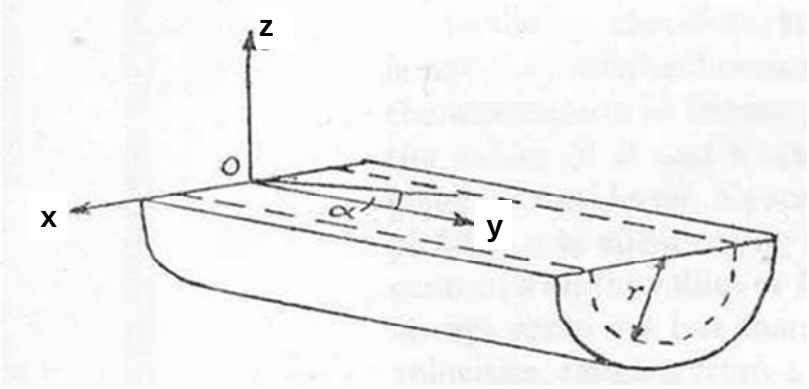

Fig 2.1 – Flow in a Half Cylinder. In a half cylinder of uniform size, shear stress increases linearly with depth and is dependent on slope, gravitational acceleration and the density of ice (Nye, 1952). Modified from Nye (1952).

2.1.2 – Surface Strain and Strain Rate

Strain analysis through the measurement of surface deformation is common practice in glaciology. It is an important way to gather information about the surface flow dynamics of a glacier. Velocity and compressive and tensional strain rates can be gathered from these data to determine stress values. One method of strain analysis in the field involves measuring the movement of stakes drilled into the surface of the ice relative to one another. Alternatively, a strain grid of velocity stakes can be used in the collection of field data, where the strain rate is derived using velocities rather than relative positions (van der Veen, 1999). This method of strain analysis is used in this thesis (see 3.4.2).

The analysis of deformation in glaciers is similar to the analysis of deformation in materials such as rock and metal. Some differences between the two have arisen, such as the convention in glaciology to refer to compression in terms of negative numbers and extension in positives (Paterson, 1994), whereas in geology it is the opposite (Price and Cosgrove, 1990). The glaciological convention is used consistently throughout this thesis.

Strain is defined as the change in length of a given line divided by the original length of the line and is a response of a material to all the stresses (normal and shear) acting on the material (Hooke, 2005). Ice and the analogue material are considered viscoplastic materials. A perfectly plastic material does not deform at stress levels below its threshold yield, however, ice and the analogue material respond to continued stress levels relative to the amount the stress exceeds their critical yield. Glen's flow law predicts very small strain rates at low stress levels but suggests that ice has a threshold yield. Ice and the ice analogue materials' response to stress can be seen along line c in Fig. 2.2 (Hooke, 2005).

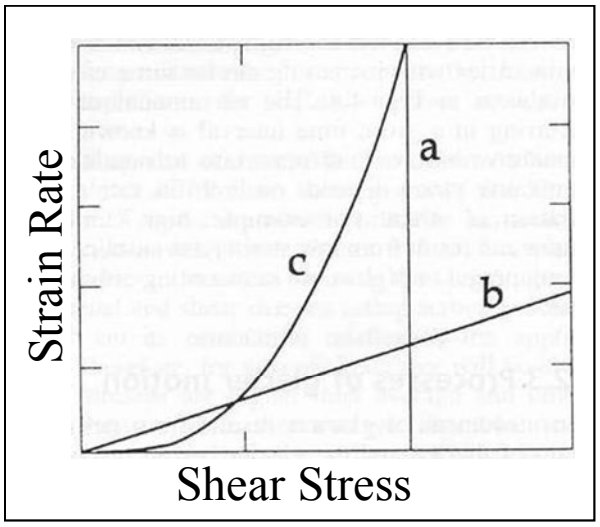

Fig. 2.2 – Strain response to shear stress. Line 'a' indicates the response of a perfectly plastic material; 'b', a Newtonian viscous material; and 'c', a non-linearly viscous material (ice analogue material). Material 'a' resists deformation until its threshold yield is met and then deforms instantaneously (fractures); material 'b' responds linearly to an increase in stress with a proportional increase in strain; and material 'c' indicates very low levels of strain response to low levels of stress and demonstrates a continuous increase in response until critical failure (formation of crevasses). Modified from Paterson, 1994.

Field studies usually consist of stakes that are arranged in either strain diamonds or squares placed along a transect on the glacier surface. The initial location of each surface marker is recorded and then measured at a later date. The change in location between measurements is used to obtain the strain rate for the site.

Glaciological surveys have been conducted on Taku Glacier, Juneau Icefield, Alaska over the last half century or more (Daellenbach and Welsh, 1993). Two different studies along the same transverse profile were conducted using two different but common methods of strain analysis. The first was a study carried out by Wu and Christensen (1964) and involved the use of strain diamonds to gather surface strain rates and velocity. They drilled 3 sets of squares, 2 at each location, each with sides 30.5 m long. The three sites were measured in the last week of August and again in the first week of September of the same year. Normal strain (perpendicular to the material) was measured in each of four directions: 0° (Y-axis, perpendicular to flow), 45°, 90°, and 135°. The X-axis was

considered to be parallel to direction of flow, which was SE (~ 42°) at the profile's location. The strain squares were measured initially as they were drilled and then re-measured once in place. These two measurements were averaged to obtain a strain rate for the area covered by an individual square.

Strain rate measurements collected by Wu and Christensen (1964) indicate that along the measured profile the Taku Glacier is subject to longitudinal extension occurring at a rate of 0.55×10^{-5} hr^{-1}. The recorded strain rate correlates with the location and magnitude of crevasses associated with the profile. Wu and Christensen (1964) also measured the velocity in the same area along two profiles 500 m apart. They measured velocity in a different field season and did not use the same strain squares as surface markers. They then compared their recorded velocity measurements for the profile against the previously recorded strain rates using the equation perfectly plastic materials in Nye (1957). Wu and Christensen (1964) determined that there was little to no movement of ice adjacent to the valley walls, which is an area associated with high shear stress. The recorded transverse velocity corresponded with the derived velocity.

Daellenbach and Welsh (1993) surveyed the region established by Wu and Christensen (1964) at Taku Glacier using 3 equilateral triangles placed across the transect each with sides of 500m. They also drilled a transverse profile of 12 surface markers. The triangles and the transverse profile were measured as they were placed and re-measured 'several days' later (Daellenbach and Welsh, 1993). Their recorded strain rates were compared to the location and magnitude of a crevasse field and the strain triangle nearest it showed the greatest rates of extension perpendicular to the crevasses (Daellenbach and Welsh, 1993). The results from this site (Triangle A) correspond with the results

collected by Wu and Christensen (1964) in the same location. Their second site (Triangle B) was located mid glacier in an area with high surface velocities showed the lowest strain rates of the three sites. This central site was located in an area of the glacier that had very few crevasses and those were of a very small magnitude. Strain Triangle C showed higher strain rates than those observed in Triangle B but lower than those in A. This area did have some crevasses and the extensional strain was perpendicular to their general orientation. Daellenbach and Welsh (1993) derive a maximum extensional strain rate of 395 x 10^{-6} per day and a maximum compression rate of -333 x 10^{-6} per day. Daellenbach and Welsh (1993) also derived stress conditions for these three sites from the recorded strain using Glen's Flow Law and determined that shear stress of both Triangle A and Triangle C are much greater than those determined for Triangle B which also corresponds with the Wu and Christensen (1964) results and seems to reflect the proximity of the sites to the valley walls. This relationship is reflected both in the principal stress deviators and the hydrostatic stress.

Daellenbach and Welsh (1993) compared their transverse velocity results to existing records of velocity previously recorded in 1949, 1950 and 1952. Changes in the transverse velocities can be seen both in the magnitude of the overall velocity and in the reduction of centre flow peak velocities from the earlier records to those recorded from 1986 – 1988 (Daellenbach and Welsh, 1993).

The Taku Glacier studies provide examples of findings common in valley glacier strain surveys. Crevasses, surface features that form when stresses are greater than the critical yield of ice, result in either compressive or tensional stresses (Sugden and John,

1985). The orientation of crevasses is a reflection of the stresses that can be found at that location.

Nye (1952) described three types of crevasses and the stresses that they are associated with. “Chevron crevasses” open normal to the direction of greatest tensional stress. “Splaying crevasses” are the result of longitudinal compression that results in pre-existing chevron crevasses, which normally align to the valley wall at 45°, to shift up-ice. Longitudinal compressive stresses can be the result of a narrowing of the glacial valley, flow around the inside of a bend or the presence of a concave bed (Nye, 1952). Under conditions of longitudinal extension “transverse crevasses” open normal to the direction of flow and veer downstream where they are influenced by drag from the valley walls (Sugden and John, 1985). Longitudinal extension occurs where there is a convex bed, a widening of the valley, an ice fall, or in the outside bend of a curve (Nye, 1952).

2.2 – Surging Behaviour in Valley Glaciers

Glacial surging is defined as ice flow behaviour that oscillates between periods of fast and slow flow (Clarke, 1987). A link between tributary - trunk confluences and surge-type glaciers has been suggested but is still unknown. Tributary induced blockages in a trunk glacier may be linked with a build up of potential energy up ice from the blockage that may in turn be a trigger mechanism for surging episodes in some regions (Jiskoot *et al*., 2001). However, the mere presence or absence of tributaries does not appear to be linked to surging behaviour in the Yukon (Atkinson *et al*., 1998), Svalbard (Hamilton and Dowdeswell, 1996; Jiskoot *et al*., 2000) or in East Greenland (Jiskoot *et al*., 2003).

During periods of fast flow surge-type glaciers experience periods of rapid ice discharge (Fig 2.3). The flow rate during these surge periods is often 10 to 100+ times

faster than the quiescent flow rate (Post, 1969). In order for a surge phase to be initiated there must be considerable accumulation of ice that is held in a reservoir until a threshold is met and the ice is released into the receiving area (Clarke, 2005). Though it is generally accepted that there is a trigger mechanism that results in this sudden, large-scale displacement, what this mechanism is, is not known. Several possible causes for this behaviour have been suggested and it is thought that it may be an interaction between different factors that causes a change in the flow of a surge-type glacier (Clarke *et al*., 1986; Murray *et al*., 2003; Hamilton and Dowdeswell, 1996).

A  **B** 

Fig 2.3 - Variegated Glacier, Alaska, U.S.A. The first image was taken in 1964 during a period of normal flow (Post, 1964). The second image is the same glacier during the 1965 surge event. The glacier has pushed its mass into the adjacent valley and obstructed the outwash flow of that glacier**.** Image A - Post. 1964; Image B - Unknown. 1965. *Variegated Glacier*. From the *Online glacier photograph database*. Boulder. CO: National Snow and Ice Data Center / World Data Center for Glaciology. Digital Media.

A relationship between surging glaciers and their underlying substrate has been suggested by Post (1969) and has been generally accepted as a contributing factor to surging behaviour. Hamilton and Dowdeswell (1996) noted that glaciers overlying sedimentary bedrock were more likely to be of surge type than those overlying coarse-grained bedrock. They concluded that this increased probability is support for the

deformable bed theory suggested by Clarke *et al.,* (1984). Hamilton and Dowdeswell (1996) suggested that subglacial geology has an influence on the probability of a glacier surging but that it cannot account for the geographic distribution of surge-type glaciers. Post (1969) indicated surging behaviour may be correlated with the permeability of the substrate, thus areas of highly permeable sedimentary bedrock or regions that have experienced severe deformation are more likely to have surge-type glaciers.

Substrate permeability, however, cannot be the only requirement for surging behaviour as regions that are not underlain by soft beds can have surge-type glaciers as well as regions of highly deformed bedrock can underlie glaciers that are not surge-type (Post, 1969).

Kamb (1987) suggested a linked-cavity model to explain surging. He suggested that the trigger mechanism for a surge phase is instability caused by a switch from a tunnel system operating at low pressure to a linked cavity system at high pressure in the basal drainage system. This switch in hydrological regimes results in a restriction of water within the linked cavity system. According to Kamb (1987) high water pressure at the ice-bed interface can result in very rapid basal sliding and surging. The surging episode ends when the cavity linking capillaries become unstable and collapse into tunnel flow. Once this occurs there is a decrease in water pressure and lower basal sliding velocity and a subsequent return to the glaciers quiescent flow rate.

It has been shown that there is a correlation between the length of a glacier and its probability for surging and several studies have indicated length as the most significant variable associated with surging (Clarke, 1991; Hamilton and Dowdeswell, 1996; Jiskoot *et al.*, 2000; Jiskoot *et al*., 2003). The cyclic nature and geographic distribution of surge-

type glaciers suggests a trigger mechanism that is a function of the combination of climate (Clarke, 1984), lithological features and subglacial geology (Post, 1969; Hamilton and Dowdeswell, 1996; Jiskoot *et al*, 2000; Jiskoot *et al*., 2003), and basal sliding as a result of subglacial hydrology (Kamb, 1987).

Few links have been made between tributaries and surging behaviour. As mentioned previously these studies focused on the presence/absence of tributaries as a factor in surging behaviour of a trunk glacier (Post, 1969; Hamilton and Dowdeswell, 1995; Atkinson *et al*., 1998; Jiskoot *et al*., 2000; Jiskoot *et al*., 2003)**.** A possible connection between tributaries and surging in the trunk glacier may be linked to the flow dynamics and the blocking potential of a tributary glacier (see Kargel *et al.'s* (2005) classification in section 2.4). This thesis is the first attempt to quantify the blocking potential of flow obstructions such as tributaries and thus its possible effect on surge behaviour.

2.2.1 – Geological Controls on Surging

In the last couple of decades there has been a major change in the way glaciologists approach the examination of subglacial bed and related ice-flow dynamics (Murray, 1997). Prior to this it was generally assumed that glaciers scoured and removed sediment beneath them and therefore flowed over completely rigid beds. Under these conditions ice creep and sliding were the only methods of glacial movement (Boulton, 1986). Boulton and Hindmarsh (1987), however, suggested that where glaciers overlie soft basal sediment that can become saturated high rates of basal shear stress can contribute to the overall forward velocity of the glacier. The theory of subglacial deformable sediment has become an important aspect of current glaciological research (Murray, 1997).

Clark (1994) suggests that large-scale fluctuations in the Laurentide Ice Sheet were a result of the deformation of subglacial sediment. Once the Laurentide had retreated onto a mostly rigid bed its retreat was nearly continuous and lacked the highly lobate margin seen in regions underlain by deformable sediment. He also states that because the processes and flow dynamics of a glacier that is underlain by deformable sediment are different from those of a glacier underlain by rigid bedrock, the landforms associated with each will also differ. Deformable sediment generally refers to that which is derived from sedimentary rocks such as carbonates, shale and siltstone as well as fine-grained igneous rocks such as basalt. Course grained rocks such as most igneous, metamorphic and sandstones are generally associated with rigid beds (Clark, 1994).

The concept of a deformable bed is important to understanding surging glaciers (Hamilton and Dowdeswell, 1996; Jiskoot *et al*., 2000). Post (1969) suggested that surging behaviour in glaciers is linked to the surface roughness of the bedrock but that there is no specific link to bedrock types as surge–type glaciers are found over all variations of bedrock. He also states that the relationship between surge-type glaciers and subglacial geology is related to the level of deformation and permeability of the underlying rock. Course-grained sediments are associated with higher hydraulic conductivity than fine-grained, clayey or silt sediments (Clark, 1994). Clarke (1987) suggests that subglacial sediment is responsive to water flux, overburden pressure, and basal shear stress.

Hamilton and Dowdeswell (1996) examined several factors that relate to surging probabilities in Svalbard. Although a relationship between bedrock geology and glacier surging was established, they could not say specifically what that relationship was.

Nevertheless, their results support a deformable bed origin for surging events in Svalbard. Jiskoot *et al*. (2000) support the conclusion of a soft bed mechanism, though they suggest that it is thermally controlled in the region of Svalbard.

2.3 - Early Analogue Modelling

Early modelling attempts provide insight into several aspects of valley glacier morphology and surface formations. These experiments were important qualitative steps in the evolution of analogue modelling. Even as strictly observational tools analogue models are valuable because they allow the observation of processes that access may otherwise be limited due to financial barriers, safety risks or any other factors that may influence the practicality of field observations (Fleisher and Sales, 1972).

These early modelling attempts were primarily designed to model glacier flow in order to observe the formation of both the surface and internal structures. They were, however, limited in their accuracy by the flow properties of their analogue materials and their tendency to dry and crack, thus obfuscating any further analysis. Lewis and Miller (1954) conducted some of the earliest known modelling attempts in glaciology. These experiments were conducted with a material comprised of kaolin clay and water mixed in different ratios. Despite being unable to conduct a quantitative analysis on any of their model trials, they were successful in building a model valley glacier that displayed features such as en echelon crevasses and bergschrunds. Ogives were also created, through the addition of material wedges at the top of the valley with a sprinkling of dust that allowed discrimination between each of the ‘seasonal’ ice additions. The experiments conducted by Lewis and Miller (1954) were primitive and somewhat dubious in their

scientific methodology but did provide some useful insights into analogue modelling of glaciers and the formation of glacial surface features.

Fleisher and Sales (1972) experimented with an analogue model of a valley glacier using moulding plaster. They were successful in displaying surface features and some internal deformation structures, as well as adequately displaying various flow features. Fleisher and Sales (1972) were able to 'consistently and accurately' recreate crevasse and ogive formations, in addition, they were able to observe strain ellipses through the presence of deformed bubbles that were preserved once the material set, as well as through the addition of reference markers internally and on the surface of the model glacier. Despite the advances made in almost 20 years since the experiments of Lewis and Miller (1954), these experiments were marred by the same problems as earlier attempts. The analogue material was subject to cracking and desiccation, and like Lewis and Miller (1954), Fleisher and Sales (1972) used a material that did not conform to Glen's Flow Law.

Shoemaker (1981) attempted to model and quantify the creep slump behaviour of a cold-based surge-type glacier using an analogue model. The material used was viscous, thickened malt that was not subject to any attempts to control or maintain viscosity of the material. A single line of plastic beads was placed in the centre flow line and movement of the beads was measured relative to lines stretched above the surface of the material and attached to the model walls. These lines remained rigid and perpendicular to direction of flow. The experiments were photographed with a still 35mm camera and the time of each photo recorded. The trial run time varied between 1 and 20 minutes. Presumably, a single line of markers was used in this case rather than a strain grid or

diamond because the experiment was predominately concerned with longitudinal extension along the centre flow line prior to critical collapse of flow preceding a 'surge' (Shoemaker, 1981).

The model appears to provide data that corresponds with that recorded from the Trapridge Glacier and was designed to recreate large bulges that have been observed at the transitional boundary between cold and warm based ice (Clarke *et al*., 1984). Accurate recreation of the complex thermal structure found in subpolar surge-type glaciers would be difficult, as it requires the creation of a lower zone of flow that is not subject to basal sliding as well as an upper region that is (Clarke *et al*., 1984). Clarke *et al*. (1981) suggest that the transition between cold and warm based ice acts as a 'thermal dam' to flow in this type of glacier.

Of Shoemaker's (1981) 33 experimental trials, 9 returned favourable results. Of these 9 trials, 8 resulted in a wave-like structure being formed in the malt material that broke from the reservoir and rapidly moved down valley. This behaviour was thought to simulate the behaviour of a subpolar surge-type glacier reaching the critical yield of a thermal damming mechanism as suggested by Clarke *et al*. (1981) though not the surge itself (Shoemaker, 1981). The last of the 9 trials resulted in the creation of a wave-like slump that presumably did not reach the threshold levels required for it to detach from the reservoir. The lack of detachment of the slumped material in this single trial was suggested to represent slump creep in a cold-based glacier. This behaviour could potentially be a result of a change in the viscosity of the malt, as it was subjected to numerous trials and extensive exposure to air and air-borne debris.

2.3.1 - Modelling the Malaspina Glacier

The modelling of the Malaspina Glacier during an undergraduate project at the Analogue Modelling Facility, University of Maine was an important step in glaciological research (Stearns and Osterberg, 2003). They used an ice analogue material that reflected the flow properties of ice and adhered to Glen's Flow Law. It has been shown to have the same flow properties as temperate glacial ice and will be discussed in greater depth in Chapter 3.2.

Stearns and Osterberg (2003) designed the experiment to recreate the folded lateral moraines seen at the Malaspina Glacier, a large piedmont glacier located in Alaska. The model consisted of a 75 cm long Plexiglas 'valley' with a width of 12 cm and 15 cm high walls inclined at 20°. The model was not designed to mimic flow in a half cylinder but to recreate a more U-shaped valley. They also recreated a 'coastal plain' at the mouth of the 'valley' of approximately 36 cm wide and 30 cm long. This was created using 6cm high walls lined with sand paper (150 grit), which were arranged to resemble the contact between the Seward lobe and the Agassiz lobe and to allow the analogue material to spread into a piedmont. Stearns and Osterberg (2003) placed a strain grid on the surface of the material and recorded the flow experiments using a digital camera. The resulting images were manually digitized.

Results from the Malaspina Glacier model were converted into vector maps displaying velocity, rotation, dilation and strain rates (Stearns and Osterberg, 2003). They found that the material flowed fastest in the centre of the valley, slowest near the valley walls and base, with a basal velocity approaching zero. They also found that the material folded underneath itself as it flowed as a result of basal coupling (Stearns and Osterberg,

2003). They also noted that the velocity of the material was significantly reduced as it left the 'valley' and entered the 'plain', responding instantly to the abrupt change in slope. They did successfully create features that resembled the heavily folded lateral moraines. Although they were unable to definitively state what process created these features, they suspect it was a direct result of the change in flow velocity as the ice left the constraints of the valley to spread out on the coastal plain as piedmont rather than a result of surging events (Post, 1969).

Gherbi (2003) carried out a rheological testing of the ice analogue material used by Stearns and Osterberg (2003) during an undergraduate project. The material was subjected to a compression test, in which a sample was placed under a constant stress and the length of time it took to deform to a given height was recorded. Glen (1955) used a similar lab-based creep test by subjecting blocks of ice with known dimensions to constant stress, the results of those experiments are discussed in greater detail in Chapter 4. This type of creep test is commonly used to measure the rheological behaviour of rock and metal, though it is also frequently used with other materials (Price and Cosgrove, 1994).

It is assumed that an ice analogue material will respond in three phases to this loading (Fig 2.4). Initially the material will respond immediately to the loading with elastic strain. If the weight is removed the material will return to its original form after a period of recovery time. The second phase of creep is initiated with continued loading of the material beyond the first phase. During this period the material will once again instantly respond and begin to recover if the loading is removed. However, the material will not recover fully and will experience some permanent deformation and will not return to its

original form. Accelerated creep, the third phase, is entered into if loading is continued through the second phase and leads to the eventual and permanent failure of the material. Crevasses can be observed in areas of glacial flow that have experienced material failure in areas of continued stress (Price and Cosgrove, 1994) and the ice analogue material has been shown to fracture when under continued high levels of stress (Gherbi, 2003).

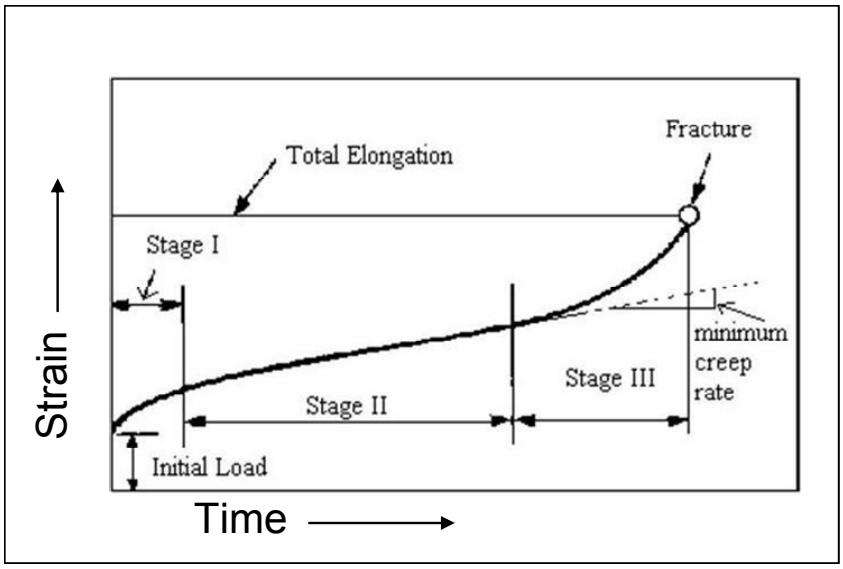

Fig 2.4 – Creep test. A materials strain response to continued loading over time (Modified from Metallurgical Consultants, 1999). http://www.materialsengineer.com/CA-Creep-Stress-Rupture.htm). Digital Media.

2.3.2 – Problems with Early Analogue Modelling

The earliest analogue models used materials such as moulding plaster, variations on a clay mixture or viscous malt. None of these substances possess the same flow properties as ice, and all can be subject to severe desiccation and other problems that all but nullified their usefulness for quantitative analysis. In some cases these problems lead to questions regarding their reliability and usefulness even as observational tools.

Other issues arise in the methodology of some of the early modelling experiments. These problems were not with the model *per se* but in the ways in which the experiments

were carried out. In the experiments conducted by Lewis and Miller (1954) they indicate that in the model for which they intended quantitative analysis they knocked on the valley to assist the material with its flow. They also admitted scaling and slope inaccuracies between their model and the actual glacier that they were attempting to recreate (Lewis and Miller, 1954).

2.3.3 – Problems with the Malaspina Glacier Model

Stearns and Osterberg (2003) discussed several sources of error in the Malaspina Glacier modelling experiments. Some, like those added through movements of the camera, were accounted for and controlled through the filming and digitization of fixed points in each trial. Filming fixed points during the experiments allowed for the comparison between known stationary objects and those points that were subject to motion. The average perceived displacement of the fixed points as a result of camera movement was simply subtracted from the measured surface markers (Stearns and Osterberg, 2003).

The surface markers used in the Malaspina modelling experiments were larger than a single pixel. Stearns and Osterberg (2003) found that the displacement of the marker was often not much larger than the marker itself and as a result the average error associated with manual digitizing of these points was 3.4%. The strain grid used by Stearns and Osterberg (2003) was of low spatial density. A higher density may have improved error analysis. Errors were also added through deliberate readjustment of the camera mid-trial as it followed the flow of the ice analogue material. Shifts in the perspective of the camera accounted for approximately 0 - 2 cm of horizontal displacement (Stearns and Osterberg, 2003).

In summary, the development of glaciological analogue models has experienced evolution in the complexity of design and the appropriateness of analogue materials. The earliest experiments, those conducted with modelling clay and plaster (Lewis and Miller, 1954; Fleisher and Sales, 1972) were primitive but provided a basis for the progression of analogue modelling of glaciological processes and morphology.

2.4 – Classification of Convergent Flow

A recently published classification system has been used to compare and contrast different regions of convergent flow (Kargel *et al*. 2005). According to the tributary classification system there could be several processes and characteristics that affect the flow regimes of the tributary and trunk glaciers:

1. *Tributary / trunk activity ratio (Ra)* : a ratio that compares velocity between the two converging glaciers. There can be significant variation in the flow velocities of two converging glaciers particularly in systems that experience surging behaviour in one or more glaciers. A summary of tributary / trunk activity ratios can be seen in Table 2.1, below.
2. *Size ratio*: the average size of the tributary glacier compared to that of the trunk glacier. In this thesis, measurements of tributary - trunk size are presented for several glaciated regions (see section 4.2).
3. *Entrance angle:* the angle at which the tributary glacier enters the trunk glacier. It has been hypothesised that the restriction caused by an entrance angle that results in blockage of a trunk glacier is a potential trigger mechanism for surging episodes in surge-type glaciers. Entrance angle is suggested to be largely dependent on the underlying structural geology (Gregory and Walling, 1973). In

this thesis, entrance angles are presented for several glaciated regions (see section 4.1).

4. *Entrance slope*: the slope of the tributary glacier where it enters the trunk. Slope is intricately linked to velocity and thus the tributary / trunk activity ratio. Higher velocities may result in a higher potential for trunk flow blockage at a tributary confluence. Conversely the same tributaries may be subject to higher rates of recession after detachment from the trunk glacier (Jiskoot, 2003).
5. *Entrance depth*: the depth in the trunk glacier at which the tributary glacier enters it. Though entrance depth may be a significant factor in the interaction between tributary and trunk glaciers, it is difficult to measure in areas that are still glaciated. There can be significant variation in the entrance depth and this may prove to be an important factor in the potential for flow blockage provided by a tributary glacier.
6. *Entrance location*: the location of the trunk glacier where the tributary glacier enters its flow. If the ice of the tributary flows into the accumulation zone of the trunk glacier it is considered to contribute to the accumulation of mass in the trunk glacier (Jiskoot, 2003). Jiskoot (2003) postulated that in regions where the tributary glacier has ceased feeding into the ablation zone of the trunk glacier there is the potential for a marked increase in the ablation of the trunk glacier.

According to Kargel *et al*. (2005), a tributary / trunk confluence can be assigned to one of five categories within the tributary-trunk activity ratio (Point 1 above). Each of the five categories determined by the tributary / trunk activity ratio is described in Table 2.1.

Table 2.1 – Classification of Convergent Flow Systems (Kargel *et al*., 2005). Specific tributary types are determined through a comparison of tributary and trunk activity ratios. Types II and IV indicate surging behaviour in the trunk and tributary, respectively. Activity Ratio (Ra) is the velocity of the tributary divided by the velocity of the trunk glacier.

Class	Tributary Type	Activity Ratio (Ra)	Description
I	Coalescing	Ra ≤ 1	Trunk and tributary flow at approx. the same speed, enter the confluence at a similar angle
II	Sheared	Ra << 1	Flow is faster in the trunk than tributary, can result in a tear shaped moraine
III	Bulging	Ra > 1	Tributary flows faster than trunk, tributary end moraine is pushed into the trunk glacier
IV	Overriding	Ra >> 1	Tributary flows much faster than the trunk, potentially blocking flow of the trunk
V	Detached	Ra = 0	Tributary no longer contributes ice to the trunk glacier

2.4.1 – Confluent Flow

Within Kargel *et al.*'s (2005) classification an artificial distinction has been made between 'confluent or coalescing flow' and 'tributary flow'. This distinction is based mainly on differences in the activity ratio and the entrance angle, and thus differences in blockage potential and flow regime down ice from the convergence point. The term 'confluent flow' implies a convergence between two glaciers that does not result in the blocking of either one (Fig 2.5). Most glaciers that display confluent flow regimes are classified as coalescing tributaries, or Type I in the above mentioned classification system (Kargel *etal*., 2005). It has been suggested that the blocking potential for either glacier is limited in a convergence described as confluent flow (Table 2.1).

Fig 2.5 - Confluence of two arms of the Kaskawulsh Glacier, Yukon Territory, Canada. Two valley glaciers of similar size converge with a mean change in direction by both glaciers. Source: Vic Adomaitis. (Accessed March 2006 **http://www.jovial.on.ca/vica/**)

Early research on the dynamics of a glacial confluence has been conducted on the Kaskawulsh Glacier in Kluane National Park, Yukon Territory. The Kaskawulsh Glacier exhibits a Type I confluence as the north and central arms converge and continue to flow parallel to each other (Fig 2.5). Both Collins (1970) and Anderton (1973) analysed surface deformation at the confluence of the two arms of the Kaskawulsh.

Collins (1970) examined confluent and tributary flow using slip – line field analysis, a method most commonly associated with deformation in geological structures that have undergone compression-induced deformation (Price and Cosgrove, 1994). Ice subjected to compressive flow will display a slip-line structure that is analogous to a reverse fault in geological structures that have undergone compression. Glacier ice that is subject to extensional stress will display motion more indicative of normal faulting (Sugden and John, 1985; Plummer and McGeary, 1991). Collins (1970) created several theoretical

solutions for geometrically different confluences using slip lines. Some aspects of Collins' (1970) mathematical solutions closely correspond with field data collected by Anderton (1973) at the confluence of the Kaskawulsh Glacier. Collins (1970) suggested that there is a zone of intense shear directly below a confluence, the magnitude of which is dependant upon the geometry of the confluence itself. However, Collins (1970) theoretical analyses were based on highly idealised conditions that are not found in nature and he stated that the conclusions made from his analysis could not be quantitatively compared to field data.

Anderton (1973) carried out the most detailed analysis of a glacier confluence at the Kaskawulsh Glacier. He measured both longitudinal and transverse surface velocity and strain, collected and analysed several core samples, and observed crevasse patterns at the convergence point as well as in both glaciers up ice from the confluence. Transverse, en echelon, chevron and splaying crevasses were observed (Anderton, 1973). Transverse crevasses perpendicular to the direction of flow were found predominantly on the medial moraine or very close to it. These were attributed to extensional flow at the confluence. Marginal en echelon crevasses were observed on both arms of the glacier and are generally associated with compressive flow (Sugden and John, 1985). Crevasses indicating longitudinal strain on the central arm and at the medial moraine were observed. The central arm was observed to enter the confluence at a lower velocity than the north arm but began flowing at the same velocity within 1000 m down ice from the confluence (Anderton, 1973). Both arms were observed to experience an initial reduction in velocity upon entering the confluence and a subsequent increase down ice (Anderton, 1973).

Eyles and Rogerson (1977) observed the formation of a medial moraine at a confluence on the Berendon Glacier in British Columbia. Though not specifically studying the flow dynamics of a confluence their observations of the medial moraine serve to corroborate conclusions from the Unteraargletscher and Kaskawulsh studies. At the time of study each of the merging glaciers was ~1 km wide and they met ~ 2.1 km from the terminus at an angle of approximately 50°. At this confluence there was little change in the flow direction of the north arm but the south arm changed direction slightly from NE to an E (Eyles and Rogerson, 1977). Like Anderton (1973), Eyles and Rogerson (1977) recorded different velocities in the two glaciers up ice from the confluence and a single velocity of the combined flow units within 1000 m down-ice from the confluence. Eyles and Rogerson (1977) also recorded severe lateral compression perpendicular to flow direction that was attributed to the high angle of entry into the confluence of the south arm. There is no obvious dominance of the valley by one arm of the glacier down ice of the confluence. Though there was a change in velocity in the north arm, the south arm did not exhibit an obvious end moraine that pushed into the north arm.

The most recently published research into confluent flow of glaciers is the fieldwork conducted at Unteraargletscher by Gudmundsson *et al.* (1997). Changes in the flow direction and velocity were measured at the confluence of the two glaciers that make up Unteraargletscher, Swiss Alps. The two converging glaciers are both temperate and display similar surface velocities.

Unteraargletscher displays geometry similar to both the Berendon (Eyles and Rogerson, 1977) and the Kaskawulsh glaciers (Anderton, 1973). All three glaciers are Type I according to the Kargel *et al*. (2005) classification. It can be seen in all three

regions that one arm, acting as a single flow unit, of the glacier joins another and results in the formation of a medial moraine as the two arms flow parallel to each other. Gudmundsson *et al*. (1997) found that the medial moraine, coinciding with the centre flow line, was subject to longitudinal extension as a result of the velocity increase from the point of convergence, down ice to the confluence centre point. There is a change in mean flow direction, within the confluence, that combined with the longitudinal extension results in transverse compression (Gudmundsson *et al*., 1997). These results are similar to what has been found at Kaskawulsh Glacier (Anderton, 1973). Complementary to the surface strain rate, Gudmundsson *et al*. (1997) also examined the variation in vertical strain rate. They observed substantial displacement of their bore-hole markers that increased with depth, indicating extension along a vertical column. Gudmundsson *et al*. (1997) established that this increase with velocity only occurred to a certain, unknown, threshold depth after which velocity rapidly decreased leading to compressive strain approaching the base as a result of basal drag (Paterson, 1994).

Gudmundsson *et al*. (1997) suggest there are three processes occurring at the junction of two temperate glaciers: 1) thickening of the ice from the junction to the centre flow line; 2) a change in mean flow direction as the confluence area is approached; and, 3) a velocity increase along the medial moraine from the junction point to the centre of the confluence. These three mechanisms only apply to regions where there is a Type I confluence. At a tributary and trunk intersection these mechanisms may not be the same as a result of the different flow properties of the convergence. Collins (1970) suggested that the geometry of the confluence, e.g. Y-shaped as compared to those with higher entrance angles, would influence the flow patterns of the lower portion of the glacier.

2.4.2 – Tributary Systems

Glaciers that converge in any manner that is not coalescent can be considered tributary flow. In the tributary classification system described in Kargel *et al*. (2005), tributary interactions are those that are described as Types II through IV and with an example of a Type I convergence can be seen in Fig. 2.6.

Jiskoot *et al*. (2001) hypothesised that this intrusion of tributary ice may act as a blockage to the flow of the trunk glacier and may be linked with surging behaviour of Sortebrae, East Greenland. During surging events, tributary moraines can be seen to form classic teardrop moraine formations as they are pulled down glacier by the rapid flow of the trunk glacier (Jiskoot, 1999). In the event of a surging trunk glacier the convergence is considered a Type II interaction (Kargel *et al*., 2005).

Variations in the angle of entrance will result in different levels of blockages in the flow of the trunk glacier ice. Jiskoot *et al.* (2001) suggested that blocking of a trunk glacier could result in the build up of energy to a critical point that may be the switching mechanism for surging behaviour. If a tributary partially blocks or overrides the flow of a trunk glacier the convergence is considered to be Type III or Type IV interaction, respectively.

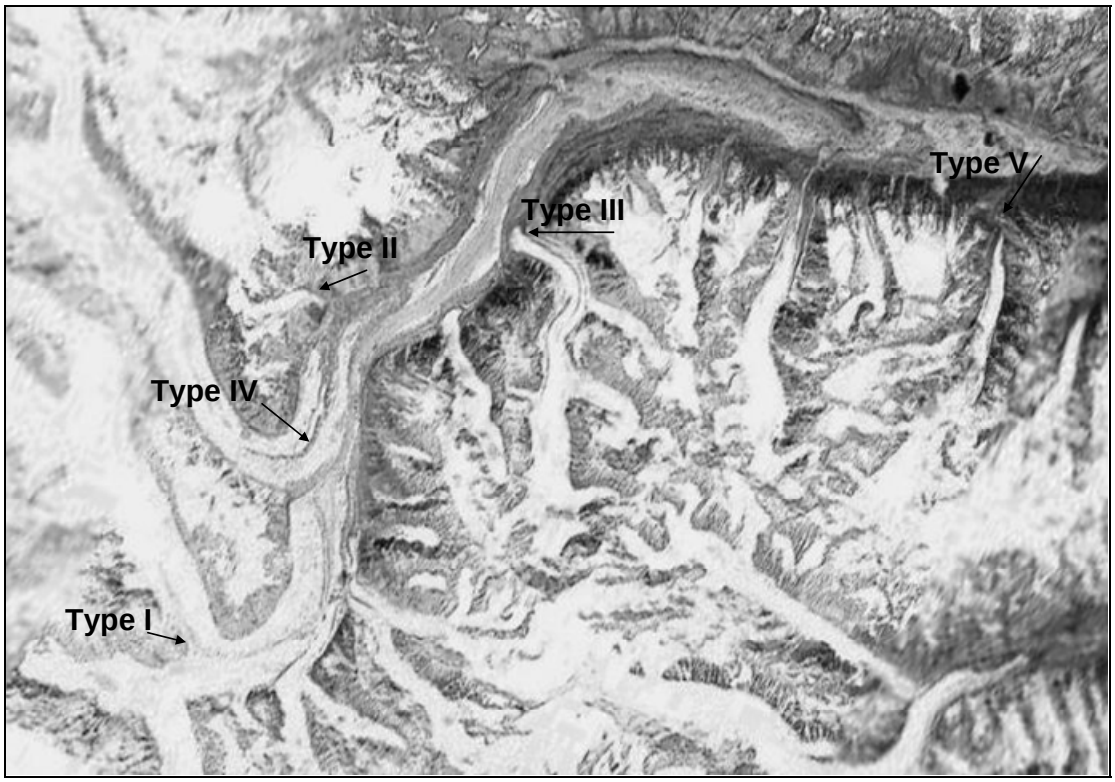

Fig 2.6 – Tributary-trunk Interactions on Steele Glacier, Yukon Territory, Canada. Steele Glacier and its various tributaries demonstrate all of the above mentioned glacier convergence types. 1:150000. Image: Modified from Google Earth (Created 03/30/2006).

Collins (1972) conducted a survey on the Rusty Glacier located within the St. Elias Range of the Yukon Territory. The Rusty Glacier is a subpolar surge-type glacier similar in size, flow patterns and thermal regime to the nearby Trapridge glacier (Clarke *et al*., 1984) but is of greater interest to this thesis due to the presence of two tributary glaciers. The upper tributary displays confluent flow as it enters the Rusty Glacier in a Y-shaped valley convergence. There are no field data to support this interpretation, however, and the assumption is based on the vector map provided by Collins (1972) which indicates low velocity NE flow in the trunk glacier at the mouth of the confluence. The blocking effect of the upper confluence is entirely speculative, as the velocity decrease also appears to coincide with the boundary between the upper portion of the glacier that is potentially sliding and the lower portion that is frozen to the bed. The second area of

convergent flow occurs within the nearly stagnant lower region of the Rusty glacier. The convergence between the Rusty and Backe glaciers can be considered a true tributary, as it can be seen to push its mass into the lower portion of the Rusty glacier and affect the generalized flow direction in that area (Fig 2.7).

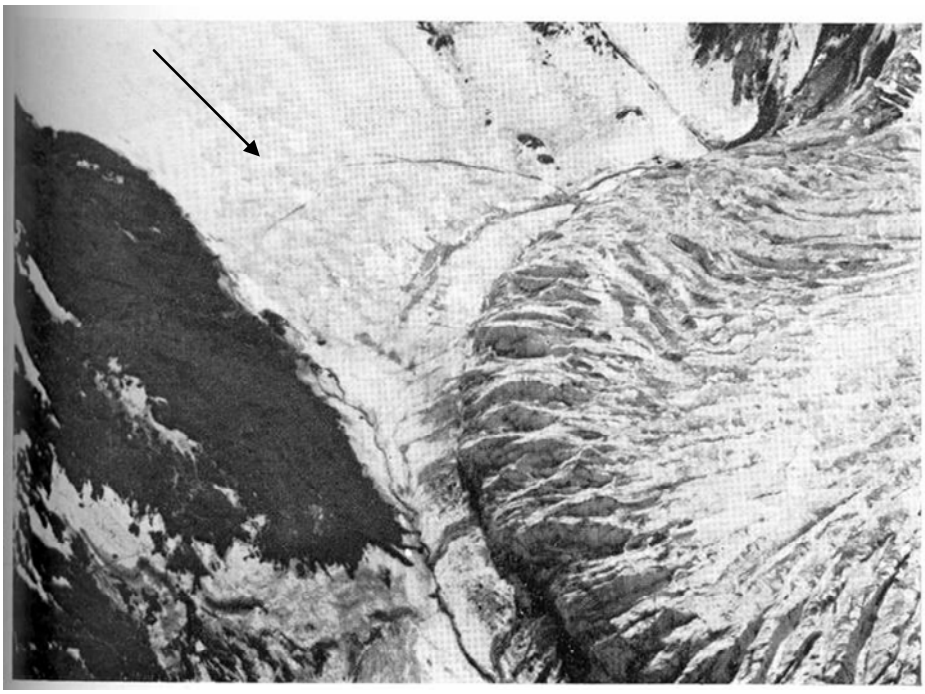

Fig. 2.7 – Rusty Glacier, Yukon Territory, Canada. The tongue of the surging Backe Glacier can be seen pushing into the quiescent Rusty Glacier. This tributary convergence would be considered a Class IV, overriding interaction where the velocity of the tributary glacier is much higher than that of the trunk (Collins, 1972). Arrow indicates flow direction of the Rusty Glacier. Modified from Collins (1972).

Above the lower tributary Collins (1972) recorded high rates of longitudinal compression. This was attributed to a change in thermal regime but may also be indicative of a blockage from the intrusion of the Backe Glacier-fed tributary. The marker stakes located directly in front of the lower tributary were the only ones in the lower region of Rusty Glacier to have indicated any significant motion. The flow direction indicated by these stakes was an Easterly direction rather than the general North flow of the Rusty glacier. These stakes seemed to record the deflection of flow caused as the Backe Glacier enters into the trunk valley of the Rusty Glacier. In fact, it was recorded by

Collins (1972) that the Backe Glacier tributary flowed over the stagnant tongue of the Rusty glacier nearly reaching the opposite valley wall (see Fig 2.7). This morphology resembled the large bulge associated with a thermal damming hypothesis for surge triggering in subpolar surge-type glaciers (Collins, 1972; Clarke *et al*., 1984).

2.5 – Geological Controls on Tributary-trunk Interactions in the St. Elias Mountains, Yukon Territory

The St. Elias Mountains are extensively glaciated and provide an excellent selection of dendritic tributary / trunk interactions within the region (Ommanney *et al*., 1973). They are located in the southwest corner of the Yukon Territory, Canada. They are both the youngest and highest mountains in the Canadian Cordillera and are the result of a relatively recent mountain building episode that occurred in the Late Cretaceous (Roberts, 1996). This region is still tectonically active as a result of the continuous subduction of the Pacific Plate as evidenced by the presence of the extensive NW trending Shakwak Fault system east of the St. Elias Mountains. This fault commonly experiences earthquakes which result in right angle offsets to glacial flow direction in the predominantly dendritic glacial system (Gregory and Walling, 1973).

Large scale faulting plays an important role in determining flow direction in a glacier system. Research into the correlation of ice flow direction through the examination of fjord formations and the major fault systems in the underlying substrata goes back to the late 19th century (Randall, 1961). Several large fault systems divide the St. Elias region and its Alaskan counterpart the Chugach range. Major faults systems, such as the aforementioned Shakwak / Denali, as well as the Hubbard, the Border Ranges, the St. Elias and the Columbus faults all have had substantial influence on the ice behaviour of

the overlying glacier systems; influencing valley orientation through offset dendritic systems (Post, 1969) (Fig 2.8).

Fig 2.8 – Offset dendritic flow, Kaskawulsh Glacier, Yukon Territory, Canada. 1:150000 Image modified from Google Earth, 03/30/2006.

The formation of dendritic glacier systems is related to the pre-glacial water flow (Harbor, 1992). The majority of the uplift of the St. Elias Mountains occurred during the Cretaceous, a period not known for extensive glaciation. There is significant support for the theory that rapid uplift during and around this period may have been the impetus for the extensive glaciation that followed later in the Pleistocene (Eyles, 1993). Glaciation in this region is likely a secondary erosional process and the flow patterns, confluence angels, confluence depths, slope and size ratio are reflections of both structural controls and pre-existing erosional structures.

Little research has been conducted to elucidate the role geology may play in the interactions between a tributary and trunk glacier (Post, 1969). It is possible in regions such as the St. Elias where the bedrock geology is variable (Post, 1964), that the activity ratio (Ra) (Kargel *et al*., 2005) of a tributary-trunk interaction is related to different underlying geologies for the tributary and trunk (see section 2.4). As it is likely that modern glaciers occupy former river valleys (Eyles, 1993) the relationship between underlying geologies and glacial flow may require an examination of the connection between the underlying geologies and the pre-glacial erosion.

2.6 – Summary

A detailed review of the literature in the field of tributary-trunk interactions has provided a method of classification that will be used in this thesis as well as an overview of the few surveys that have been conducted on glacier confluences (Collins, 1970; Collins, 1972; Anderton, 1973; Eyles and Rogerson, 1977; Shoemaker, 1981; Jiskoot, 2003; Gudmundsson *et al*., 1997; Kargel *et al*., 2005). A history of analogue modeling in glaciology has revealed both its benefits and limitations as well as provided a basis for future improvements in the process (Lewis and Miller, 1954; Fleisher and Sales, 1972; Shoemaker, 1981; Stearns and Osterberg, 2005).

Chapter 3 – Materials and Methods

This chapter provides a detailed description and discussion of the materials and methods used in this thesis. Data inventory collection method collection is discussed as is the design and set-up of the analogue model experiments. Concepts are discussed individually as well as in concert when logical to do so.

3.1 - Inventory of Svalbard, Yukon Territory, East Greenland and Arctic Canada

The design of the model valley and blockages is this thesis was based on geometric measurements gathered and analysed from a number of regions. Measurements of confluence angles and glacier length and width measurements were collected from 1:500,000 maps of Svalbard drainage basins (Hagen *et al*., 1993; Fig 3.1) as well as from pre-existing inventories of Svalbard (Hagen *et al*., 1993), the Yukon Territory (Ommanney, 1980; Atkinson *et al*., 1998) and East Greenland (Jiskoot *et al*., 2003). Measurements were also collected for a dendritic network of converging glaciers in Arctic Canada from a 1:50,000 map of the Thompson Glacier Region of Axel Heiberg Island, N.W.T.

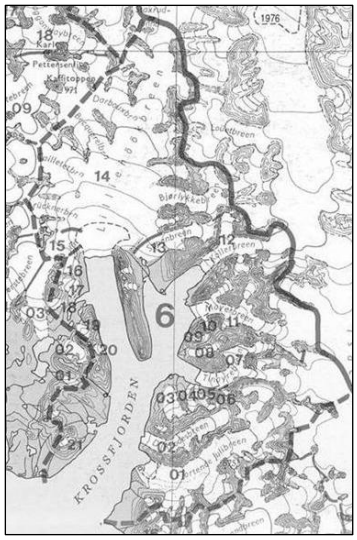

Fig 3.1 – A representative Svalbard drainage basin. Tributary confluence angles were measured manually as well as derived from pre-existing electronic databases. Modified from 1:500,000 map of Svalbard (Hagen *et al*. 1993).

Trunk width was measured directly up-ice from the confluence (Fig 3.2), as below this point the width of the trunk may be altered by the addition of ice from the tributary. Tributary width was measured where the tributary joins the trunk. However, for the inventory data, the width measurements are the average width of the trunk and tributary glaciers, and are therefore not a direct measure of the trunk/tributary ratio at the confluence. The length of all trunks and tributaries were measured from the ice divide to the snout of the glacier or to the convergence point between two glaciers, as well as collected from electronic glacier inventories as published by Ommanney (1980), Hagen *et al*. (1993) and Jiskoot *et al*. (2003) when available. Confluence angles were measured on the upstream side of the tributary-trunk intersection in order to adequately reflect the ice flow direction of both trunk and tributary. For the Yukon Territory inventory (Ommanney, 1980), confluence angles were interpreted from the mean flow direction of the ablation and accumulation areas of the trunk and tributary given in the glacier inventory. When a tributary's lowest elevation (the confluence with the trunk) was higher than its trunk's ELA then the confluence angle was the difference in compass direction in octas between the flow direction of the tributary and that of its trunks accumulation zone, and for tributaries entering below the ELA it was calculated as the difference in angle between the flow direction of the tributary and that of the ablation zone of the trunk.

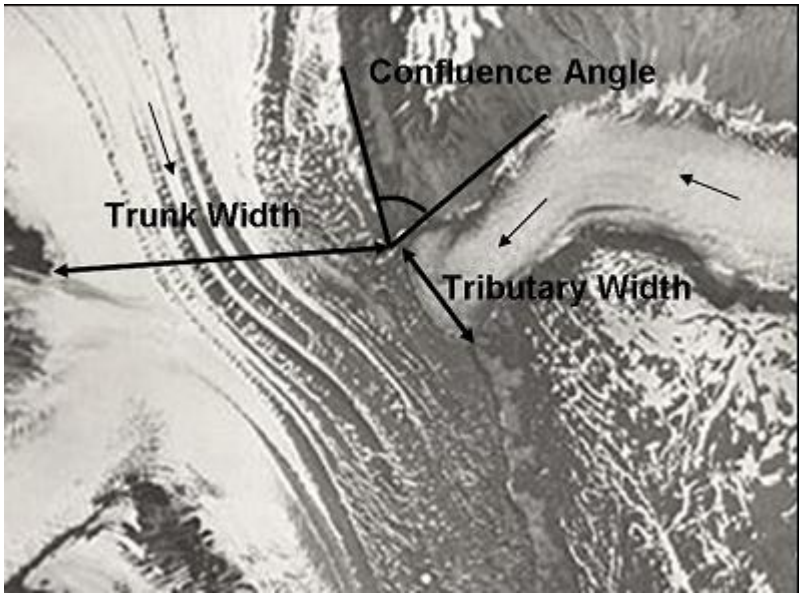

Fig 3.2 – Tsirku Glacier, Alaska. Example of tributary and trunk measurement collection of geometries for Svalbard, Yukon Territory and Arctic Canada. Short arrows indicate flow direction. Modified from NSIDC (2002).

Geometric data for East Greenland were taken from a pre-existing inventory (Jiskoot, 1999; Jiskoot *et al*., 2003). The original form of the flow direction data in this set was compass direction in octants represented by numbers ranging from 1 (N) to 8 (NW). This required that the data be transformed into degree directions to allow for comparison with the Svalbard and Yukon data collections, both of which were already in degree form. Glaciers that indicated a tributary-trunk confluence were isolated and analysed to obtain the angle of confluence between the tributary and trunk. The method used to interpret confluence angle data for East Greenland is the same as was used for the Yukon Territory data, detailed above.

3.2 – Ice Analogue Material

Stearns and Osterberg (2003) used a material for their Malaspina Glacier modelling experiments (see section 2.3.1) that has been shown to have flow properties similar to those known for ice. The material responds elastically to low stresses and will recover fully from stress until a threshold yield is met. In stresses greater than this critical value the analogue material displays brittle deformation (Figure 3.3). The behaviour of this material closely conforms to Glen's Flow Law (Glen, 1955), the flow law most commonly used in modelling simple flow in pure temperate ice (see Chapter 2.1), and thus is effective in simulating flow in a lab setting.

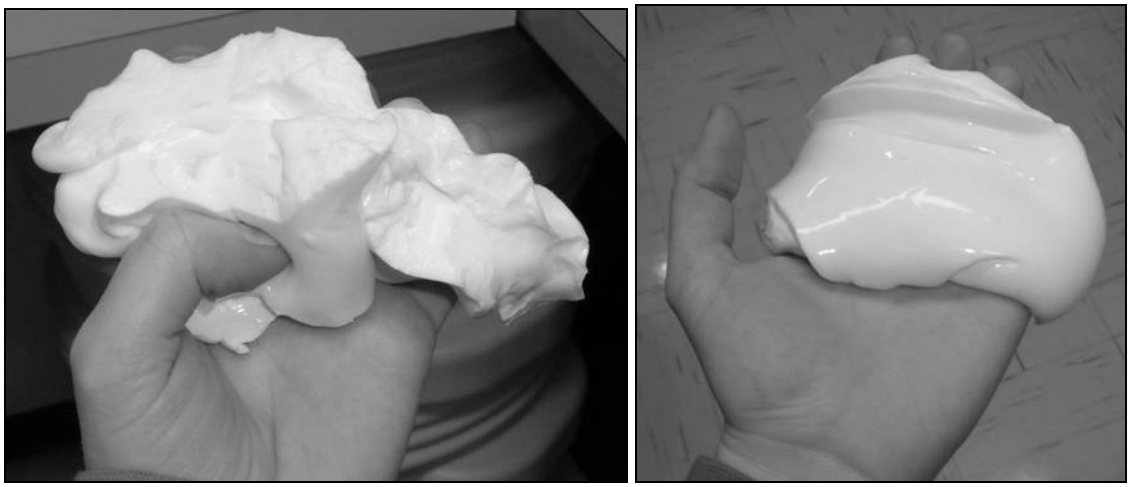

Fig 3.3 – Brittle and plastic deformation in the ice analogue material. The material on the left has been subjected to stresses higher than its critical yield and has fractured. The material on the right has been allowed to flow under its own weight.

3.2.1 – Ice Analogue Recipe

The ice analogue material consists of inexpensive household items - white glue, borax and water - and is simple to make and easy to use. The material is safe, relatively clean and can be dyed different colours to enhance the visibility of both surface and internal flow structures (Stearns and Osterberg, 2003).

The ice analogue was created in large batches that provided more than enough material for a single trial run. Each batch was then used in several experiments before being discarded and a new batch made. The following recipe was calculated from a single batch recipe to fulfill volume requirements for the model valley reservoir (3.5 L).

Ice analogue recipe for a single, large batch:

- Mixture 1
  - 1362 mL warm water
  - 1814 mL white glue
- Mixture 2
  - 185 mg borax
  - 910 mL warm water
- Mixture 2 is slowly poured through a sieve into Mixture 1 in order to strain out any undissolved Borax though ensuring that the solution is saturated.
- The two mixtures are combined and worked together by hand until completely set and then allowed to sit undisturbed overnight in a sealed container.

Changes in the characteristics of the material were observed over the course of six weeks in October and November 2005 through a series of simple experiments. The material was left for varying lengths of time both exposed to the air and in a sealed container in order to determine the effects of both conditions on the material. The material will not set, as was the case in early modelling attempts with clay based ice analogues (see Chapter 2), though it is subject to some surface desiccation and the formation of a membrane if left in the open air for several days. However, if this happens, the material beneath the protective skin will retain its viscous properties for several more days.

The ice analogue material can be stored for relatively long periods of time in a sealed container. However, after several months of inactivity it separates into water and a solid gummy substance regardless of storage. An initial batch was made on April 01, 2005 and

placed in a sealed container. No obvious changes in the materials physical properties were observed as of August 22, 2005. By September 25, 2005 the material had separated and could not be remixed.

It was also observed through tests that the material will lose mass, presumably through evaporation over a period of time, though the effects of this process can be reduced by placing the material in a container sealed with rubber or plastic. The loss of mass should not result in a significant variation in the flow properties of the material. In order to test this, the material was weighed before and after each trial run and the difference between the two recorded. Results of these tests are discussed in greater detail in Chapter 5 and details are given in Appendix II.

3.3 - Model Design

Several materials were considered in the construction of the analogue model valley. PVC pipe was briefly considered but discarded due to its lack of transparency. It was also rather expensive to purchase in the diameters required. Plexiglas was also considered, as were several other materials that were ultimately unsuitable in one manner or another. After consulting with Frank Klassen, the University of Lethbridge technician who was to build the model, it was decided to use acrylic tubing. This is an acceptable choice for a building material because it is relatively inexpensive, strong and easy to work with and can be purchased in various lengths, thicknesses and diameters. It is also entirely transparent which allows for easy viewing of the material from all angles as it flows through the model. It is also rigid so there is no error introduced as a result of sagging or flexibility of the model valley (Fig. 3.4).

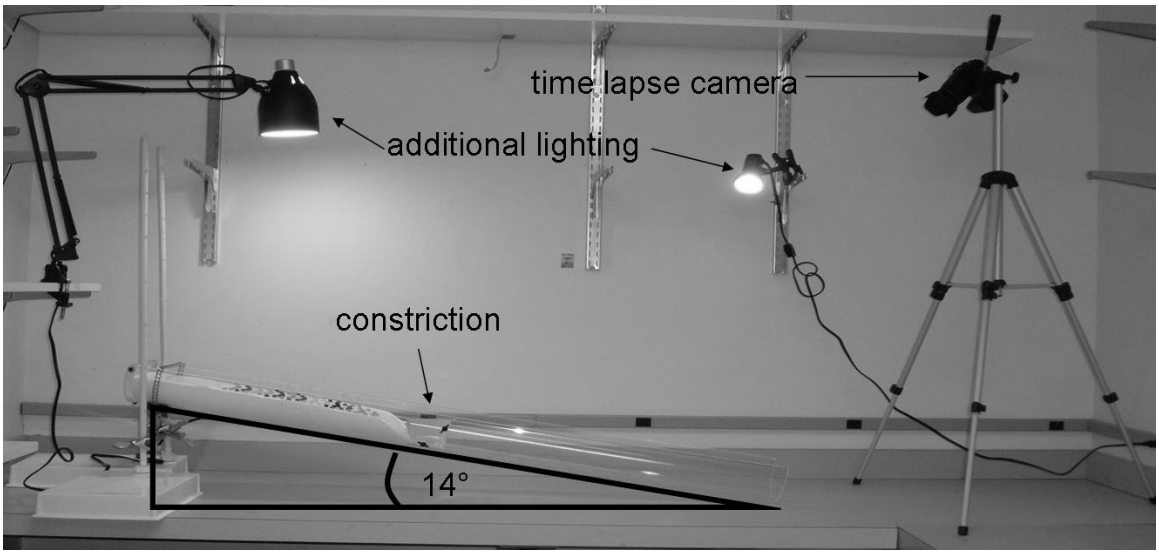

Fig 3.4 – Lab set-up for modelling experiments. The transparency of the acrylic tubing can be clearly seen in this image as can the rigidity of the model valley. No additional external supports were required along the length (125 cm) of the model.

The model was constructed from ¼ inch (0.63 cm) thick acrylic tubing with an internal diameter of 15 cm. The material was initially purchased as a length of tubing 182.22 cm (6 feet) long. This then had to be cut to a length of 125 cm and then cut again in half (lengthwise) slightly above the halfway mark. At bankful conditions the material would only fill the upper portion of the 'valley' in a 'reservoir' of 25 cm long and a depth of exactly half the diameter (7.5 cm). Because the model was designed prior to any extensive testing of the behaviour of the material the above-mentioned design specifications were made because the ice analogue material may have spilled over the edges of the model valley if its flow was impeded significantly by the blockages. The model design was based on a moderately sloped valley glacier of 10 km long with a trunk/tributary width ratio of 2, based on the most common tributary-trunk geometric properties as discussed in Chapter 4.

3.3.1 - Blockages

A series of experiments was designed to show the effects of blockages on flow in a valley glacier. Experiments consist of a single, straight, idealized glacial valley (width 15 cm x depth 7.5 cm x length 125 cm) with blockages of different sizes attached perpendicular to the valley wall 60 cm from the top of the reservoir. These blockages, indicated with letters A-E (assigned in order of testing, not in order of obstruction), represent restrictions on the trunk ice flow as a result of incoming tributary ice or the presence of a geological obstruction. These experiments consist of four different sizes of obstacles, of which the first three are perpendicular (90º) and the last oblique (45º). The first obstruction (B) blocks half the width and the full depth of the valley (depth 7.5 cm x width 7.5 cm). The second blockage (C) blocks the full depth but only ¼ of the valley's width (depth 6.5 cm x width 3.75 cm). The third (D) blockage is half the width of the valley but only half the depth (depth 3.75 cm * width 7.5 cm) and is mounted to allow the material to flow underneath the obstacle. The fourth blockage (A) has the same dimensions as the first (depth 7.5 cm x width 7.5 cm) but is designed to block flow at a 45° angle (Fig. 3.5) rather than at 90° as is the case with the first three obstructions. And in the unblocked trial (E) the material is unobstructed and in a valley of the same dimensions as the blocked experiments.

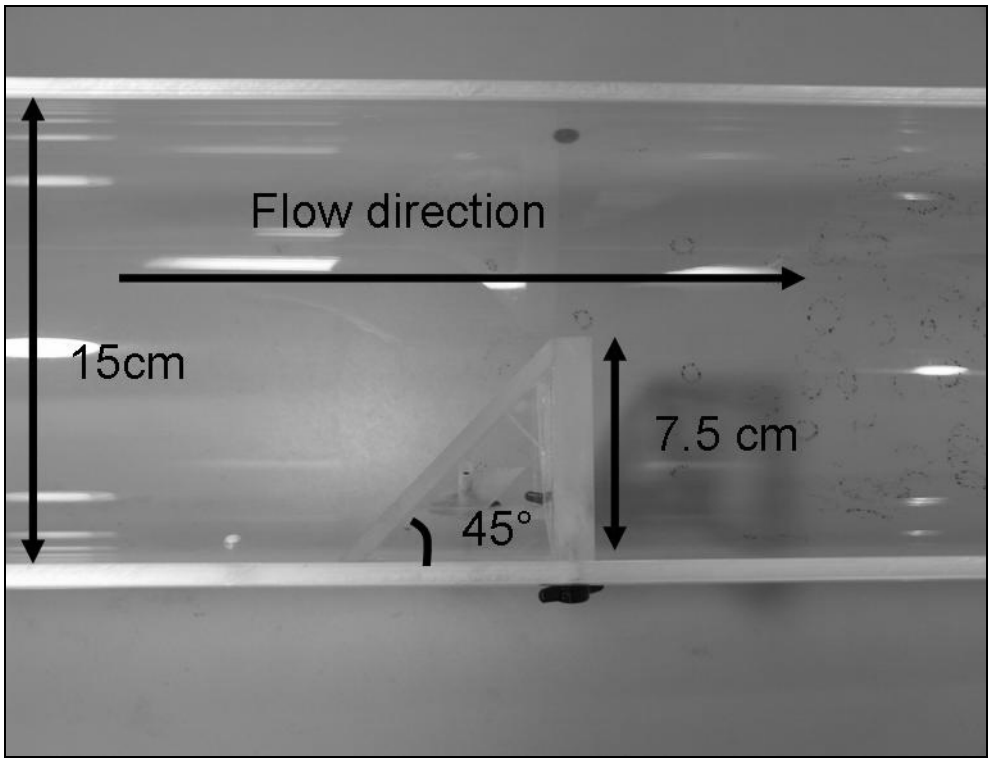

Fig. 3.5 – Model set-up for angled blockage (A). Depth is 7.5 cm. A wingnut can be seen in the lower centre portion of the image.

The four blockages were made from ½ inch (1.26 cm) thick acrylic to prevent breakage and to provide more stability and resistance against the weight of the material. Because acrylic tubing has a tendency to crack where there is any pressure put on weak points, such as the areas in the blockages where there are screw holes with wingnuts to keep the blockage in place inside the valley tube, extra precaution was taken both in the thickness of the acrylic and in the location of the attachment points.

Slope was marked on the model stands in 5 cm increments and the valley model set to a slope of 14°. This slope angle remained consistent throughout the experiments and was chosen because slopes less than 14° did not allow the material to flow at a rate that was realistic for a lab-based experiment. Furthermore, even though plotting of Yukon and East Greenland glacier inventory data indicate that for glaciers of 10 km length slopes of 7 - 10º are common (and the analogue model ideally simulates a 10 km long glacier), the

same inventories show that slopes of 14º are very common for glaciers in the 5-8 km range, and are therefore justifiable. A catchment was placed at the bottom of the model valley to collect any outflow of the analogue material, though was rarely required. The model was left attached to the stand at all times with only the lower end being raised to a slope of 0° during the filling of the reservoir and subsequent settling of the analogue material.

The reservoir was filled with 3500 g of the analogue material and left to settle for approximately 10 minutes into a flat surface before the placement of a strain grid template. This template was made from an initial grid created on a piece of graphing paper and transferred to velum using a permanent marker. A 3/16" punch was used to make holes in the velum to allow for a transfer of marker dots to the surface of the analogue material. The grid (Figure 3.6) consisted of 85 points, 13 rows of 6 or 7 marker dots, over an area of 324 cm^2 resulting in a point density of 1 marker per 4 cm^2. The strain grid was placed 7 cm above the reservoir blockage to prevent deformation of the grid as the material experienced an initial slumping motion with the abrupt removal of the reservoir wall. Once the template was in place the holes were marked with a permanent marker and the template removed. Surface marker points were then placed on top of the permanent marker dots in a predetermined and fixed order.

Several materials were tried as surface markers in the creation of an accurate strain grid on the surface of the ice analogue material before a suitable material was found. Surface markers such as permanent marker dots and chalk pieces were successfully used in the Malaspina modelling experiments (Stearns and Osterberg, 2003) but provided several problems for this thesis experiment. Permanent marker dots are easily visible in

the digital imagery but deform into lines and ellipses that could not be used for analysis. Chalk lumps were attempted but were nearly impossible to break into a useable size as well as to place, and then to remain, in a grid. All materials attempted were folded into the analogue material during the trials. The chalk lumps were no exception; they were nearly impossible to pick out and often became crushed into the material, which then turned purple. Map pins were attempted but again the problem was that they were being folded into the material and were somewhat difficult to remove without injury. The map pins also had a tendency to 'lie down' forward in the direction of flow, which resulted in the loss of the original marker position. Painted toothpicks were also considered and then discarded for the same reasons. A considerable problem with all of the above mentioned surface markers that eventually rendered them all unsuitable was the simple fact that the digitization of the markers points required 85 individual and unique points that could be recognized as such from the images. None of the above markers possessed such a quality nor could they easily be altered enough to do so while maintaining their original placement on the surface of the analogue material as it flowed.

Plastic beads were found to be the most suitable objects for markers because they are clearly visible by the camera and remain in the position in which they are placed upon the surface. They can be easily removed from the material after every trial and, conveniently, they are less dense than the analogue material. Any beads not accounted for at the end of the day will rise through the ice analogue material overnight and can be collected from the surface of the material before a new trial run is set up.

As mentioned above, in order to accurately digitize the beads from the time-lapse photos the strain grid had to be constructed from 85 unique points that could be easily

recognized and differentiated from each other in the photos. For each of the 13 rows in the strain grid, different coloured beads were used. Each row was comprised of either 6 or 7 beads depending on its location within the grid. This alternating number of beads per row exists because the grid is actually a series of strain diamonds rather than repeating rows and columns. The insetting of the rows and organization of the beads can be seen in Fig. 3.6. Each of the 85 beads was painted with one of 7 different coloured sparkles so that in any given location on the grid there was a unique point that could be identified by its combination of bead colour and filler. This simple and rather elementary step was essential to the digitizing process. Each bead was identical in every aspect other than colour with each having a diameter of 8.8 mm, a height of 6.2 mm and a weight of 0.03 g.

Beads were always placed in the same order to facilitate the digitization process and eliminate the potential for confusion between colours that may look similar in the photographs (i.e. Off-white/mixed and off-white/silver can look similar to one another but each could be looked for in a predictable location that could not be confused with the location of the other regardless of the effects of the blockage). In digitization order, points 1 through 4 refer to the fixed point locations on the surface of the lab bench (for the purpose of image correction) and points 5-89 refer to the points on the strain grid. Table 3.1 indicates the order of both bead colours and filler colours as seen on the surface of the ice analogue material.

Table 3.1 – Relative positions of unique points in the strain grid.

BEAD COLOUR	FILL COLOUR (BEAD ID #)						
AQUA	green (5)	silver (6)	gold (7)	purple (8)	blue (9)	mixed (10)	empty (11)
PURPLE	NA	silver (12)	gold (13)	purple (14)	blue (15)	mixed (16)	empty (17)
PINK	green (18)	silver (19)	gold (20)	purple (21)	blue (22)	mixed (23)	empty (24)
BLUE	NA	silver (25)	gold (26)	purple (27)	blue (28)	mixed (29)	empty (30)
DK BLUE	green (31)	silver (32)	gold (33)	purple (34)	blue (35)	mixed (36)	empty (37)
MAUVE	NA	silver (38)	gold (39)	purple (40)	blue (41)	mixed (42)	empty (43)
RED	green (44)	silver (45)	gold (46)	purple (47)	blue (48)	mixed (49)	empty (50)
OFF-WHITE	NA	silver (51)	gold (52)	purple (53)	blue (54)	mixed (55)	empty (56)
YELLOW	green (57)	silver (58)	gold (59)	purple (60)	blue (61)	mixed (62)	empty (63)
BLACK	NA	silver (64)	gold (65)	purple (66)	blue (67)	mixed (68)	empty (69)
GREEN	green (70)	silver (71)	gold (72)	purple (73)	blue (74)	mixed (75)	empty (76)
ORANGE	NA	silver (77)	gold (78)	purple (79)	blue (80)	mixed (81)	empty (82)
WHITE	green (83)	silver (84)	gold (85)	purple (86)	blue (87)	mixed (88)	empty (89)

Fig 3.6 – Detail of the 85 points included on the strain grid prior to flow. Strain grid is 13.5 cm wide and 24.0 cm long with a total area of 324 cm^2 before flow begins.

3.3.2 – Materials Used in the Collection of Data

Time-lapse still photos of the trial runs were captured using an 8 Mega pixel Konica Minolta Dimage 2 camera equipped with anti shake and 7x optical zoom. The camera was mounted on a tripod at the foot of the model glacier on the lab table and adjusted to an appropriate height, which then remained consistent throughout the series of experiments. Additional lighting was necessary and was mounted at two locations above the model. The additional light sources had to be bright enough to illuminate the surface of the material and allow for easy distinction between the unique points of the strain grid without resulting in over-exposure of the photographs as a result of the highly reflective surface of the ice analogue material. A non-descript, 60W desk lamp was placed above the reservoir at the top of the model and a second smaller, 40W light was placed above and slightly down flow from the location of the blockages (Fig 3.4).

3.4 – Digital Images

The camera was set at an oblique angle at the end of the model valley due to space limitations in the lab. Four markers were affixed to the lab bench and within the image frame to allow for a correction in any error that may have resulted from slight movements in the camera and/or model valley placement. Markers were also placed on the bench under the tripod. The camera had to be removed and remounted between every trial so its battery could be recharged and images uploaded to a desktop computer after each experiment. The markers on the bench allowed the camera to be replaced in the original location.

Each series of experiments was filmed with a digital camera so that precise measurements could be taken from the time-lapse images through the use of digitizing

software. A single image was captured every thirty seconds for a total of 103 frames and an individual trial time of 51.5 minutes. The time-lapse sequence was activated while the valley was still blocked and at a slope of 0°, which resulted in 100 (002 to 101) images indicating flow. To initiate flow of the material the reservoir blockage was removed and the valley set to a 14° slope for the remainder of the 100 frames.

3.4.1 – Digitization of Images

Each of the four blockages (A, B, C, and D) and the straight valley (E) were subjected to 10 analogue flow repeats for a total of 50 runs (A01-A10, B11-B20, C21-C30, D31-D40, E41-E50). Initially, 30 repeats were proposed for each of the blockages and the straight valley for the purpose of statistical significance. However, this was reduced to 10 as a result of time limitations for the digitizing process. For each run, only 10 of the 100 frames were digitized. The following table indicates the ten frames chosen for digitization and its corresponding time within the trial. Time 00:00 corresponds with the unusable frame (Frame 001) of the valley at a slope of 0°. Time and image frames used in the digitization of images can be seen in Table 3.2.

Table 3.2 – Selected frames and corresponding time intervals digitized in each of the trials

Frame ID	002	013	024	035	046	057	068	079	090	101
Time (min : sec)	00:30	06:00	11:30	17:00	22:30	28:00	33:30	39:00	44:30	50:30

Hence, from each of the 50 trials conducted, 10 frames were selected at specific time intervals for a total of 500 frames. Each frame included the 85 points in the strain grid and 4 fixed points, which equals a grand total of 44,500 manually digitized points. The 89 points in each frame were digitized in exactly the same order for all frames and trials so that each of the unique points corresponded to a specific number between 1 and 89. This

system allowed for an error check in the digitization process through the creation of indicator points throughout the grid: For instance, the red bead with no fill colour was always Point ID# 50. If, when digitizing, the red bead was counted but did not correspond with Point ID# 50 there had obviously been an overlooked marker point that could then be tracked by double checking the previous indicator beads to pinpoint the exact location of the error and then digitizing it properly. In the event of a bead point disappearing from the surface of the analogue material by folding under, the beads' corresponding unique ID# was then given the coordinates 0,0 (top left pixel of the digital image, and well outside the experiment frame). These positions could then be removed from the data before final analysis.

Digitization was done from digital frames saved in JPEG format, which were imported Image J (Figure 3.7). Image J (http://rsb.info.nih.gov/ij/index.html) is a downloadable freeware Java image-processing software originally designed for biology applications and was chosen because it lends itself well to identifying the point data required by this thesis. Image J creates an arbitrary X/Y grid over each image allowing the usage of the *Crosshair (mark and count)* tool that is found on the Image J toolbar. This manual count tool allowed for the exact location on each of the multi-pixel beads to be pinpointed and digitized. Points recorded from the beads were given a pair of coordinates on the arbitrary X/Y grid, which were recorded in numerical order in a *Results* window and saved as .txt file.

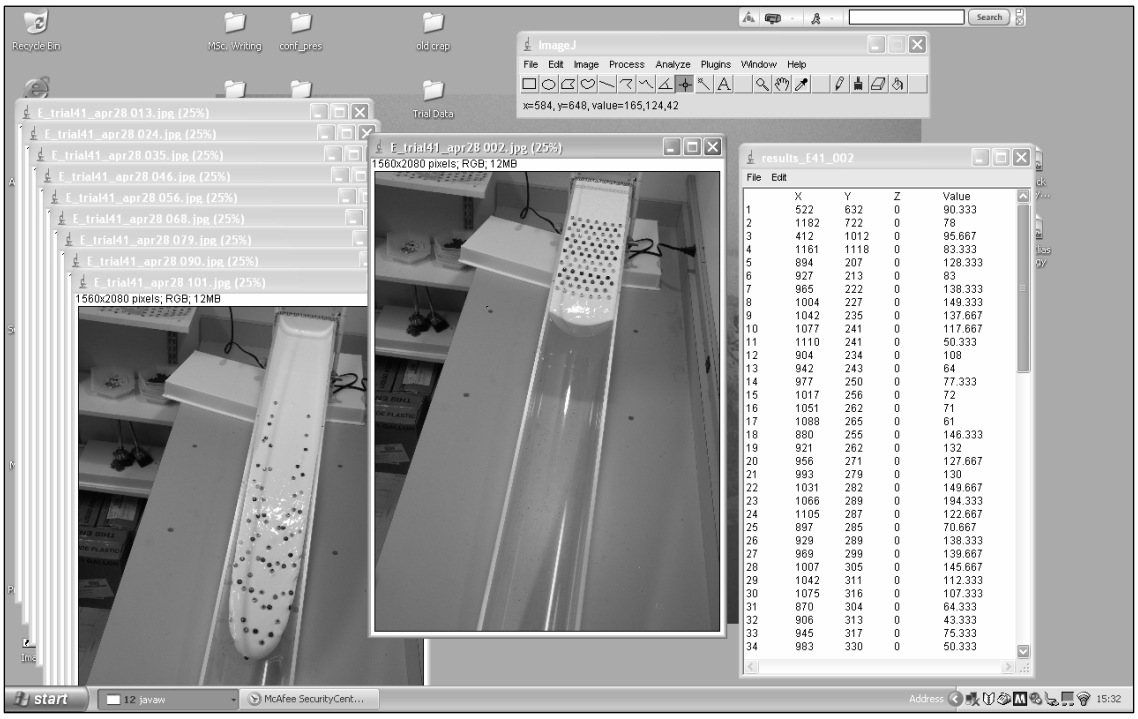

Fig. 3.7 – Image J, Java image processing software, as seen during digitization. All images in a trial could be opened, cascaded and then digitized in order, allowing the user to move between frames and facilitate point tracking between images. The Image J toolbar can be seen at the top of the screen with the crosshair tool selected. Coordinates are shown directly below the tool bar and when selected appear in the results window beneath it to the right.

3.4.2 – Data Analysis

The coordinate data for all 50 trials were imported to an excel file containing coding written for these data by Dr. Hester Jiskoot in April, 2006. Once imported into this file the coordinate data were subjected to a number of trigonometric corrections. These corrections were required to remove the effect of errors due to camera motion and to make adjustments in the coordinate data in order to account for the camera angle and photo distortions. From these calculations, lateral (X), longitudinal (Y) and total surface flow velocities as well as lateral, longitudinal and shear strain rates for each of the 50 trials were derived using the excel code.

The method used to analyse the flow of the model glacier is through speckle-tracking of the beads, using a mid-point average velocity calculation and a Lagrangian infinitesimal 1D strain calculation (e.g. Middleton and Wilcock, 1994; Price, 2006), an approach widely used in glaciology (e.g. Meier, 1957; Raymond, 1969; van der Veen, 1999; Murray et al., 2003; Pattyn, 2003).

1. The raw data (unique bead ID and XY coordinates), initially saved in a text file (.txt) were copied into an excel template containing the coding. For each Trial, data for 10 frames were entered, each with a 5.5 min interval (Table 3.2). Hereafter these are referred to as time 002, 013, 024, etc., up to 101.
2. The 'uncorrected' X and Y distance, the distance the bead appears to have moved between time intervals was calculated by subtracting the bead XY position at time t_i from that of the same bead at t_{i+1}. This is done for all the beads at all the time intervals.
3. The 'corrected' distance was then calculated by subtracting the average of the uncorrected distance for the four fixed points compared to time 002 (the distance that the fixed points appear to move as a result of slight digitization errors or camera movement) from the uncorrected distance acquired for each of the beads in step 2. This correction is generally a fraction of a pixel, but can occasionally be up to a maximum of 4 pixels in the x and y directions.
4. Grid rotation adjustments were then made to the bead locations to account for the distortion in the image caused by the angle of the camera during filming and the camera perspective. It was assumed that the undistorted y-axis (the centre flow

line) runs parallel to the valley walls, hence to the lines on each side of the initial regular strain grid at time 002.

5. Using points 5, 83, 11 and 89 (four corners of the strain grid) at time 002, the y-axis rotation angles on the left and right side of the image were calculated using simple right triangle trigonometry and Pythagoras theorem. Dependent on the camera position in each trial, this angle (α) is ~10-12º for the left-hand side of the grid, and ~6-8º for the right-hand side of the grid. This method was then extrapolated to each of the 7 points on the even lines, and each of the 6 points on the odd lines, so that in total 13 grid-adjustment angles were calculated, decreasing in value from the left to the right-hand side of the valley.
6. Using the angles calculated in step 5, the 'corrected' y- and x-distances from step 3 were adjusted to the grid-rotated distances, $\hat{y}$ and $\hat{x}$ using:

[Eq 3.1] $$\hat{y} = \frac{y}{\cos(\alpha)},$$

and

[Eq 3.2] $$\hat{x} = \frac{x}{\cos(\alpha)} + \left(\tan(\alpha) \times \hat{y}\right),$$

where α is the rotation angle calculated in step 5. The grid rotation method in step 5 introduces a small error for beads that do not remain on their straight path, which is <1 pixel in the y-direction and <3 pixels in the x-direction for beads that travel furthest off-line (from the valley wall flow-line to the centre flow-line).
7. Velocities for each marker were calculated using the mid-point average method, where the average displacement (grid-rotated distance in pixels) between frame times t_{i+1} and t_{i-1} was calculated (e.g. for frame 13 this is the average of the grid-

rotated displacement between frames 002-013 and 013-024). Since this is the velocity for the observed time interval between the digitized frames (11 intervals of 30 seconds = 5.5 minutes), this displacement was divided by 5.5 minutes to obtain the velocity in pixels per minute.

[Eq 3.3]

$$\overline{V}_{\hat{x}} = \frac{0.5\left((\hat{x}_{t_{i+1}} - \hat{x}_{t_i}) + (\hat{x}_{t_i} - \hat{x}_{t_{i-1}})\right)}{\delta t}$$

[Eq 3.4]

$$\overline{V}_{\hat{y}} = \frac{0.5\left((\hat{y}_{t_{i+1}} - \hat{y}_{t_i}) + (\hat{y}_{t_i} - \hat{y}_{t_{i-1}})\right)}{\delta t}$$

8. The pixel size in cm was calculated in order to convert the data into the useable units of cm min^{-1}. Pixel size was determined using the known distances in cm between the four corner grid points and their immediate neighbours on the same line (2 cm) and those on the next line with the same number of beads (4 cm) in the original regular strain grid at time 002. The distance in cm was then divided by the corrected and grid-rotated pixel-distance between the same points on the image. In this way four pixel sizes in the x and four in the y direction were determined, one for each of the four corners of the grid. These pixel sizes varied between 0.09-0.011 cm for the y direction, and 0.06-0.08 cm for the x direction.
9. The average x- and y-pixel size was then calculated and used to determine the movement of the beads in cm min^{-1}. This was done by taking the distance in pixel/min and multiplying it by the average pixel size of the strain grid.

10. The total velocity in cm min^{-1} was then determined by using Pythagoras theorem.

[Eq 3.5]
$$\overline{V} = \sqrt{\overline{V}_{\hat{x}}^{\,2} + \overline{V}_{\hat{y}}^{\,2}}$$

11. Strain rates ($\dot{\varepsilon}$) were determined in the x (lateral) and y (longitudinal) directions and from those the shear strain rate was derived using the following equations (e.g. van der Veen, 2002).

[Eq 3.6]
$$\dot{\varepsilon}_x = \frac{\delta \overline{V}_{\hat{x}}}{\delta x}$$

[Eq 3.7]
$$\dot{\varepsilon}_y = \frac{\delta \overline{V}_{\hat{y}}}{\delta y}$$

[Eq 3.8]
$$\dot{\varepsilon}_{xy} = \frac{1}{2}\left(\left[\frac{\delta \overline{V}_{\hat{x}}}{\delta y}\right] + \left[\frac{\delta \overline{V}_{\hat{y}}}{\delta x}\right]\right)$$

where x is the displacement of a single pixel over the same time as its velocity difference was calculated. The strain rates are given in the unit min^{-1} (c.f. the usual notation of s^{-1} or day^{-1} on real glaciers: Paterson, 1994) and the results of these calculations will be presented in Chapter 4.

Chapter 4 – Results

4.1 - Data Inventory

Glacier inventory data were collected to find characteristic geometries of tributary-trunk systems and thus to provide a foundation for the construction of the valley glacier model. Data was collected manually as well as derived from existing glacier inventories for the regions of Yukon Territory, East Greenland, Svalbard and the Thompson Glacier system (Canadian High Arctic). Histograms of measured entrance angles and trunk-tributary width ratios are given in Appendix I.

Fig 4.1 – A complex system of tributary- trunk interactions in Kong Christian IX Land, East Greenland. 1:3,000,000. (Modified from Benn and Evans, 1998).

4.1.1 – Confluence Angles

The confluent flow data for East Greenland and Yukon Territory were derived from pre-existing data inventories and because of this, the flow directional precision of these data has been given in 45° increments in order to correspond with the original directional

data, which was given in octants. Glaciers that exhibit confluence angles of 0° and 180° have a parallel confluence where both glaciers flow in the same direction.

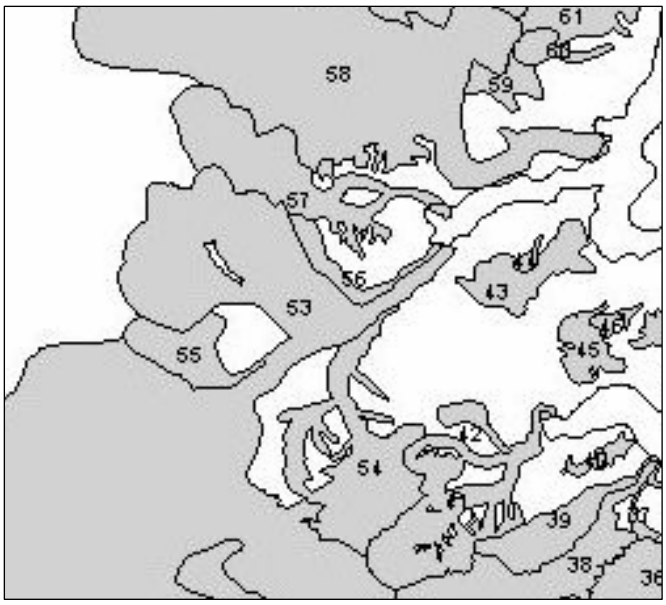

Fig 4.2 – Parallel confluent flow. A 0°/180° confluence can be seen at the glacier indicated by the convergence of glacier #53 and glacier #56 in the centre of the image. Down ice from the confluence the tributary flows directly parallel to the trunk glacier. (Modified from Jiskoot, pers.comm., 2006).

Of a total of tributary-trunk interactions sampled from the Yukon Territory data (n=358) inventory it was found that 116 (32%) had 45° confluence angles and 118 (33%) had 90° confluence angles (Appendix I). Results derived from manipulation of the East Greenland inventory data agree with those from the Yukon Territory. Of the 53 East Greenland tributary-trunk confluence angles collected 22 (42%) were 45° and 14 (30%) were 90°. Interestingly, 16 (30%) of the 53 were 0°/180° confluences, an example of which can be seen in Fig 4.2.

The data collected from manual measurements of glacier maps (Svalbard and the Thompson Glacier system) were measured with a protractor to within 5°. The previous trend towards the common occurrence of 45° and 90° tributary entrance angles that was noted in the Yukon Territory and East Greenland data is also apparent in the data

collected from the Svalbard inventory (Appendix I). The distribution of angles is bi-modal with 41 (29%) of 142 measured confluences having angles of 80° - 95° and 47 (33%) with angles 40° - 60°. Of the 15 glacier interactions measured from the Thompson map sheet, 6 (40%) had confluence angles between 40° and 55°. Examination of these inventories provided enough evidence to ensure that the model glacier would include blockages that would simulate those potentially created by a tributary glacier entering at both 45° and 90° angles.

4.1.2 – Trunk / Tributary Width Ratios

The Yukon Territory data inventory also yielded results regarding tributary-trunk width ratios, which are the width of the trunk measured at the confluence divided by the width of the tributary also measured at the confluence (see Chapter 3.1). These ratios were used to determine the width and depth of the blockages used in the experiments. From the Yukon Territory data inventory 515 tributary-trunk interactions were measured and it was determined that the most common trunk / tributary width ratios were those between 1 and 3 (Appendix I), indicating that tributaries in this region are commonly more than 1/3 the width of their trunk glaciers. Another relatively common occurrence in this region was the convergence of tributaries that were wider than their trunks (138 or 26.7%). It is important to note, however, that the Yukon and East Greenland width data are based on average widths of both glaciers and so are not necessarily entirely indicative of their widths at the confluence. Tributary width ratios 3 - 5 occurred less than the smaller ratios, approximately half as often as those with lower ratios (99 or 19%) and even fewer tributary - trunk width ratios were greater than 5 (81 or 16%).

The tributary-trunk width ratio data from the East Greenland inventory correlate with those of the Yukon Territory in this respect as well (Appendix I). Of the measured tributary-trunk interactions (n= 49) the most commonly occurring width ratio is that of 1 - 3 (1 - 2, n=13 or 26.5%; 2 - 3, n= 7 or 14.2%) and the second are those between 3 and 4 (n=8 or 16.3%). There were 5 (10.2%) of the 49 ratios measured that were between 4 and 5 and 12 (24.4) that were greater than 5. East Greenland also had a few tributaries that were wider than their trunks with width ratios of less than 1, though again these measurements are based on average widths of the entire glacier, not the measured widths at the confluence.

The Svalbard (n=208) and Thompson Glacier (n=12) data have a higher level of precision with the width ratios because they were both manually measured and so indicate the precise ratio at the confluence. The Svalbard data corresponds with the Yukon Territory and East Greenland data in that the most commonly occurring recorded width ratio is that of 1 - 2 (n=65 or 31%) with the second most common being those of 2 - 3 (n=54, or 26%). Svalbard had 21 (10%) of its total of 208 tributary glaciers that were larger at the confluence than the trunk. The most commonly occurring width ratio from the Thompson map sheet is that of 1.5 - 2. There were no tributaries in this system larger than their trunks though there was a single confluence where the tributary and trunk were nearly the same width. There were 4 of the 12 (33.3%) tributaries that had width ratios between 2 and 3 as well as two others that had width ratios between 4 and 4.5 (16.6%). The remaining three glacier confluences had width ratios of 1 - 1.5, 3 - 3.5 and 4.5 - 5 (8.3% each).

4.2 – Modelling Experiments Results

This section provides qualitative and quantitative descriptions of the general flow patterns in the form of results from the experimental model trials that are presented for three time intervals. Each of the three times corresponds with a frame captured during the filming of the experimental trials (see Appendix III). As noted in Chapter 3, a digital photo was taken every 30 s during the model trials (see Table 3.2). Frame 024 shows the behaviour of the analogue material early in the trial as it first encounters the blockages and corresponds with time 11:30 after the start of the trial (Frame 002). The second described time is that of frame 057 (time 28:00), a mid point in the flow trial at which time the material continues to move past the obstructions and flows into the valley below. The third displayed time, frame 090, occurs near the end of the flow trial at time 44:30. Flow patterns of the trials are revealed through the examination of longitudinal and lateral (transverse) velocities as well as longitudinal, lateral and shear strain rates from each of the five different experiments. Velocity and strain rates falling within the margin of error (see section 4.5) are excluded from serious consideration though remain on the maps, excluding the shear strain rate maps, to allow observation of the pattern of low versus high velocities and strain rates.

Results for the lateral velocity (X), or cross-valley flow are given in both negative (-) and positive (+) values. Negative values indicate movement of a marker bead to the left of its original location within the strain grid and positive values indicate movement to the right. Longitudinal flow (Y) is always given as a positive value (down-valley, toward the viewer). Longitudinal and lateral strain rates can be positive (extensional/tensile) or negative (compressive), but the lateral strain rates can only be analysed for direction

when viewed in combination with the lateral velocities (Figs 4.4, 4.10, 4.15, 4.20 and 4.25). The sign of the shear strain rate is an indication of the orientation of the angle change between the originally perpendicular lines of x and y directions (negative is left angle, positive right angle). Results for a total speed were also returned but indicated patterns nearly identical to the longitudinal velocity results and were not mapped.

Invalid data ('zeros' were returned by beads that did not move between images and 'outliers' by those beads that folded under and returned false high velocity results) were removed from the datasets. Statistical analysis of the 10 repeats (section 4.3) shows that the variation between trials within a blockage experiment was low which allowed for the use of a single a representative trial from each blockage experiment to be mapped. These five trials (A06, B19, C25, D31 and E43) were copied into separate files, the unused data removed and the corrected X and Y coordinates imported into Arcmap GIS software. Each point's unique X and Y coordinate is linked to lateral and longitudinal velocity and strain data, which were then mapped and displayed in Figures 4.3 to 4.28. Table 4.1 is an example of data from a single trial as it appears before being mapped.

Table 4.1 - The top two transects of the strain grid as they appear in the cleaned excel file used in the mapping of the results (trial A06, time 024). 'ID#' is the unique point ID for the markers in the strain grid. X and Y are their respective coordinates after the fixed points correction has been implemented. Strain rates are given in min^{-1}, velocities in cm min^{-1}.

ID#	X	Y	X strain	Y strain	shear	X velo	Y velo	Total velo
5	668	213	-0.124	-0.018	-0.071	0.043	0.296	0.300
6	688	252	-0.062	-0.010	-0.077	0.040	0.544	0.550
7	715	282	-0.579	-0.009	-0.808	0.017	0.750	0.750
8	744	294	3.760	-0.010	2.737	0.017	0.823	0.820
9	775	292	2.929	-0.005	3.040	-0.002	0.740	0.740
10	805	277	0.157	-0.009	0.115	-0.015	0.590	0.590
11	843	240	0.048	-0.009	0.034	-0.024	0.276	0.280
12	672	257	-0.148	-0.014	-0.109	0.034	0.419	0.420
13	698	299	-0.383	-0.010	-0.190	0.040	0.710	0.710
14	723	321	-0.138	-0.010	-0.135	0.030	0.850	0.850
15	751	325	0.056	-0.008	0.085	-0.014	0.844	0.840
16	781	315	0.014	-0.009	0.068	-0.023	0.745	0.750
17	822	283	0.087	-0.008	0.048	-0.024	0.465	0.470

All data maps that follow are drawn using the same legend scale intervals for the ease of comparison and interpretation. The boxes drawn around the data points are simple frames and don't show the exact valley extent. Further, they are not of the same length scale, and therefore don't show the same valley length portion, but the bottom edge is simply at the leading edge of the analogue glacier at frame 090 for each trial.

4.2.1 – Straight Flow in an Unblocked Valley (E Trials)

The unblocked model experiments are analogous to flow in a straight, unblocked valley glacier and provide a basis of comparison for the blocked trials.

Longitudinal velocity patterns (Fig 4.3) - Flow in the unblocked trials consistently displays parabolic flow with the lowest longitudinal velocities found near the margins and the flow velocity of the analogue material increasing towards the centre flow line. The general range in velocities between the valley sides and centre is of the order of ~ 2.0 cm min^{-1}, with the highest velocities being recorded in centre flow-line of the lower transects in frame 024 (2.58 cm min^{-1}, bead 80). Both right and left marginal beads

consistently experience low rates of longitudinal velocity throughout the trial (<0.5 cm min^{-1}). The difference in flow velocity between the slowest moving bead (left margin, upper transect, 0.29 cm min^{-1}) and the fastest moving bead (centre flow-line, lowest transect, 2.58 cm min^{-1}) is 2.29 cm min^{-1}. An overall reduction in the longitudinal velocity is indicated as the material flows through the valley over time (see time 024, time 057 and time 090). The centre flow-line in the later time intervals continues to flow faster than marginal beads though does so at a lower velocity than in the early parts of the trial. In frame 090 the fastest velocity is only 1.81 cm min^{-1}. However, the larger patterns of longitudinal velocity remain consistent throughout the trial with areas of low longitudinal velocities in frame 024 also indicating low velocities in frames 057 and 090.

Total velocities of nearly 4 cm min^{-1} were common for points 85, 86 and 87 though these high velocity rates were recorded in trials run with new batches of material. The highest recorded velocity from a point in a trial run with older material was 3.2 cm min^{-1}. Trial E43 was the last trial run with a batch of analogue material made 16 days prior and had been used in a total of 33 trials.

The longitudinal velocity in this trial is approximately 0.5 cm min^{-1} slower than the velocity found in the following trial, E44, which was run with a new batch of material. New batches of material also affected the range of velocity across a row. The difference in the velocities between the centre flow line and the margins was greatly increased in trials that were run with a new batch of material. Marginal beads in trials run with new material moved only slightly faster than those in trials with older material, however, velocities of beads in the centre flow line of trials with new material were often more than 1 cm min^{-1} higher than those of the same position in earlier trials.

Lateral velocity patterns (Fig 4.4) - Lateral velocity in either the right (0 - 0.1 cm min^{-1}) or the left (-0.1 - 0 cm min^{-1}) direction is consistently low throughout the duration of the trial. Higher rates of lateral velocity are associated with directional movement at the leading edge of the analogue flow, but are still approximately ten times lower than the longitudinal velocities. Early in the trial (frame 024) the upper transects very clearly indicate a confluent lateral movement towards the centre of the valley where the material is flowing faster. Later time intervals indicate very little movement towards the right of the valley. Only in the upper portion of the transect markers are moving towards the centre flow line, in the lower portion the flow is divergent when the material is spreading at its leading edge, with the highest velocities as they are folded under the leading edge of the analogue material.

Longitudinal strain rate patterns (Figs 4.5 and 4.6 (optimal scale)) - Longitudinal strain rates in the unblocked trials are low, and are almost consistently negative, showing an overall slowing down and longitudinal compression. Relatively high rates are indicated at the leading margin of the material where marker beads are folding under and the material is thinning so that the driving stress is lower. Side markers also show higher longitudinal compression than the centre flow line. This pattern indicates that there is very high basal drag and drag by the valley walls. Disregarding the points that are folding under the overall compressive longitudinal strain rates are between -0.025 - 0 min^{-1}. Only the centre flow-line beads appear to experience very low extensional strain rates (0 - 0.025 min^{-1}).

Lateral strain rate patterns (Fig 4.7) - The majority of lateral strain occurring early in the unblocked trials is extensional, meaning that the lateral velocity in both directions is increasing. In frame 024 a small area of compression occurs in the upper left-hand

margin, as well as a few isolated marker beads throughout the strain grid appear to also experience lateral compression. The entire glacier seems to be slowly speeding up its left lateral movement, possibly due to the valley leaning slightly to the left in the beginning of this experiment, and hence the material filling the valley flowing slightly down and left (the compression in the upper left is possibly due to the confluence of this dominant left flow: this is corroborated in Figure 4.4). At later intervals in the trial the dispersion of compression throughout the strain grid increases. The majority of lateral strain in the unblocked trial occurs at very low rates of both extension (-0.25 - 0 min^{-1}) and compression (0 - 0.25 min^{-1}) throughout the trial with the majority of higher strain rates in frame 90 being compressive. Only a single marker returns an extensional lateral strain rate higher than 0.25 min^{-1}. It is difficult to discern a pattern of lateral strain in the unblocked flow trials. However, it should be noted that at the beginning of the trial lateral strain is largely extensional and at the end of the trial it is mostly compressive, as the material slows.

Shear strain rate patterns (Fig 4.8) - Shear strain rates that fell below the error margin (<0.73 min^{-1}: see error analysis section 4.5) are excluded from the results and appear as crosses on the shear strain maps for each of the blockages but will not be mentioned again. Early in the unblocked trials the recorded shear strain rates are predominantly positive, however, there are two regions of negative shear strain rates. In the upper left corner of the strain grid low shear strain occurs at various rates and in the lower right corner of the strain grid there is a region of negative shear strain that reaches rates of <-0.2 min^{-1}. This pattern is the result of the general direction of flow (right lateral versus left lateral flow), and, as explained in section 4.2, the magnitude rather than the direction

is important for the interpretation of shear strain rate patterns. Figure 4.8 does not show a distinct pattern of maxima and minima, however, the centre flowline in frame 024 appears to have very low values. The shear strain rate in the later times of the unblocked trials is substantially lower than earlier in the trials with the majority of shear strain rates occurring between -0.1 min^{-1} and 0.1 min^{-1}.

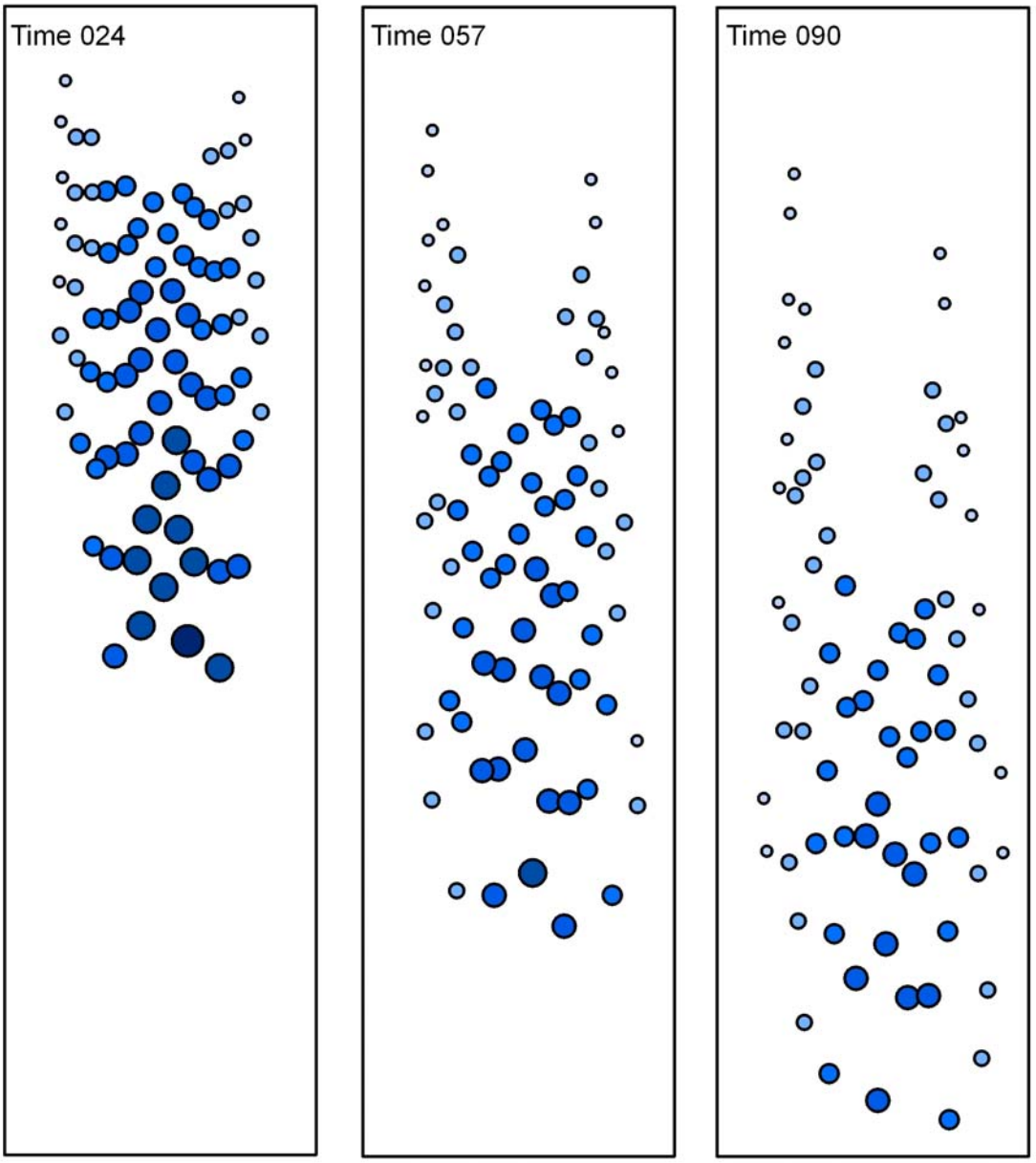

Fig 4.3 – Trial E43 longitudinal velocity (cm min^{-1}). A sample from the unblocked trials showing three time intervals. Each coloured dot corresponds with the location of a bead marker on the surface of the model glacier. Higher velocities are indicated by darker colours and larger symbols.

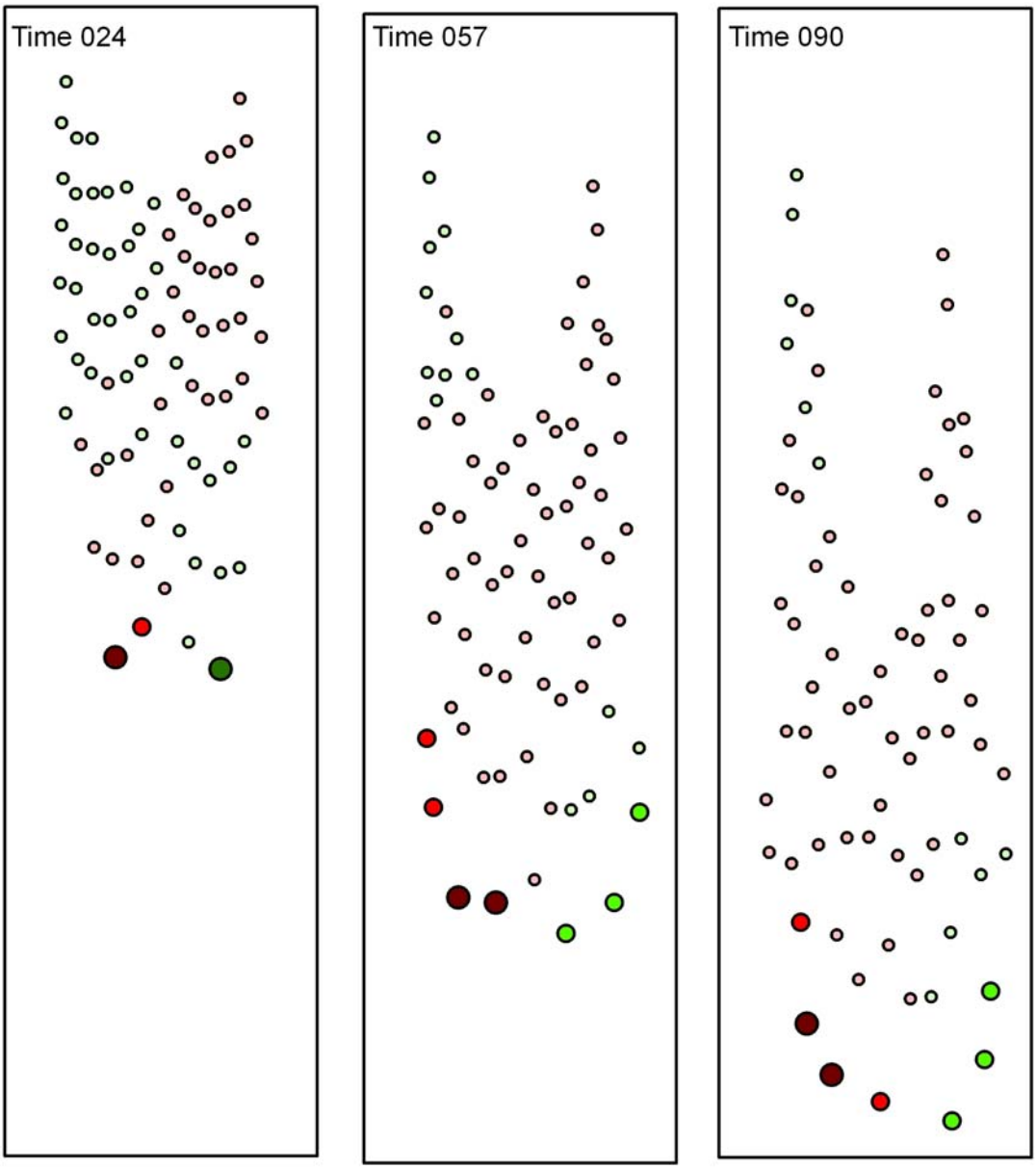

Fig 4.4 – Trial E43 lateral velocity (cm min^{-1}). A sample from the unblocked trials showing three time intervals. Each coloured dot corresponds with the location of a bead marker on the surface of the model glacier. Higher velocities are indicated by darker colours and larger symbols.

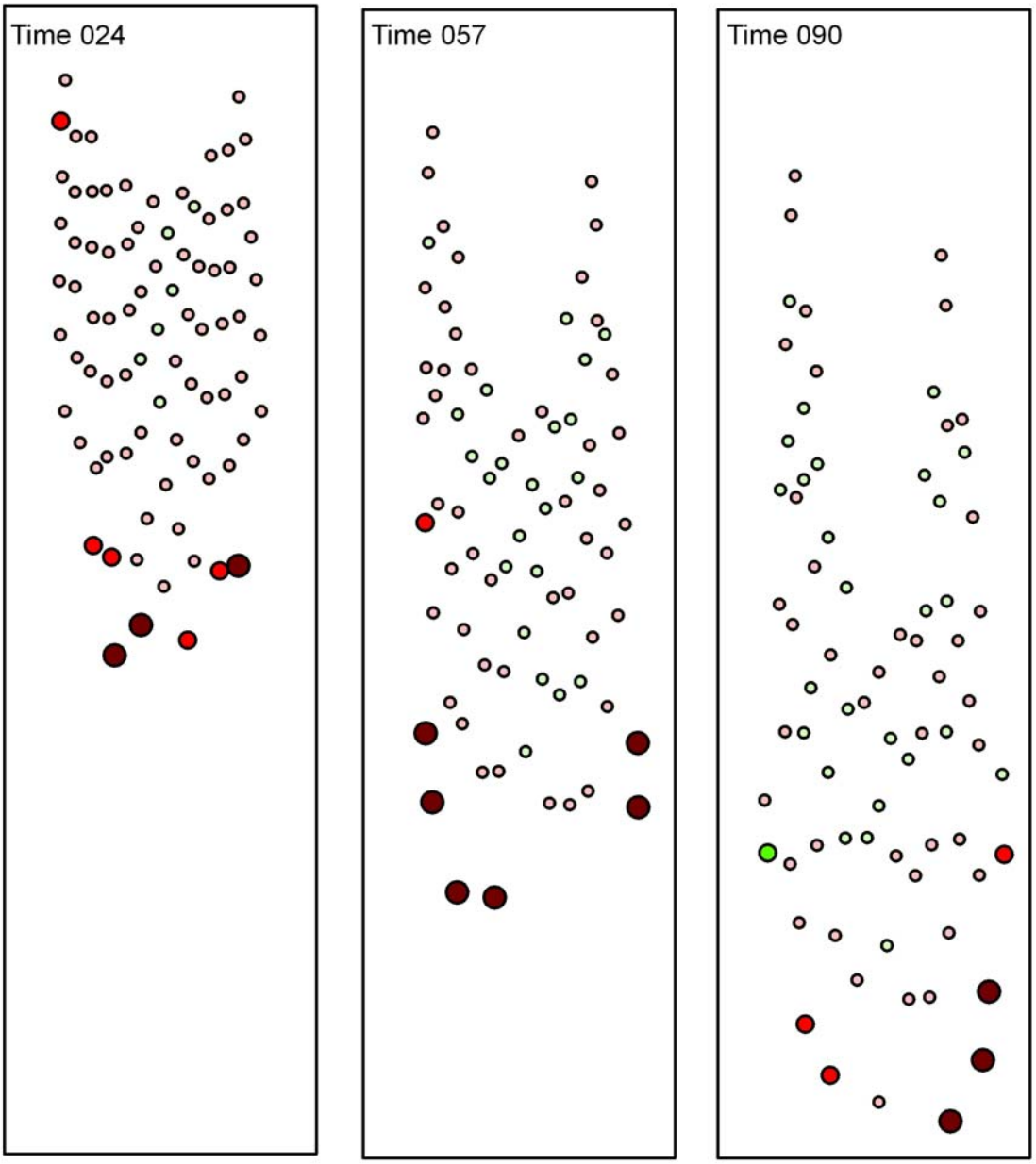

Fig 4.5 – Trial E43 longitudinal strain rate (min^{-1}). A sample from the unblocked trials showing three time intervals. Each coloured dot corresponds with the location of a bead marker on the surface of the model glacier. Higher velocities are indicated by darker colours and larger symbols.

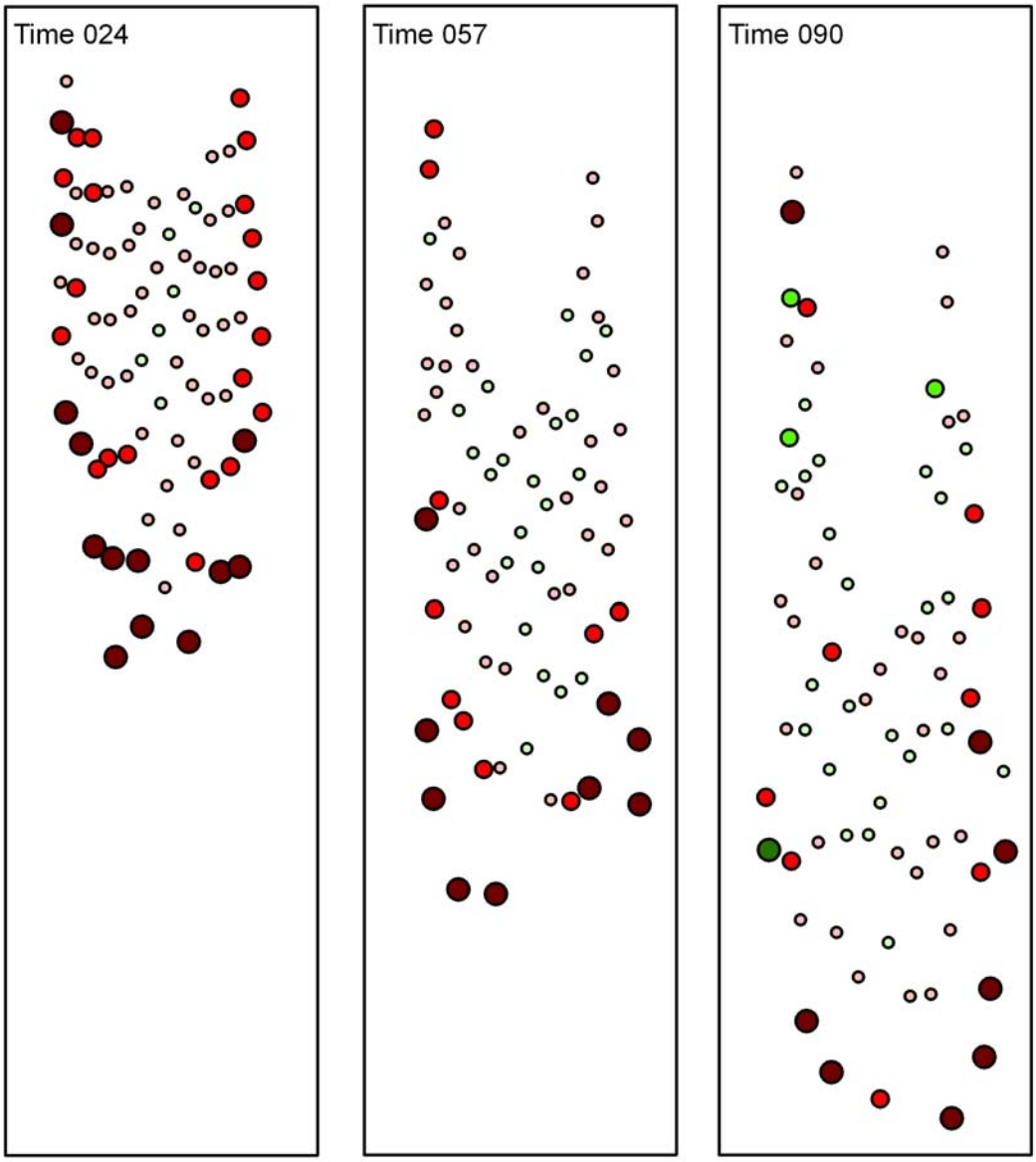

Fig 4.6 – Trial E43 longitudinal strain rate (min^{-1}). A sample from unblocked trials showing three time intervals. Each coloured dot corresponds with the location of a bead marker on the surface of the model glacier. Higher velocities are indicated by darker colours and larger symbols.

Note the reclassification in the legend (as compared to Fig 4.5)

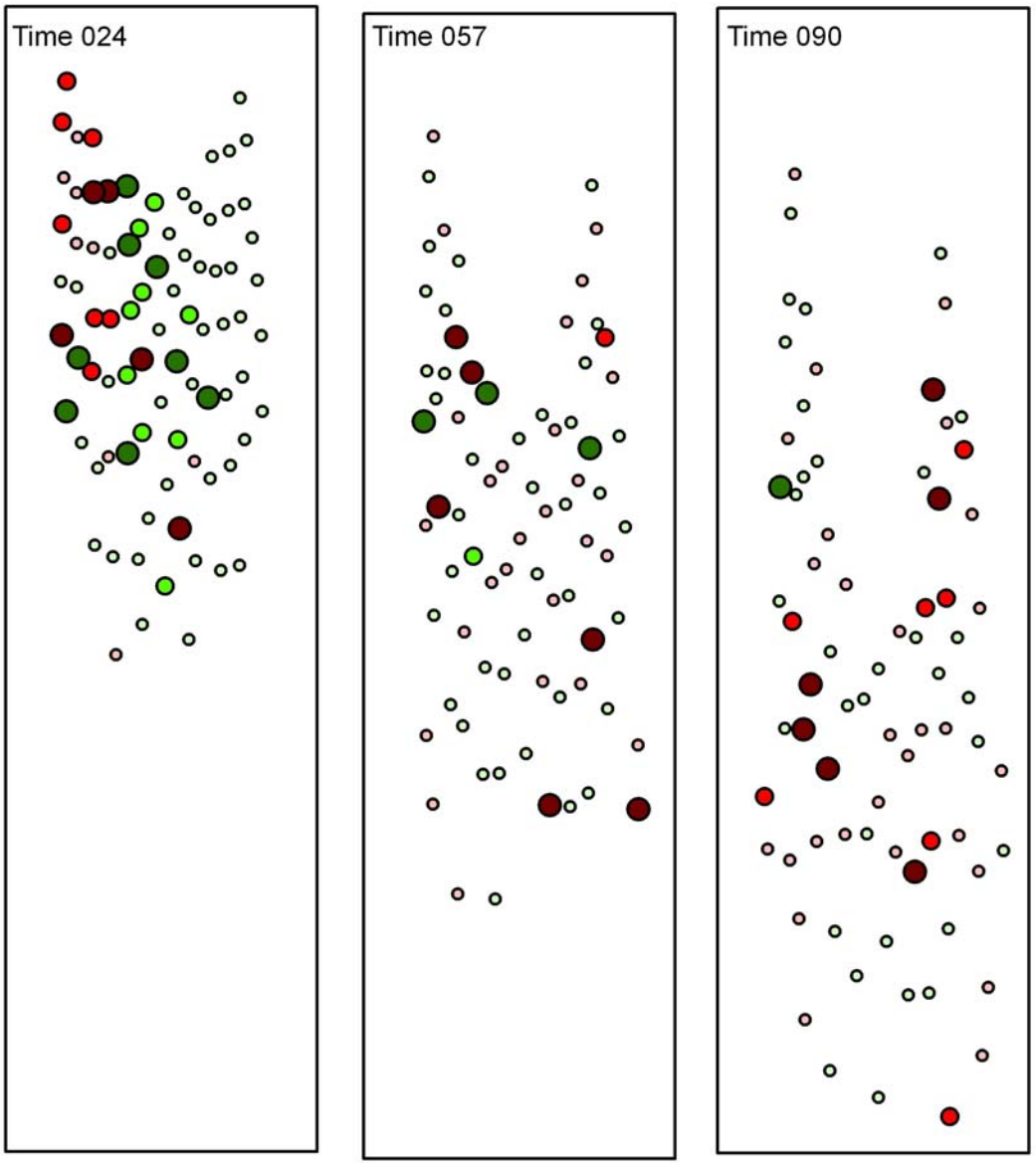

Fig 4.7 – Trial E43 lateral strain rate (min^{-1}). A sample from the unblocked trials showing three time intervals. Each coloured dot corresponds with the location of a bead marker on the surface of the model glacier. Higher velocities are indicated by darker colours and larger symbols.

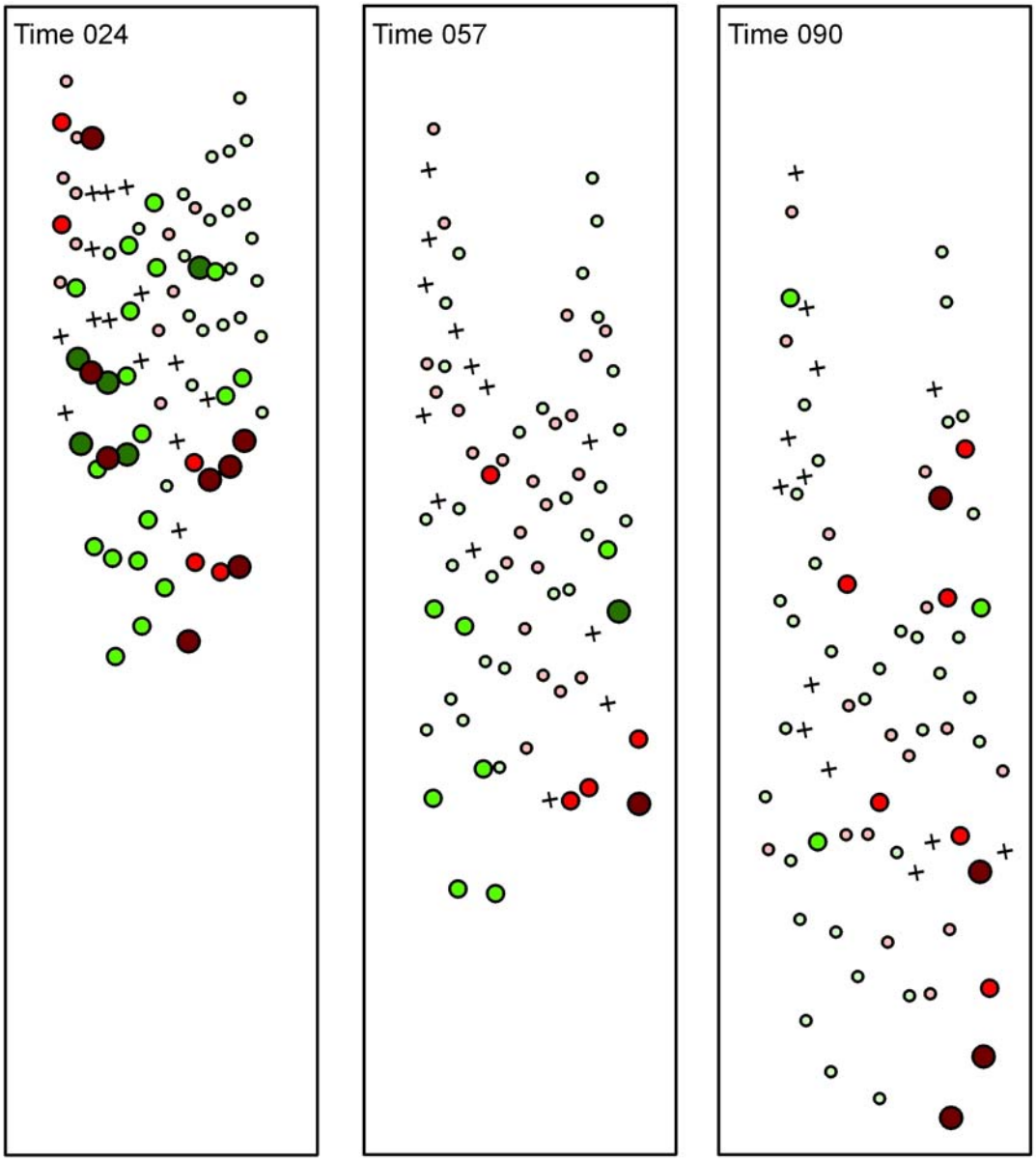

Fig 4.8 – Trial E43 shear strain rate (min^{-1}). A sample from the unblocked trials showing three time intervals. Each coloured dot corresponds with the location of a bead marker on the surface of the model glacier. Coloured dots indicate both positive (green shades) and negative (red shades) shear strain rates. Higher strain rates are indicated both by darker colours and by larger size.

4.2.2 - Angled Blockage (A Trials)

The angled (45°) blockage trials simulate the potential obstruction created by a large, fast moving tributary (Class III or IV, see Chapter 2.4) flowing at a 45° entrance angle into a trunk glacier. In this experiment the blockage obstructs half the width and the full depth of the valley. Because of the orientation of the angled blockage the material on the left side of the valley encounters the upper portion of the blockage at approximately the same time as the centre flow line encounters the 'point' of the blockage at the centre of the valley (~ time 013). Appendix III Frame 024 illustrates this situation.

Longitudinal velocity patterns (Fig 4.9) - Above the blockage the longitudinal velocity patterns are similar to those of the unblocked trials with the material in the centre of the valley (1 - 1.5 cm min^{-1}) flowing an average of 1 cm min^{-1} faster than at the margins (0 - 0.5 cm min^{-1}). Beads that directly contact the blockage in the early time intervals flow slower (0 - 0.5 cm min^{-1}) than those that do not directly contact it (1 - 1.5 cm min^{-1}). Overall, the almost symmetrical longitudinal flow pattern as found in the unblocked trial (E) is deflected slightly to the right in blockage A. In frame 057 the overall decrease in longitudinal velocity, and particularly upstream of the blockage as compared to downstream, imply a reduction in velocity as a result of contact with the blockage. The general parabolic flow pattern is still visible (flow in the centre flow-line is approximately 0.5 cm min^{-1} faster than at the margin) however, the velocity is ~1.0 cm min^{-1} lower than at time 024, and ~1.5 cm min^{-1} lower than in the unblocked trials. There is a subsequent increase in longitudinal velocity as the material passes through the constriction and into the valley below the blockage in the later frames (times 057 and 090).

Lateral velocity patterns (Fig 4.10) - Lateral velocity in the angled blockage trials demonstrates two important patterns:

The first is that upstream of the blockage the material is generally directed to the right as it is forced into the narrow unblocked portion of the valley (constriction), with higher right velocities (>0.2 cm min^{-1}) as it encounters the angled blockage. In the early times of the trial the majority of the strain markers are being moved to the right except for a small number of marginal beads in the right side of the upper transects that are still slowly moving (-0.1-0 cm min^{-1}) towards the centre flow-line.

Secondly, the beads next to and below the blockage are subject to high right and then left lateral velocities (>0.2 cm min^{-1}) as they move past the blockage and into the open valley downstream of the constriction. Once they have flown into the area directly below and behind the blockage on the left side of the valley there is large-scale left lateral movement (velocities up to <-0.2 cm min^{-1}). This pattern persists throughout the trial (frames 057 and 090).

Longitudinal strain rate patterns (Fig 4.11) - At time 024, there is a small group of strain markers near the blockage that indicate low rates of longitudinal extension (0 - 0.025 min^{-1}); however, the majority of the markers in the upper strain grid indicate compression. High rates of compression (<0.05 min^{-1}) are found directly above the blockage where beads on the left side of the strain grid come into direct contact with it. These have compressive strain rates two times higher than areas on the right side of the valley. Extension occurs where the material begins to flow through the unblocked portion of the valley throughout the trial. Notably, the mid-trial frame indicates higher tensional strain rates (>0.05 min^{-1}) than either early (0 - 0.025 min^{-1}) or later (0 - 0.025 min^{-1}) in

the trial, almost suggesting a wave-like flow pattern rather than a gradual slowing down and evening out of the velocity distribution as encountered in the unblocked trial. Increased longitudinal compression is measured up to about ½ the blockage width (3.75 cm) upstream of the blockage. Below the blockage the material is subject to an overall compression as it slows. Here, the majority of strain marker beads indicate low longitudinal strain rates (-0.025 - 0 min^{-1}) though a few markers indicate rates <-0.05 min^{-1}.

Lateral strain rate patterns (Fig 4.12) - Lateral strain rates in the angled blockage trials are approximately equal in the distribution of compressive and extensional strain rates. In the earlier frames of the trial (024, 057) the area above the constriction experiences low rates of lateral compression (-0.25 - 0 min^{-1}) before it flows through the opening and is subjected to low rates of extension (0 - 0.25 min^{-1}) once it has flowed past the blockage and speeds up leftwards into the empty valley. In frame 90 this pattern still exists though there are only two marker beads indicating compression and the rest extension at the blockage location.

Shear strain rate patterns (Fig 4.13) - Shear strain in the angled blockage trials is higher in frames 024 and 057 than that seen in the unblocked trials, as is the case in all ½ valley width obstructions (A, B and D). High values of both positive and negative shear strain occur early in the trial though the strain grid is dominated by shear strain rates of <-0.2 min^{-1}. Directly above the blockage there is a region of low shear strain rates occurring between -0.1 min^{-1} and 0.1 min^{-1}. This region of low shear strain persists throughout the duration of the trial beginning as predominantly positive strain in the early trial and becoming a region of low rates of largely positive shear strain (0.1 min^{-1}).

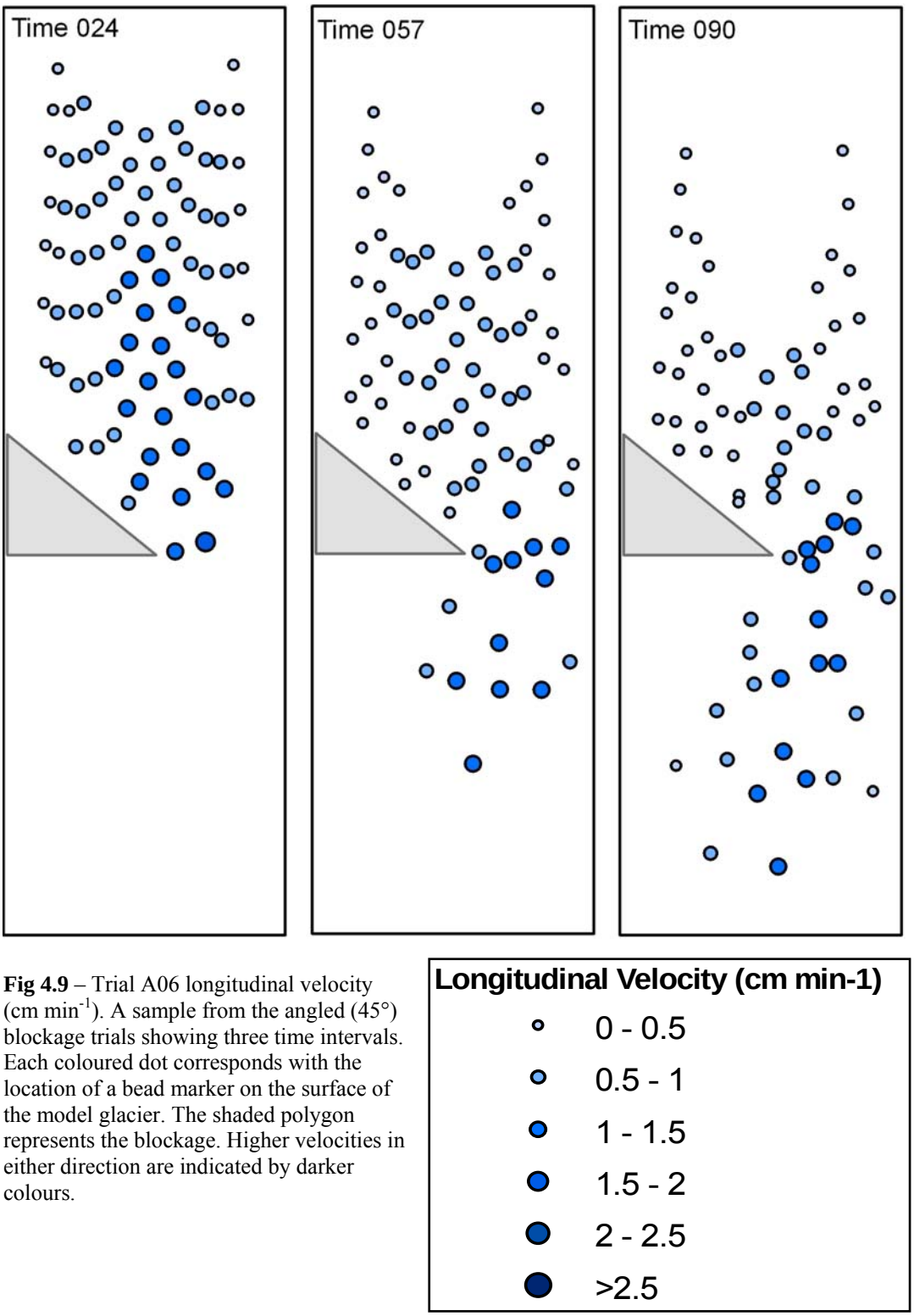

Fig 4.9 – Trial A06 longitudinal velocity (cm min^{-1}). A sample from the angled (45°) blockage trials showing three time intervals. Each coloured dot corresponds with the location of a bead marker on the surface of the model glacier. The shaded polygon represents the blockage. Higher velocities in either direction are indicated by darker colours.

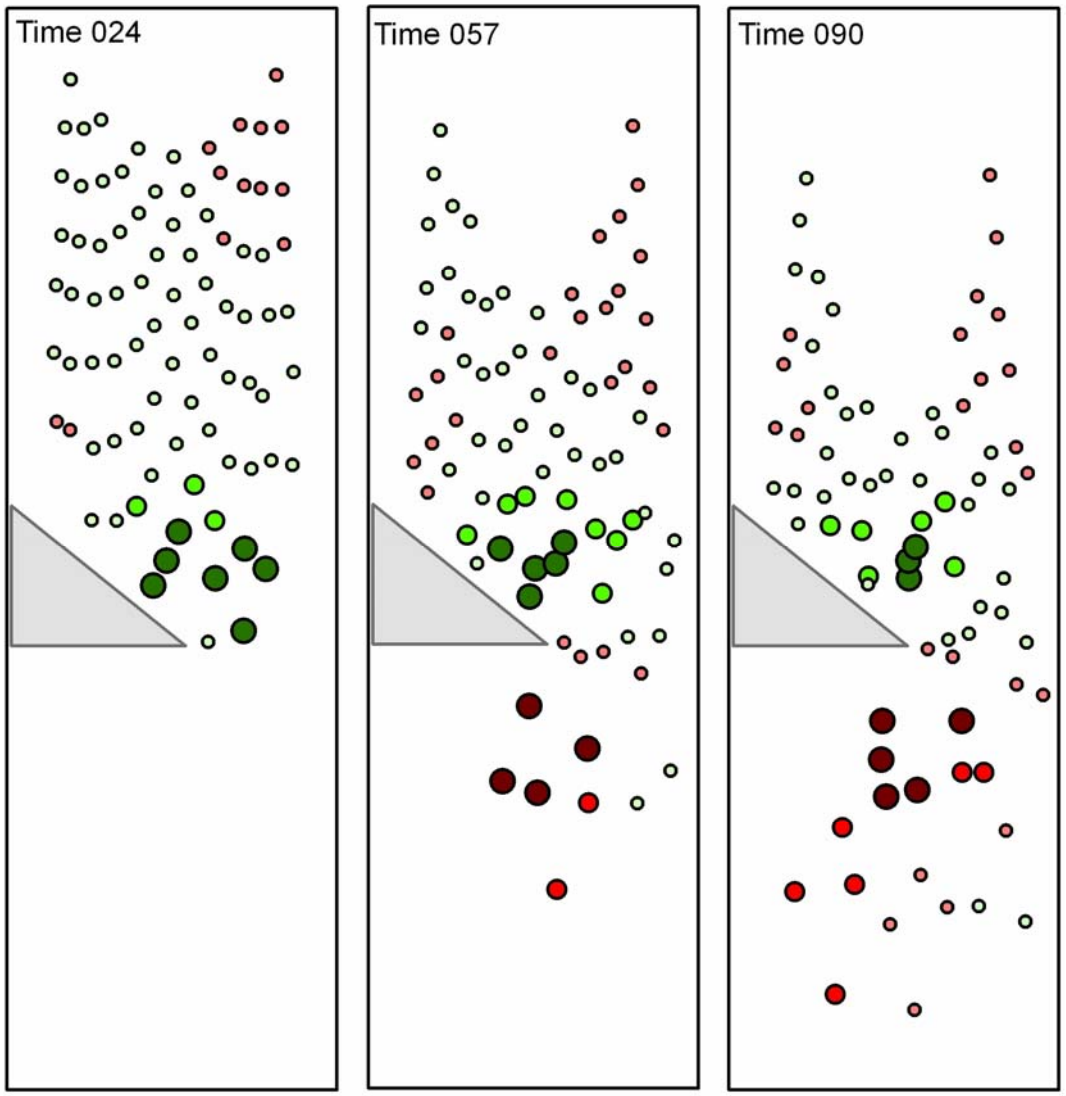

Fig 4.10 – Trial A06 lateral velocity (cm min^{-1}). A sample from the angled (45°) blockage trials showing three time intervals. Each coloured dot corresponds with the location of a bead marker on the surface of the model glacier. The shaded polygon represents the blockage. Lateral velocity occurs in two directions; to the right (positive values/green shades) and to the left (negative values/red shades). Higher velocities in either direction are indicated by darker colours and larger symbols.

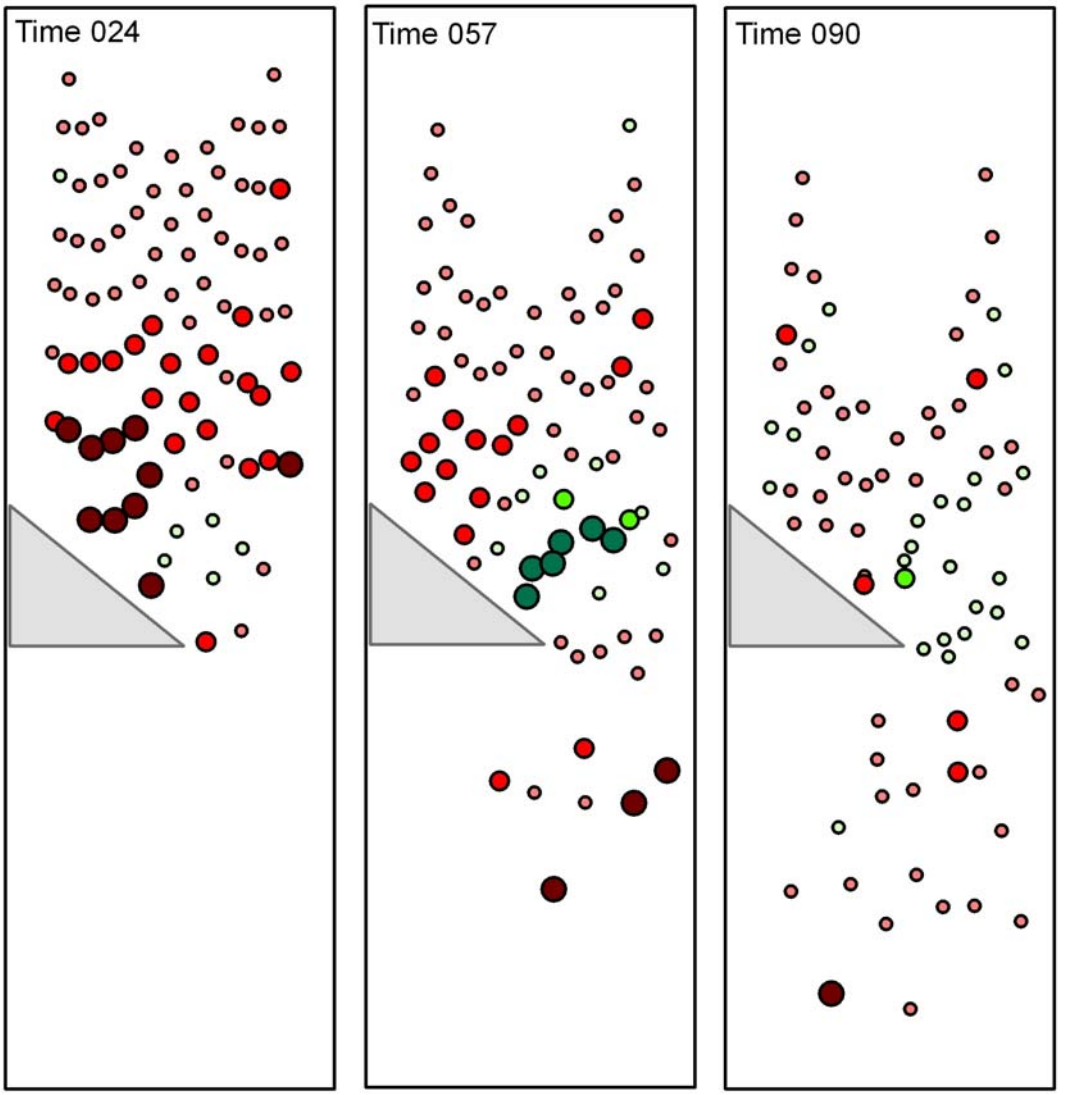

Fig 4.11 – Trial A06 longitudinal strain rate (min^{-1}). A sample from the angled (45°) blockage trials showing three time intervals. Each coloured dot corresponds with the location of a bead marker on the surface of the model glacier. The shaded polygon represents the blockage. Coloured dots indicate both longitudinal extension (positive values/green shades) and compression (negative values/red shades). Higher strain rates are indicated both by darker colours and by larger size.

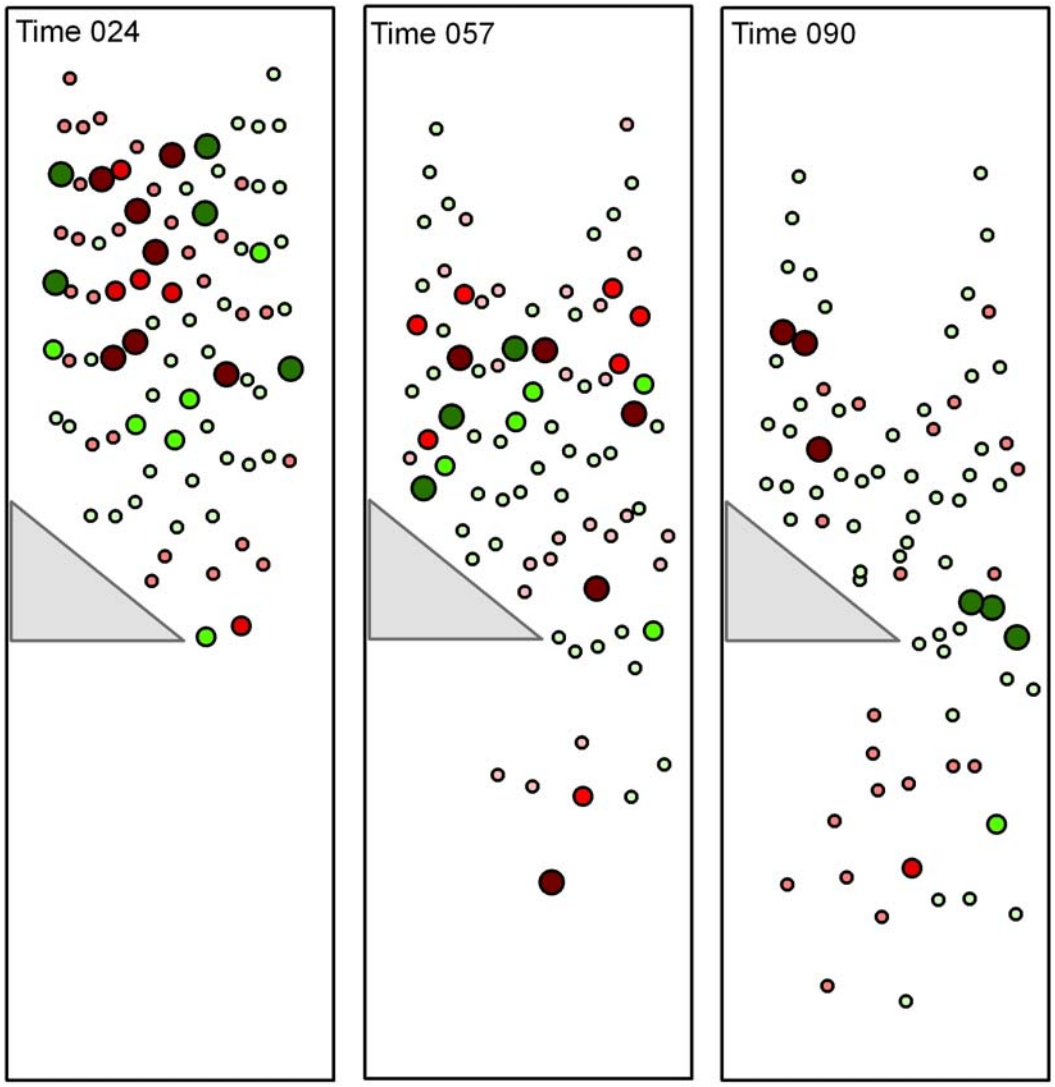

Fig 4.12 – Trial A06 lateral strain rate (min^{-1}). A sample from the angled (45°) blockage trials showing three time intervals. Each coloured dot corresponds with the location of a bead marker on the surface of the model glacier. The shaded polygon represents the blockage. Coloured dots indicate both (non-directional) extension (positive values/green shades) and compression (negative values/red shades). Higher strain rates are indicated both by darker colours and by larger size.

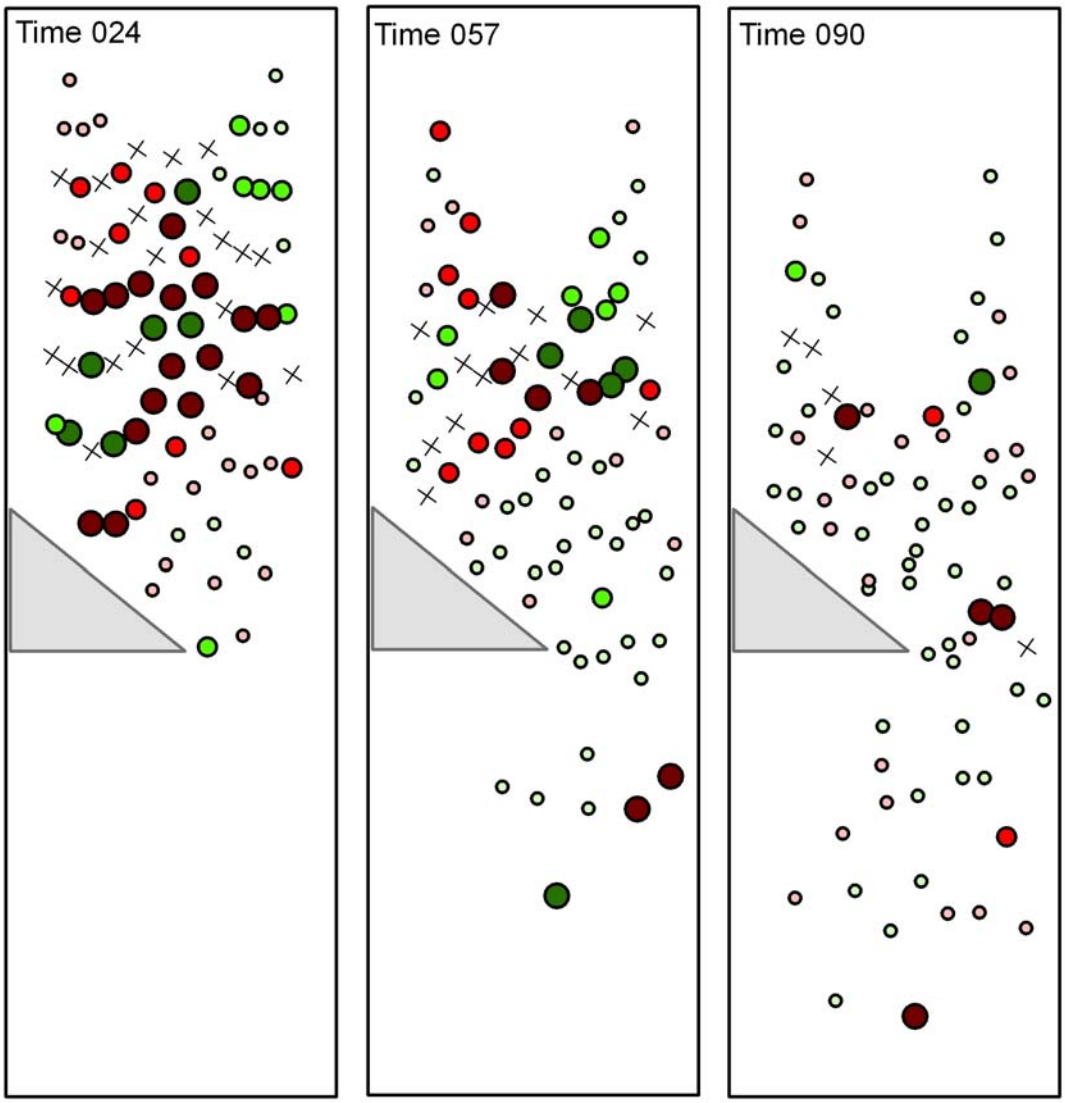

Fig 4.13 – Trial A06 shear strain rate (min^{-1}). A sample from the angled (45°) blockage trials showing three time intervals. Each coloured dot corresponds with the location of a bead marker on the surface of the model glacier. The shaded triangle represents the blockage. Coloured dots indicate both positive (green shades) and negative (red shades) shear strain rates. Higher strain rates are indicated both by darker colours and by larger size.

4.2.3 - Perpendicular Blockage, ½ width and full depth (B Trials)

Blockage B was designed to block flow of the analogue material for half of the width and the entire depth of the model valley. This blockage approximates a large-scale geological obstruction or the blocking potential created by orthogonal flow of an active tributary glacier into an equal sized trunk glacier.

Longitudinal velocity patterns (Fig 4.14) - Blockage B has a significant and obvious effect on the longitudinal velocity pattern. Velocities of beads that flow through the constriction on the right side of the valley do not appear to be affected by the blockage, but those on the left side are substantially lower above the blockage than those that flow through the constriction. The highest velocities (>2.5 cm min^{-1}) in the early frame (024) occur as the material flows past the blockage. Where the beads directly contact the upstream side of the blockage the longitudinal velocity is reduced to 0 - 0.5 cm min^{-1}; this is consistent throughout the trial though is particularly pronounced at time 057. The marginal beads in the upper transect of the early frame have overall higher longitudinal velocities than those at later times, which is consistent with the overall observations in the unblocked trial. By time 057 the longitudinal velocity of the marginal beads is ~ 1.0 cm min^{-1} lower than in the previous frame. Longitudinal velocities in all frames are consistently higher as the material flows past the blockage and into the valley below.

Lateral velocity patterns (Fig 4.15) - Lateral velocities above the blockage occur at various magnitudes to the right, with a small group of markers at the upper right corner of the strain grid indicating low rates of left lateral flow (-0.1 - 0 cm min^{-1}) towards the centre of the valley. Three beads at the left margin, directly above the blockage, also experience low rates of left lateral flow (-0.1 - 0 cm min^{-1}). Right lateral movement

directly above the blockage is observed across the entire width of the model valley in the later frames, with the highest rates (>0.2 cm min^{-1}) occurring directly above the blockage. The material begins to move left immediately after it has flown past the blockage. Beads adjacent to the blockage indicate sudden left lateral movement as they move into the space below it, and are subjected to high rates of left lateral velocities (<-0.2 cm min^{-1}) throughout the trial. This below-blockage left lateral movement is of similar magnitude as that found in blockage A. At time 057 the majority of the lower valley is experiencing flow to the left at rates that decrease as the material flows away from the effect of the blockage. By the end of the trial (090) beads flowing out of the constriction are still subject to left lateral movement, but a large portion of beads flowing lower in the valley indicate some movement to the right of the valley and a more general or divergent flow. High lateral velocities in either direction that occur near the bottom of the valley are those at the leading edge of the analogue material and are in the process of folding under.

Longitudinal strain rate patterns (Fig 4.16) - The analogue material in this full 90º blockage is largely subject to longitudinal compression. The area directly above the blockage is subject to high compressive strain rates (<-0.05 cm min^{-1}) where material is forced to pile up behind the blockage (see also Fig 5.1). This effect can be seen clearly in time 024 and still somewhat in time 057 though by time 090 most of the analogue material has flown past the blockage and the effect is less pronounced. A small area less than a valley width above the unblocked portion of the valley experiences low to moderate (0-0.025 min^{-1}) rates of extension at time 024, and higher rates (>0.05 min^{-1}) at time 057. It appears that this region is squeezed through the constriction and hence is speeding up. Longitudinal strain rates are low over the entire surface once the analogue

material has flown past the blockage. The only markers indicating high rates of compression below the blockage are those at the margin. Low rates of extension are returned from markers flowing in the centre of the material below the blockage (0 - 0.025 min^{-1}), indicating that the flow is slowly speeding up.

Lateral strain rate patterns (Fig 4.17) - Two distinct zones of positive extensional lateral strain occur in the early times of the B trials. Low rates of extension (0 - 0.25 min^{-1}) occur as the analogue material flows through the constriction. Higher rates (>0.5 min^{-1}) occur in the centre of the strain grid well above the blockage, indicating a forced flow towards the right and into the constriction. These two zones of lateral extension are separated by a band of low lateral compression at rates of -0.25 - 0 min^{-1}, which appears to increase with proximity to the opening of the constriction, indicating slowing down of the right lateral movement. This pattern remains visible throughout the rest of the trial. Compressive strain is also recorded in the upper margins of the strain grid on either side of the model valley at rates of -0.25 - 0 min^{-1}. Once the material flows past the blockage a region of high compressive strain (<-0.5 min^{-1}) is recorded and persists through the remainder of the trial. Otherwise, the later time of the trial is characterised by low overall extensive strain rates of 0 - 0.25 min^{-1}.

Shear strain rate patterns (Fig 4.18) - Most notable in the shear strain results of the B trial is the distribution of high rates of shear strain occurring early in the trial. Values of <-0.2 min^{-1} dominate the upper central portion of the strain grid while the upper right portion experiences positive shear strain rates >0.2 min^{-1}. In contrast, the region above the constriction experiences low positive and negative shear strain rates between -0.1 - 0.1 min^{-1} that persist throughout the trial.

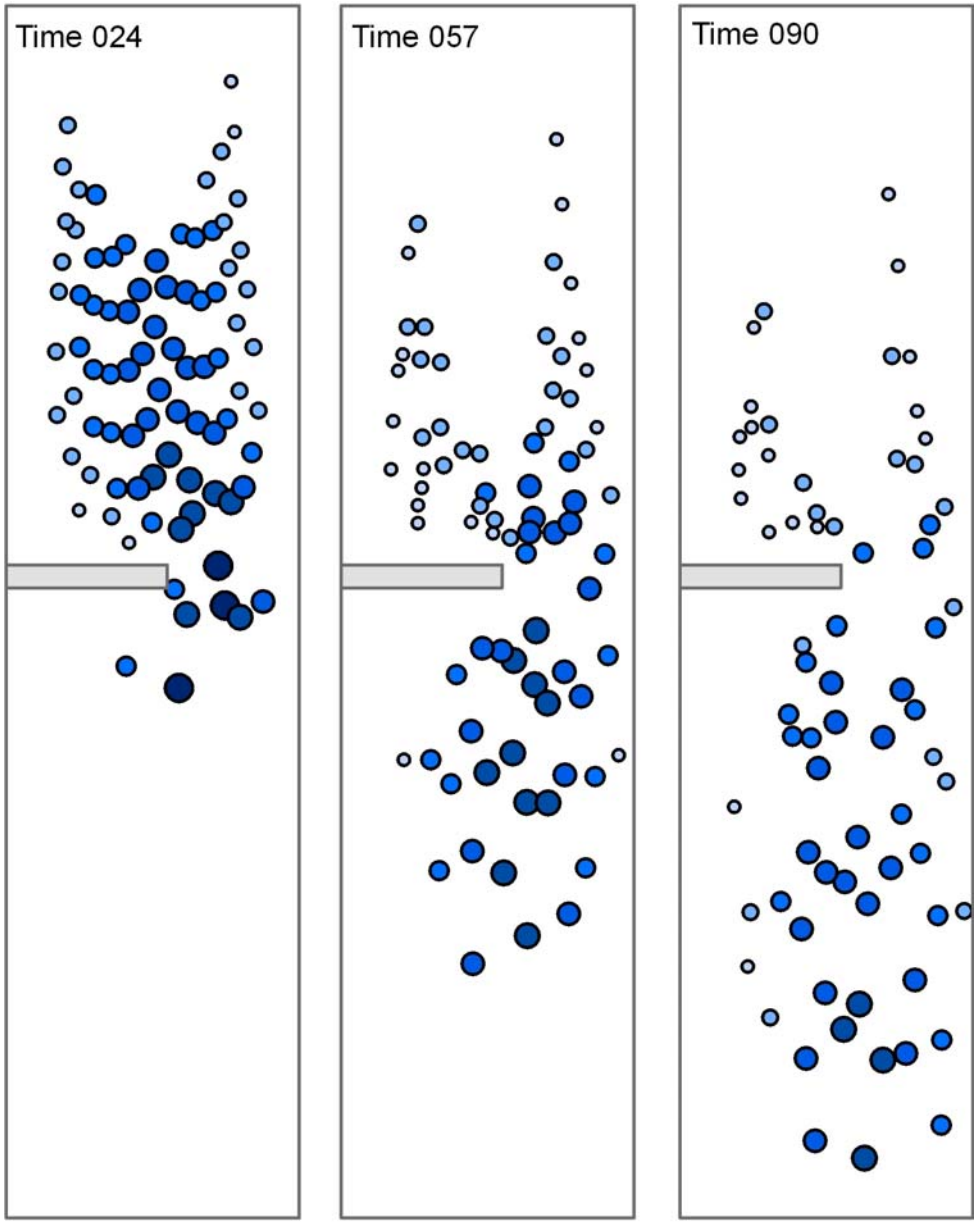

Fig 4.14 – Trial B19 longitudinal velocity (cm min^{-1}). A sample from the straight blockage trials (½ width, full depth) showing three time intervals. Each coloured dot corresponds with the location of a bead marker on the surface of the model glacier. The shaded polygon represents the blockage. Higher velocities are indicated by darker colours and larger symbols.

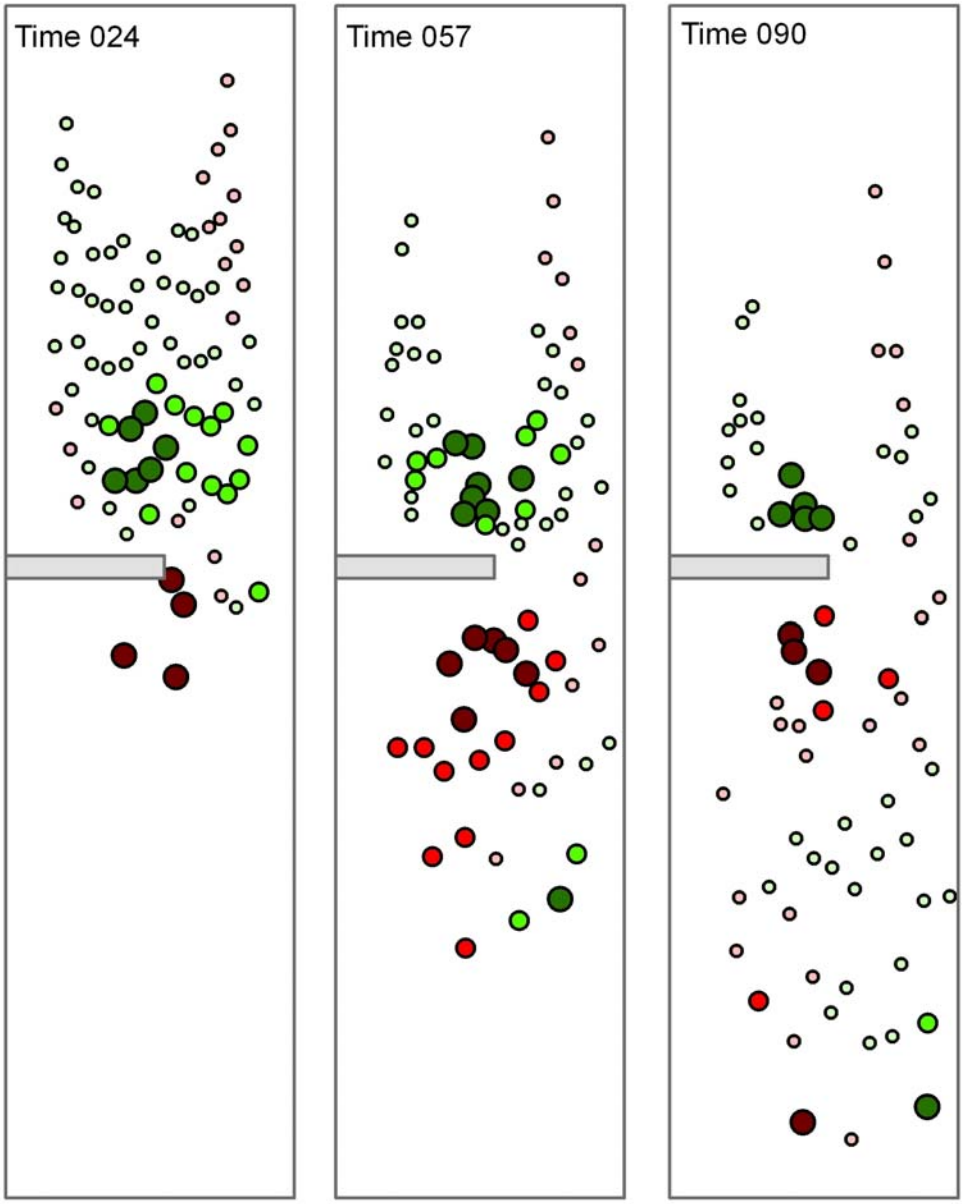

Fig 4.15 – Trial B19 lateral velocity (cm min^{-1}). A sample from the straight blockage trials (½ width, full depth) showing three time intervals. Each coloured dot corresponds with the location of a bead marker on the surface of the model glacier. The shaded polygon represents the blockage. Lateral velocity occurs in two directions; to the right (positive values/green shades) and to the left (negative values/red shades). Higher velocities in either direction are indicated by darker colours and larger symbols.

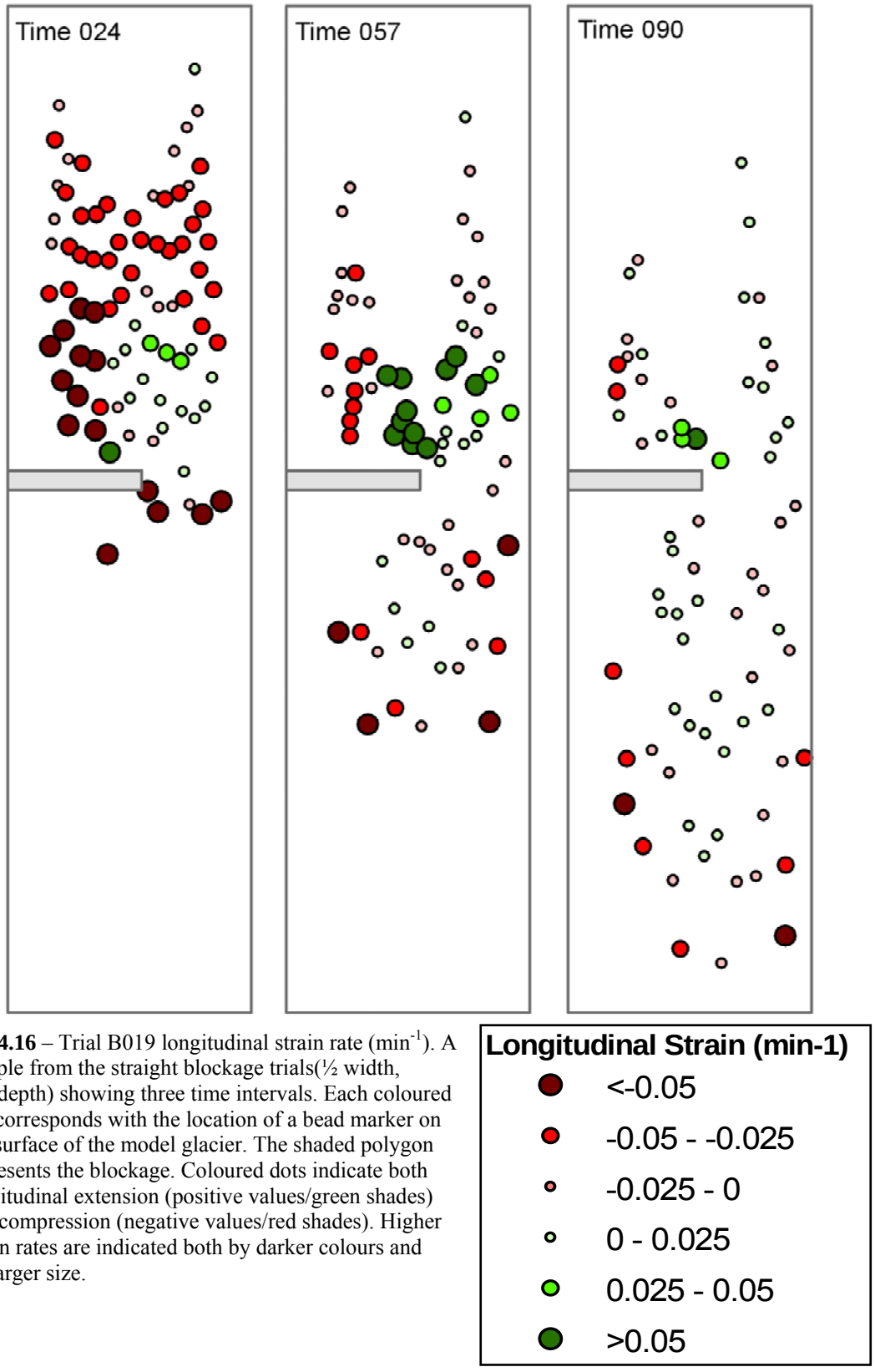

Fig 4.16 – Trial B019 longitudinal strain rate (min^{-1}). A sample from the straight blockage trials(½ width, full depth) showing three time intervals. Each coloured dot corresponds with the location of a bead marker on the surface of the model glacier. The shaded polygon represents the blockage. Coloured dots indicate both longitudinal extension (positive values/green shades) and compression (negative values/red shades). Higher strain rates are indicated both by darker colours and by larger size.

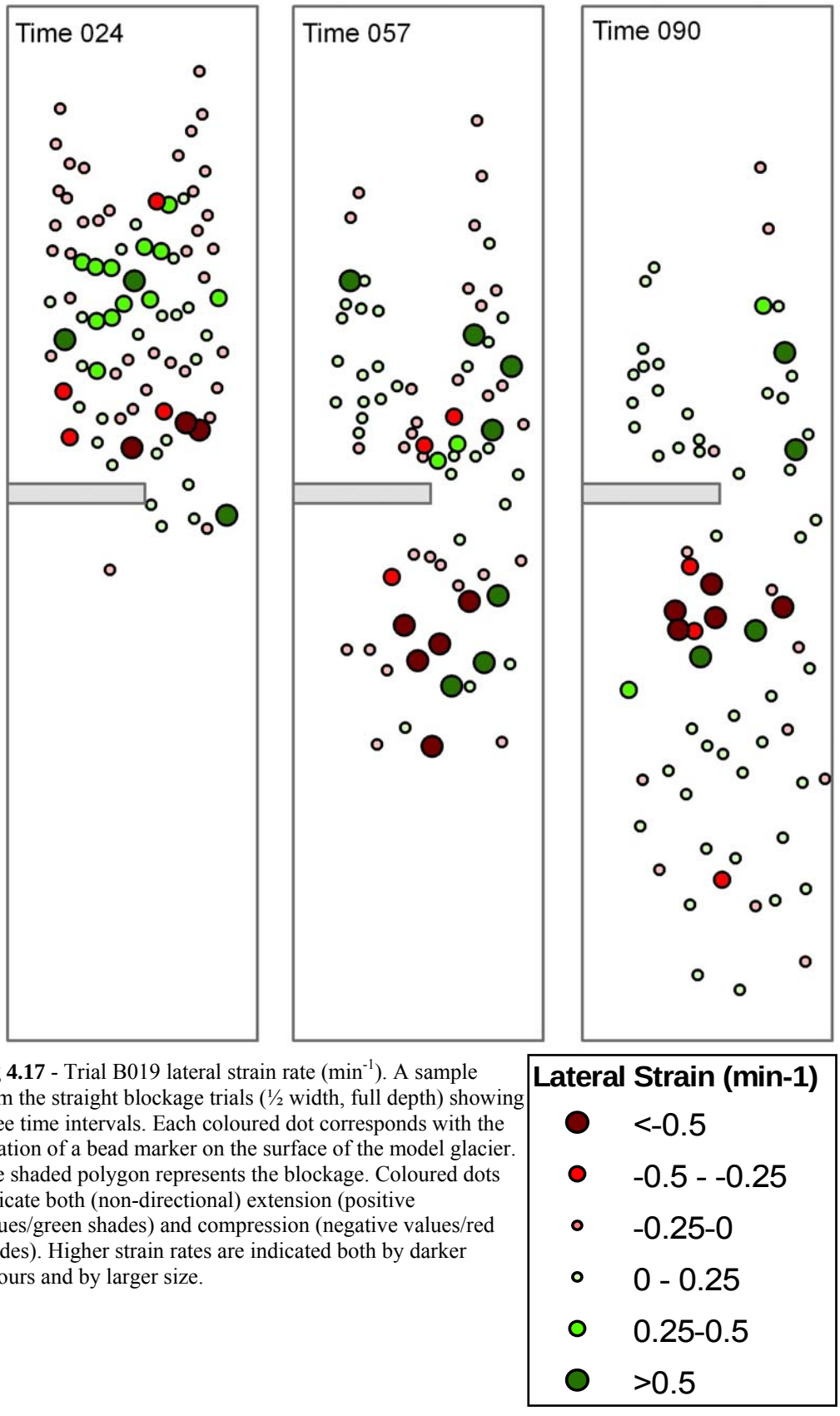

Fig 4.17 - Trial B019 lateral strain rate (min^{-1}). A sample from the straight blockage trials (½ width, full depth) showing three time intervals. Each coloured dot corresponds with the location of a bead marker on the surface of the model glacier. The shaded polygon represents the blockage. Coloured dots indicate both (non-directional) extension (positive values/green shades) and compression (negative values/red shades). Higher strain rates are indicated both by darker colours and by larger size.

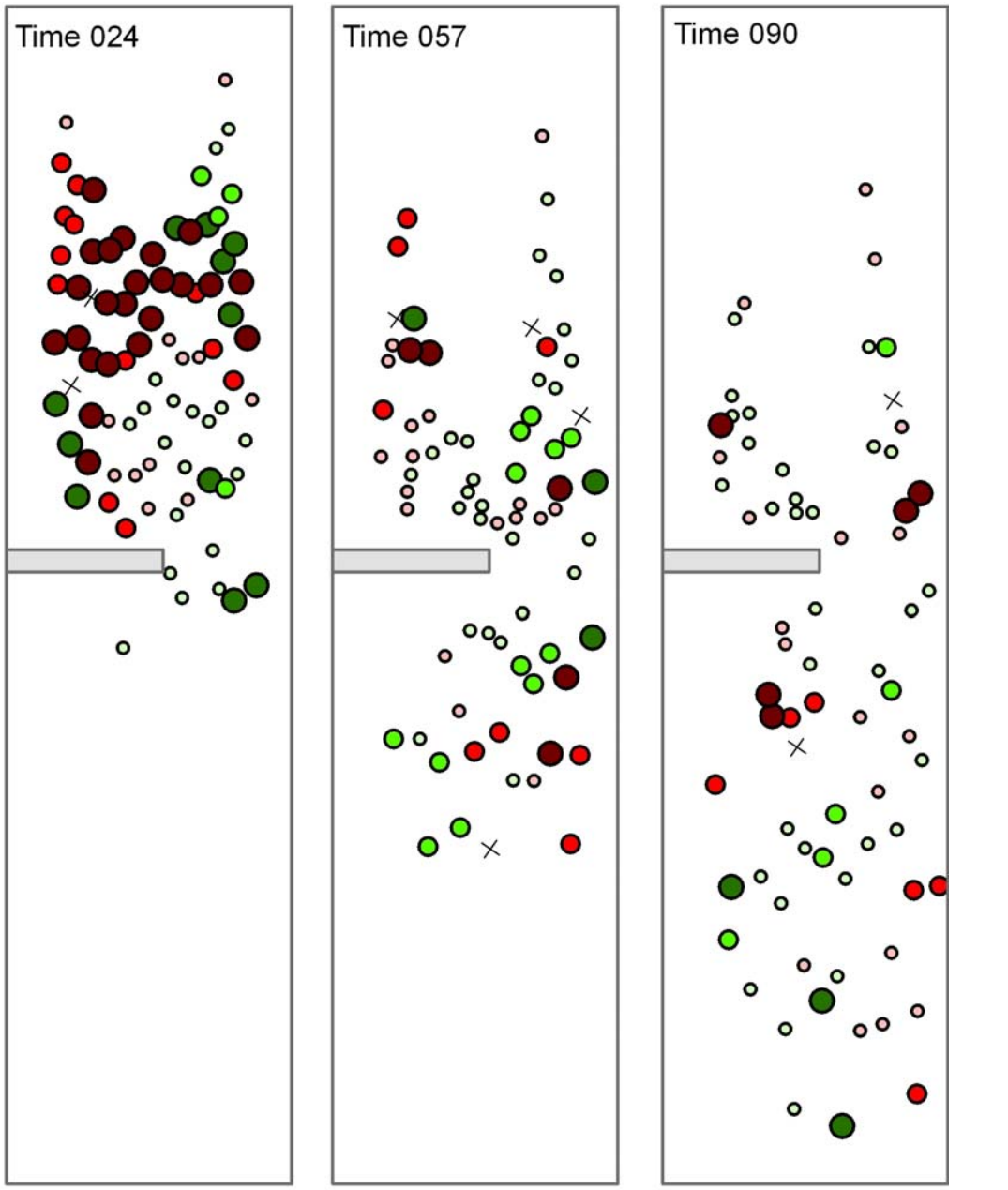

Fig 4.18 – Trial B19 shear strain rate (min^{-1}). A sample from the perpendicular blockage trials (½ width, full depth) showing three time intervals. Each coloured dot corresponds with the location of a bead marker on the surface of the model glacier. The shaded polygon represents the blockage. Coloured dots indicate both positive (green shades) and negative (red shades) shear strain rates. Higher strain rates are indicated both by darker colours and by larger size.

4.2.4 – Perpendicular Blockage, ¼ width and full depth (C Trials)

The C blockage is similar in structure to the B blockage; however, it blocks only ¼ of the width of the model valley and is therefore less deep as well. This blockage approximates the blocking potential created by a small bedrock protrusion or the potential blockage created at the confluence of a relatively small tributary glacier and/or one with a low activity ratio (see Kargel *et al*.'s (2005) classification in section 2.4) into a larger trunk glacier.

Longitudinal velocity patterns (Fig 4.19) - The longitudinal velocity patterns of the C trials are similar to those recorded in the unblocked trials. However, the C trial mapped here indicates higher velocities than those seen in the unblocked trial. Several bead markers in the centre flow-line return velocities higher than 2.5 cm min^{-1}. These high rates of velocity occur as these markers are passing the blockage, indicating that a blockage of this size and shape has little blocking effect on the longitudinal flow pattern of the analogue material in the model valley, but rather the narrowing of the valley causes acceleration through this area. Early in the trial there are only a few beads (upper transect, left marginal) that have longitudinal velocity rates of <0.5 cm min^{-1}. Throughout the remainder of the trial the overall longitudinal velocity decreases somewhat though continues to remain higher in the centre flow-line that at the margins. There is some indication in frame 057 and frame 090 of blocking of the analogue material occurring to bead markers in the left margin of the strain grid. The maps of frames 057 and 090 indicate a single bead returning low velocity rates (0 - 0.5 cm min^{-1}) sitting directly above the blockage on the left side of the valley. When the corresponding images are examined it is revealed that these are two different beads that get held up above the blockage in the

same place. They are not stationary behind the blockage but are significantly slowed down. After time 024 the greatest longitudinal velocity rates occur at the leading edge of the material where beads from the centre flow-line are beginning to fold under. The pattern of longitudinal velocity for the C trials does not change substantially throughout the trial.

Lateral velocity patterns (Fig 4.20) - Above the blockage, in the upper transects, the marker beads move directionally towards the centre flow-line in a pattern very similar to the unblocked trials. Low rates of lateral velocity are returned in both the left (-0.1 - 0 cm min^{-1}) and the right (0 - 0.1 cm min^{-1}) in the upper valley. Markers directly adjacent to the blockage indicate flow to the left as they pass the blockage while those on the opposite side of the valley flow right with a similar speed. The lowest rows of beads indicate higher rates (>0.2 cm min^{-1}) of flow to the right at the margin of the material. The majority of markers below the blockage in frame 057 indicate movement to the left of the valley, except those few at the right leading edge of the material. Directly above the blockage the material continues to flow to the right at a relatively high rate (0.1 - 0.2 cm min^{-1}). Directly below the blockage the material is also subject to high lateral velocity rates (-0.2 - -0.1 cm min^{-1}) as it flows around the blockage into the area below it. These two areas indicate similar lateral velocity rates throughout the entire trial though fewer markers experience higher rates in the later time frame. From these lateral velocities it appears that the C blockage might have some significant blocking effect, which did not transpire from the longitudinal velocity data.

Longitudinal strain rate patterns (Fig 4.21) - In the early frames of the trial the longitudinal compression occurs at low rates (-0.025 - 0 cm min^{-1}) in the upper transects

of the strain grid. Higher rates of compressive strain (up to <-0.05 min^{-1}) occur on either side of the leading edge of the analogue material, and just upstream of the blockage in frame 024. Low rates of extension (0 - 0.025 min^{-1}) occur in the centre flow-line of the material. This area continues to experience low tensional strain rates throughout the trial. Overall, longitudinal strain rate patterns are very similar to those in the unblocked trial (E).

Lateral strain rate patterns (Fig 4.22) - The majority of the strain grid in the C trials experience low rates of compressive lateral strain rates (-0.25 - 0 min^{-1}) though there are a few points in the centre flow-line that experience slightly higher rates of -0.5 - -0.25 min^{-1}. Tensional strain is recorded along the left margin of the strain grid as bead markers pass the blockage, the majority of these beads experience extensional strain of 0.25 – 0.5 min^{-1} though a few indicate rates >0.5 min^{-1}. Both compressive and extensional lateral strain rates that occur later in the trial are largely within +/- 0.25 min^{-1}.

Shear strain rate patterns (Fig 4.23) - Low shear strain rates occur in the centre of the strain grid while higher shear strain rates of both positive and negative values occur near the margins with the exclusion of the extreme upper margins where low negative shear strain rates occur on the left (-0.1 - 0 min^{-1}) and on the right where low positive shear strain rates occur (0 - 0.1 min^{-1}). As the analogue material flows through the constriction it is subject to moderate rates of positive shear strain rate (0.1 - 0.2 min^{-1}) on the blockage side and negative shear strain rates of <-0.2 min^{-1} on the unblocked side of the valley. This pattern persists throughout the trial though does so at a reduced magnitude.

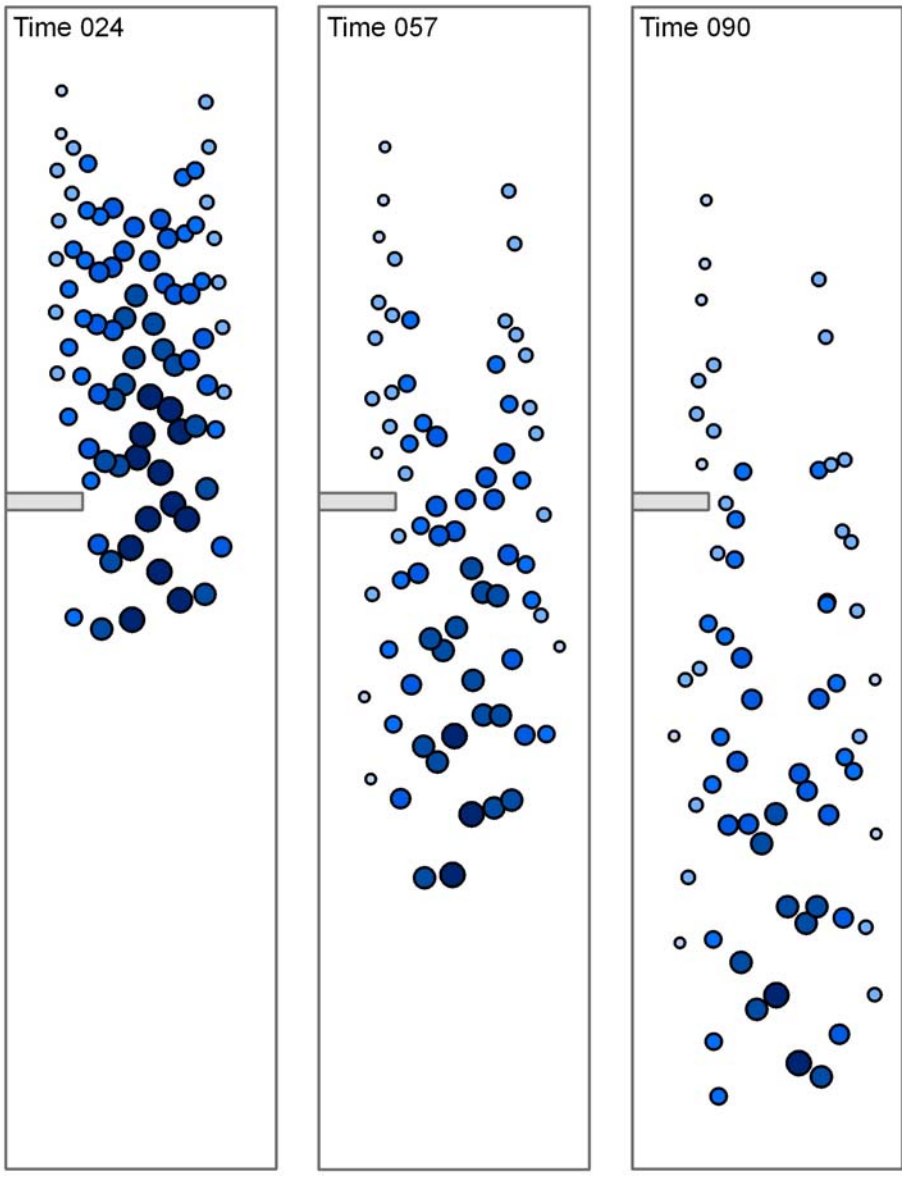

Fig 4.19 – Trial C25 longitudinal velocity (cm min^{-1}). A sample from the perpendicular blockage trials (1/4 width, full depth) showing three time intervals. Each coloured dot corresponds with the location of a bead marker on the surface of the model glacier. The shaded polygon represents the blockage. Higher velocities are indicated by darker colours and larger markers.

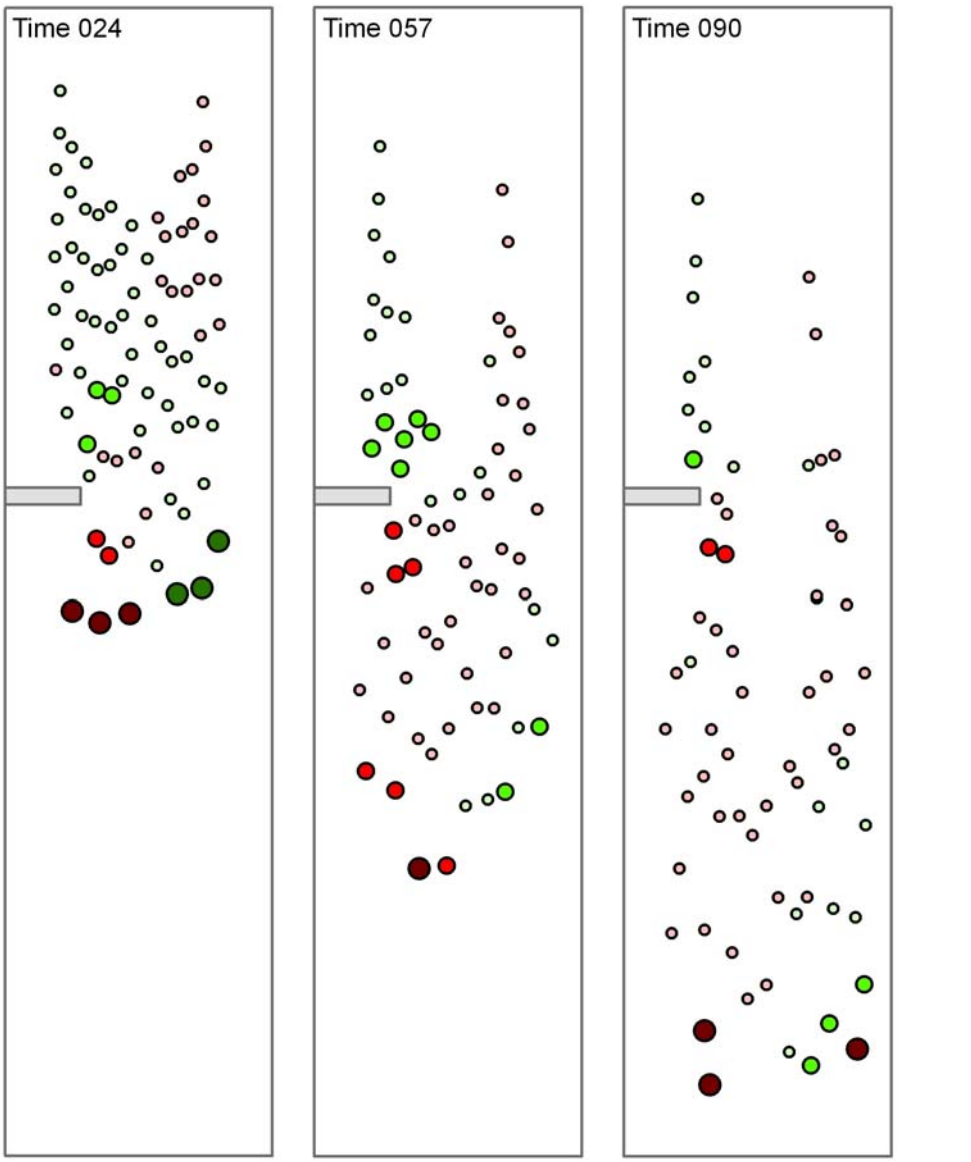

Fig 4.20 – Trial C25 lateral velocity (cm min^{-1}). A sample from the perpendicular blockage trials (1/4 width, full depth) showing three time intervals. Each coloured dot corresponds with the location of a bead marker on the surface of the model glacier. The shaded polygon represents the blockage. Lateral velocity occurs in two directions; to the right (positive values/green shades) and to the left (negative values/red shades). Higher velocities in either direction are indicated by darker colours and larger symbols.

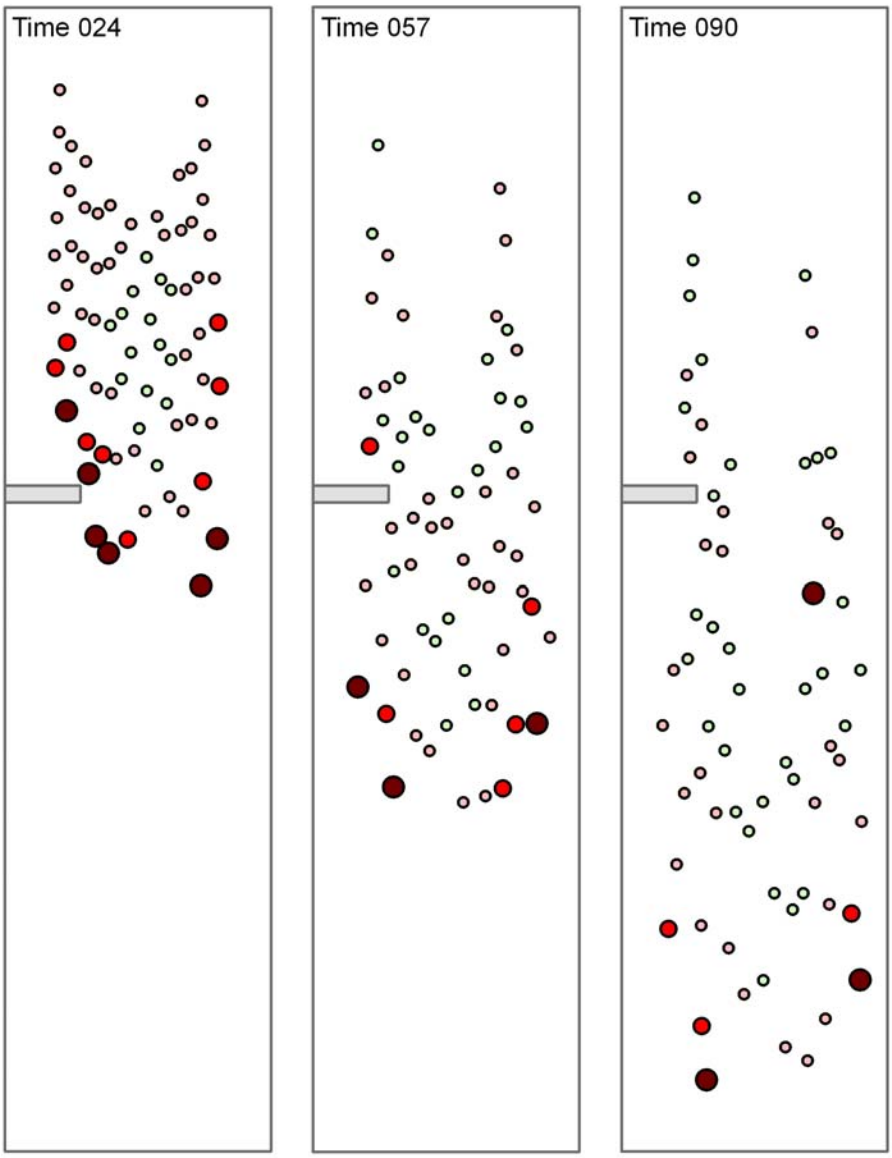

Fig 4.21 – Trial C25 longitudinal strain rate (min^{-1}). A sample from the perpendicular blockage trials (1/4 width, full depth) showing three time intervals. Each coloured dot corresponds with the location of a bead marker on the surface of the model glacier. The shaded polygon represents the blockage. Coloured dots indicate both longitudinal extension (positive values/green shades) and compression (negative values/red shades). Higher strain rates are indicated by darker colours and larger symbols.

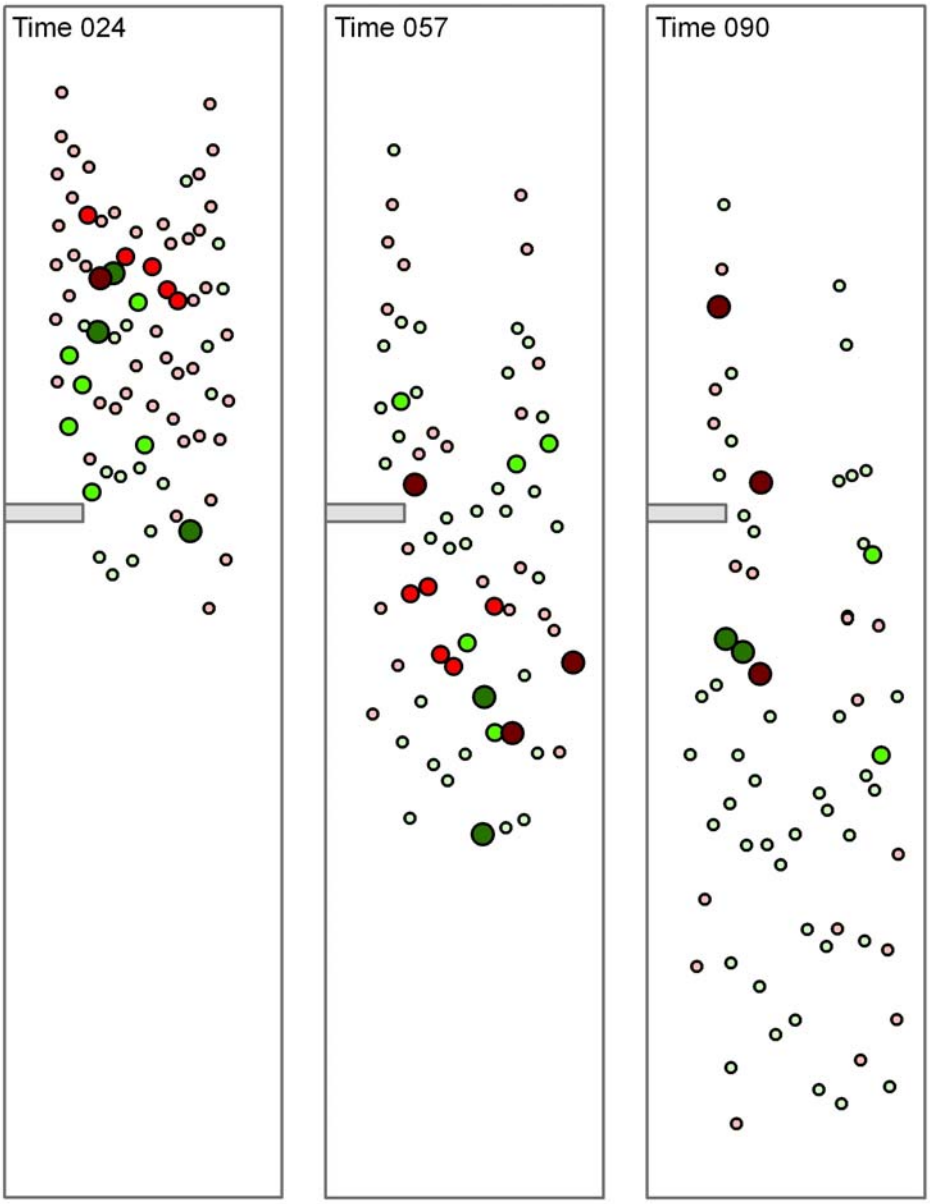

Fig 4.22 – Trial C25 lateral strain rate (min^{-1}). A sample from the perpendicular blockage trials (1/4 width, full depth) showing three time intervals. Each coloured dot corresponds with the location of a bead marker on the surface of the model glacier. The shaded polygon represents the blockage. Coloured dots indicate non-directional extension (positive values/green shades) and compression (negative values/red shades). Higher strain rates are indicated both by darker colours and larger symbols.

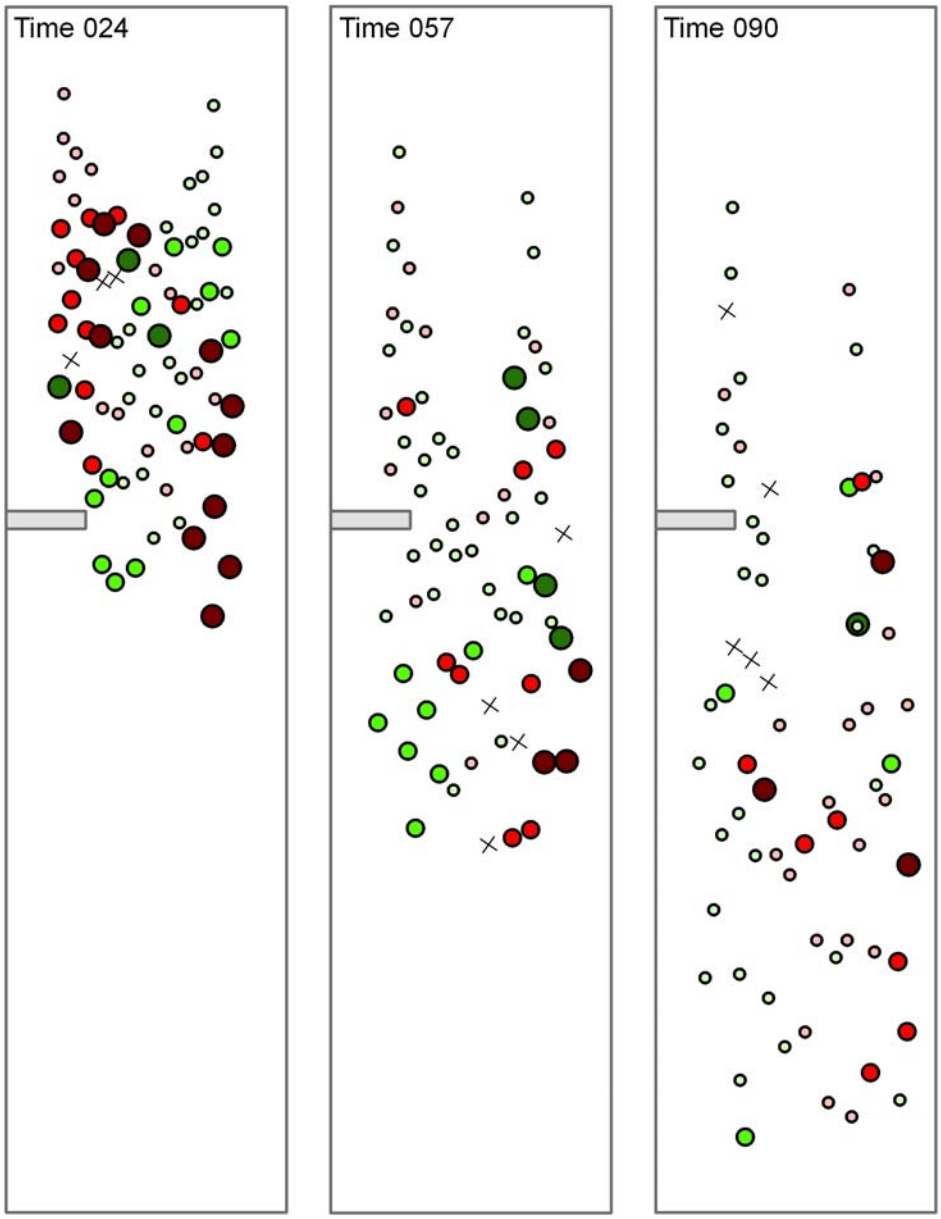

Fig 4.23 – Trial C25 shear strain rate (min^{-1}). A sample from the perpendicular blockage trials (1/4 width, full depth) showing three time intervals. Each coloured dot corresponds with the location of a bead marker on the surface of the model glacier. The shaded polygon represents the blockage. Coloured dots indicate both positive (green shades) and negative (red shades) shear strain rates. Higher strain rates are indicated both by darker colours and by larger size.

4.2.5 – Perpendicular Blockage, ½ width and ½ depth (D Trials)

The D blockage obstructs half the width and half the depth of the valley. This blockage differs from the others because it allowed the material to flow underneath it, which creates a difficulty comparing this trial to the other trials, as no beads were able to move under the blockage (but were held against the upstream side of the blockage) while some of its underlying material continued to move. Flow in this experiment indicated several differences in the behaviour of the material around the blockage; however, there is no published glaciological comparison for this trial. It could be suggested that this blockage recreates the potential obstruction by a tributary glacier with a basal depth substantially less than that of the trunk glacier that it flows into or that is entering from a hanging valley and pushing its terminus with a loop-shaped moraine into its trunk (see e.g. Scheelebreen in Jiskoot *et al*. (2000)).

Longitudinal velocity patterns (Fig 4.24) - Throughout the trial the longitudinal velocity above the blockage is higher at the centre flow-line (1.5 - 2 cm min^{-1}) than at both the left (0 - 0.5 cm min^{-1}) and the right (0.5 - 1 cm min^{-1}) margins, indicating near-normal parabolic flow such as in Trials E at time 057. The longitudinal velocity of the beads above the blockage is lower than those that are flowing through or below the constriction. Below the blockage lower longitudinal velocities are found only at the right valley wall. In the centre of the valley the material that is forced around the blockage flows confluent with the material that flowed under the blockage and thus is not slowed by contact with the valley wall. However, the analogue material that flowed under the blockage does not have any strain markers on it and so no data is available to compare its flow rate to that which flowed around the blockage. The analogue material that flowed around the

blockage has longitudinal velocities between 1 - 2.5 cm min^{-1} for the remainder of the trial.

Lateral velocity patterns (Fig 4.25) - Most markers in this trial indicate low rates of lateral velocity to either the right (0 - 0.1 cm min^{-1}) or the left (-0.1 - 0 cm min^{-1}). Overall, the lateral velocities in this trial are lower than those in trial B. Above the blockage the lateral velocity pattern is similar to that in the blockage B trials. The majority of the lateral flow occurs at low speed and to the right (0 - 0.1 cm min^{-1}). The same small group of markers that indicated low rates of lateral flow to the left in the blockage B trials also do so in the D trials (-0.1 - 0 cm min^{-1}). There are also similar right lateral flow patterns in blockages B and D as the material flows through the constriction. However, below the blockage the lateral flow rates are different, with a much higher left-lateral flow in blockage B than in blockage D. Because the D blockage allows the analogue material to flow beneath it as well as around while the geometry of the B blockage forces all the material to flow to the right around the obstruction. In D, there is no empty space below the blockage that the material experiences sudden, left lateral displacement into.

Longitudinal strain rate patterns (Fig 4.26) - In frame 024, longitudinal strain rates above the blockage are highly compressive (up to a valley width above the blockage, but decrease further upstream. Directly above the blockage the analogue material is subject to the highest longitudinal strain rates (<-0.05 min^{-1}). Lower rates occur in the strain markers higher in the valley (-0.05 - 0.025 min^{-1}) and the lowest occur above those in the upper transects (-0.025 - 0 min^{-1}). Because the analogue material is flowing confluent with its left side flow unit that moved under the blockage, there are very low rates of

longitudinal tensile strain occurring. The marginal beads adjacent to the right valley wall indicate an area of compression (-0.05 - -0.025 cm min^{-1}) while those marker beads flowing in the centre of the valley indicate low rates of extension (0 - 0.025 cm min^{-1}), which are normal for centres of confluence (e.g. Gudmundsson *et al*., 1997).

Lateral strain rate patterns (Fig 4.27) - Lateral strain behaviour early in the D trials is similar to that indicated in the B trials. Marker beads in the D trial indicate a band of low rates of compressive strain above the constriction similar in location and magnitude to that which occurs in the B blockage trials. Also similar is the zone of low rates of extension (0 - 0.25 min^{-1}) that occurs in bead markers flowing through the constriction. Below the blockage in frame 057 the lateral strain rate indicates compression up to rates <-0.5 min^{-1}.

Shear strain rate patterns (Fig 4.28) - Early in the trial the shear strain rates indicate equal magnitudes of both negative (<-0.2 min^{-1}) and positive (>0.2 min^{-1}) shear strain values. The region above the constriction and extending well into the centre and upper left margin of the strain grid indicates a varying range of negative shear strain rates. Directly above the blockage several bead markers return shear strain rates of >0.2 min^{-1}; this magnitude of positive shear strain is seen in the upper right region of the valley. The majority of both positive and negative recorded shear strain rates at the end of the trial are within -0.1 - 0.1 min^{-1} with a few scattered bead markers indicating areas of high shear strain such as those seen above the blockage (frame 090) which indicate a value of >0.2 min^{-1}.

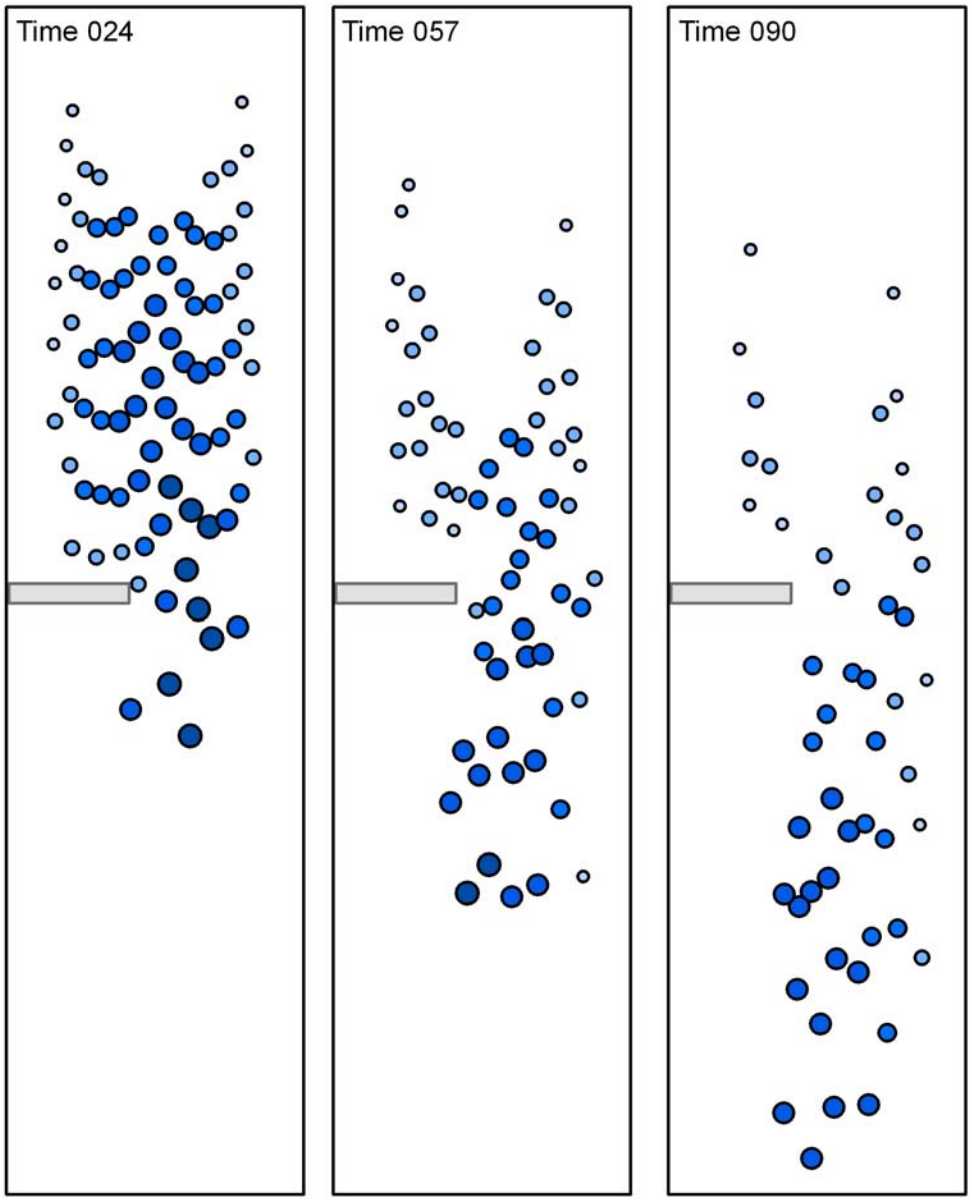

Fig 4.24 – Trial D31 longitudinal velocity (cm min^{-1}). A sample from the perpendicular blockage trials (½ width, ½ depth) showing three time intervals. Each coloured dot corresponds with the location of a bead marker on the surface of the model glacier. The shaded polygon represents the blockage. Higher velocities are indicated by darker colours and larger symbols.

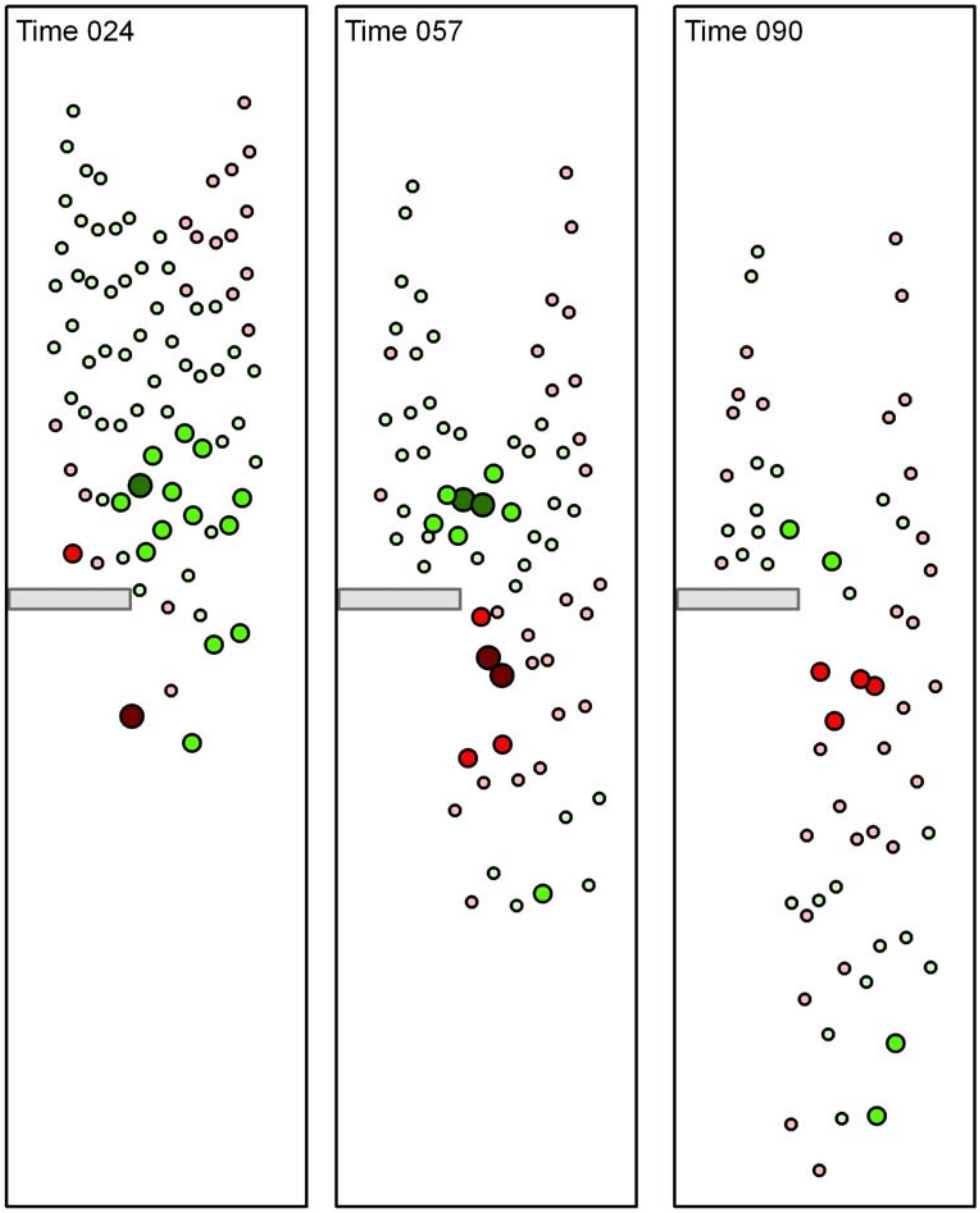

Fig 4.25 – Trial D31 lateral velocity (cm min^{-1}). A sample from the perpendicular blockage trials (½ width, ½ depth) showing three time intervals. Each coloured dot corresponds with the location of a bead marker on the surface of the model glacier. Lateral velocity occurs in two directions; to the right (positive values/green shades) and to the left (negative values/red shades). Higher velocities in either direction are indicated by darker colours and larger symbols.

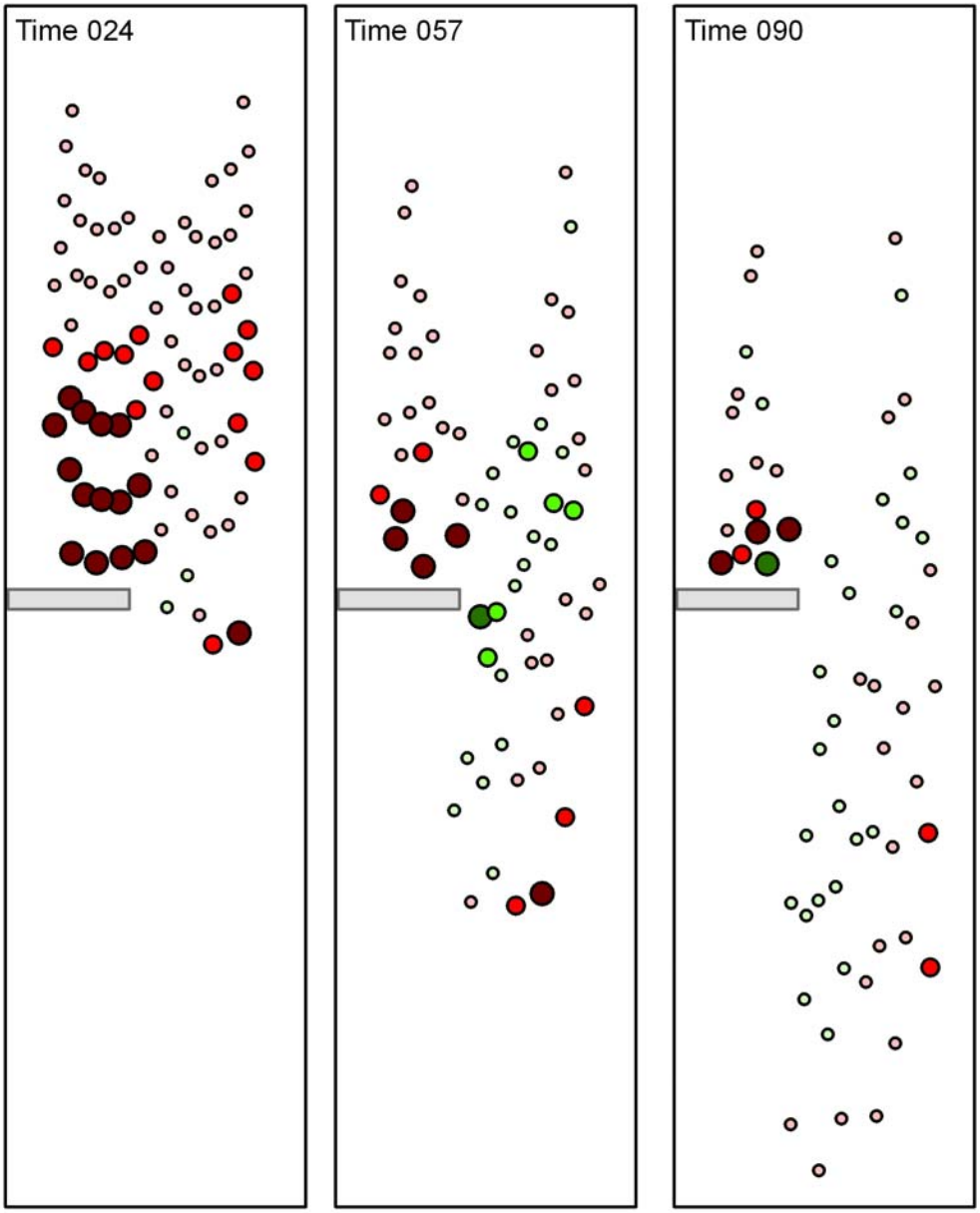

Fig 4.26 – Trial D31 longitudinal strain rate (min^{-1}). A sample from the perpendicular blockage trials (1/2 width, 1/2 depth) showing three time intervals. Each coloured dot corresponds with the location of a bead marker on the surface of the model glacier. The shaded polygon represents the blockage. Coloured dots indicate both longitudinal extension (positive values/green shades) and compression (negative values/red shades). Higher strain rates are indicated both by darker colours and larger symbols.

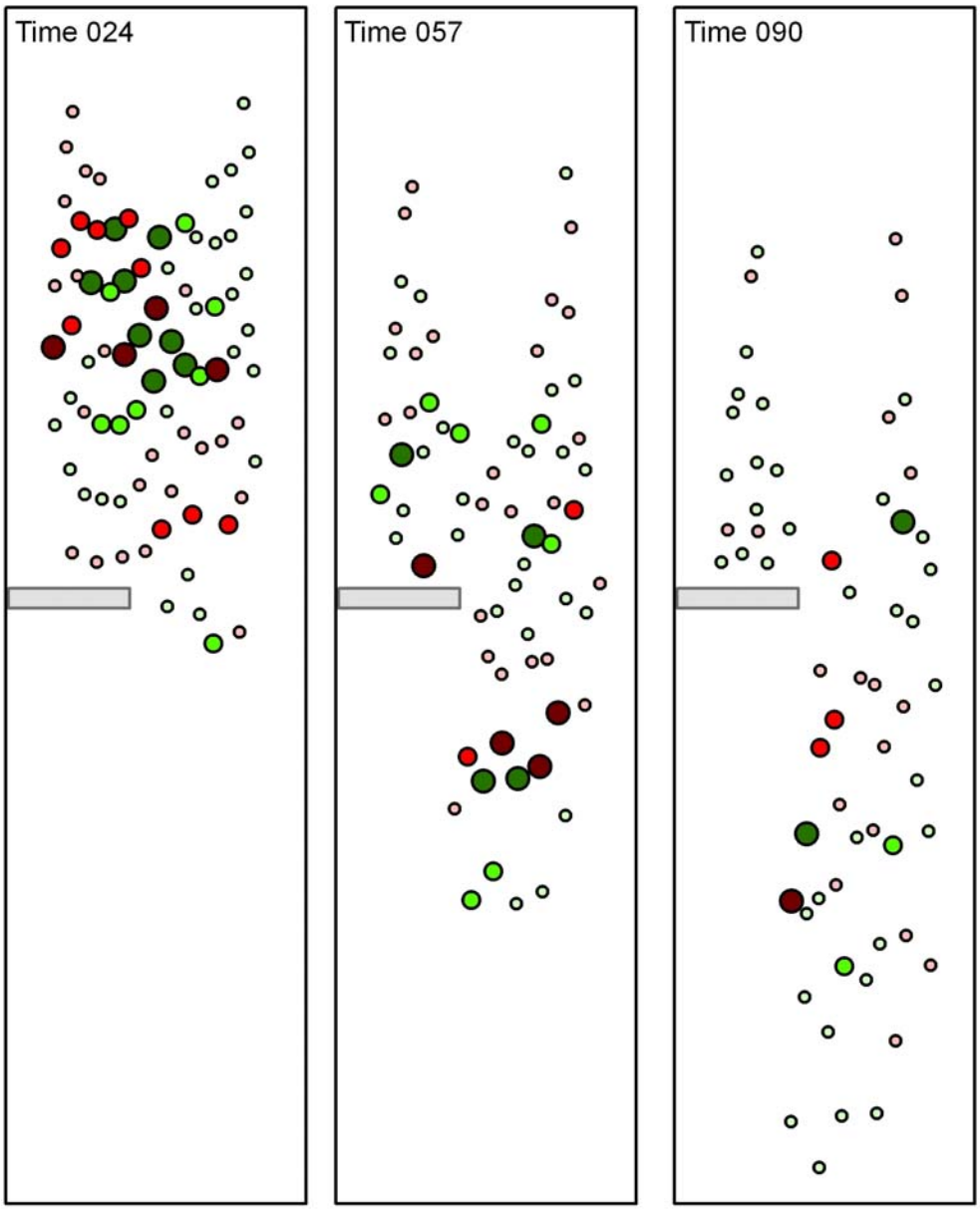

Fig 4.27 – Trial D31 lateral strain rate (min^{-1}). A sample from the perpendicular blockage trials (1/2 width, 1/2 depth) showing three time intervals. Each coloured dot corresponds with the location of a bead marker on the surface of the model glacier. The shaded polygon represents the blockage. Coloured dots indicate non-directional extension (positive values/green shades) and compression (negative values/red shades). Higher strain rates are indicated both by darker colours and larger symbols.

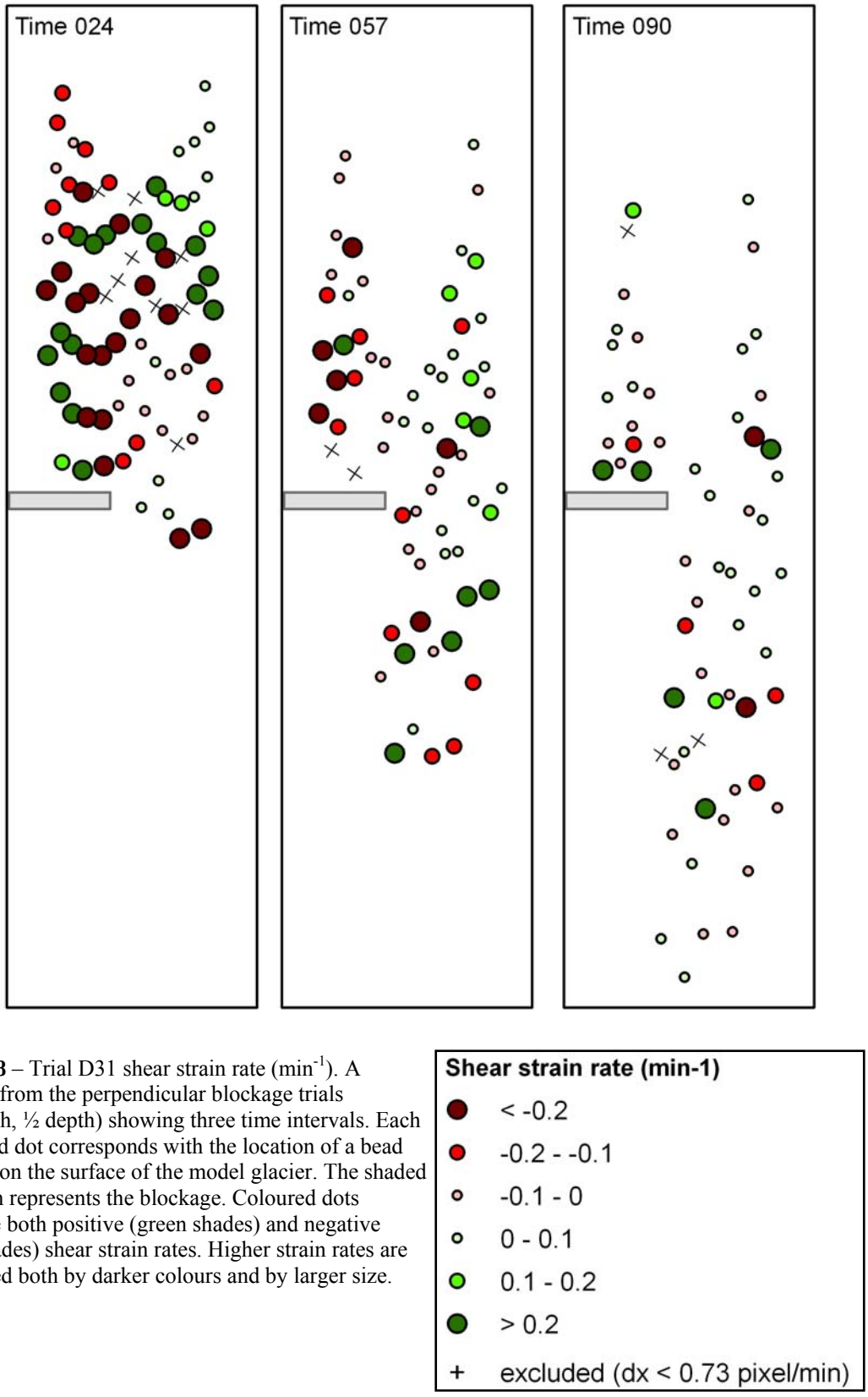

Fig 4.28 – Trial D31 shear strain rate (min^{-1}). A sample from the perpendicular blockage trials (½ width, ½ depth) showing three time intervals. Each coloured dot corresponds with the location of a bead marker on the surface of the model glacier. The shaded polygon represents the blockage. Coloured dots indicate both positive (green shades) and negative (red shades) shear strain rates. Higher strain rates are indicated both by darker colours and by larger size.

4.3 - Statistical Analysis

Mean velocities and standard deviations were calculated for each individual bead in the experiments by taking the arithmetic mean of the 10 repeat runs of each trial. Only 9 runs were used to calculate the means of trial A frame 024 and trial D frame 057, as one run in these trials returned erroneous data because of missing images due to camera errors. These results were plotted to provide an overall comparison of the effects of each blockage on the analogue material at frames 024 and 057. Figures 4.29 and 4.30 are the plotted results of the mean velocities for the five trials in both the longitudinal and lateral directions in frames 024 and 057.

The standard deviation of the means is plotted in the longitudinal velocity graphs as error bars. The relatively small error bars indicate that the velocity for individual beads does not vary significantly between the ten runs. Standard deviation for the lateral velocity is considerably larger and the bars are omitted from Figure 30 for clarity. Gaps in the graphs indicate missing beads that were folded under the leading edge in all 10 runs of a trial.

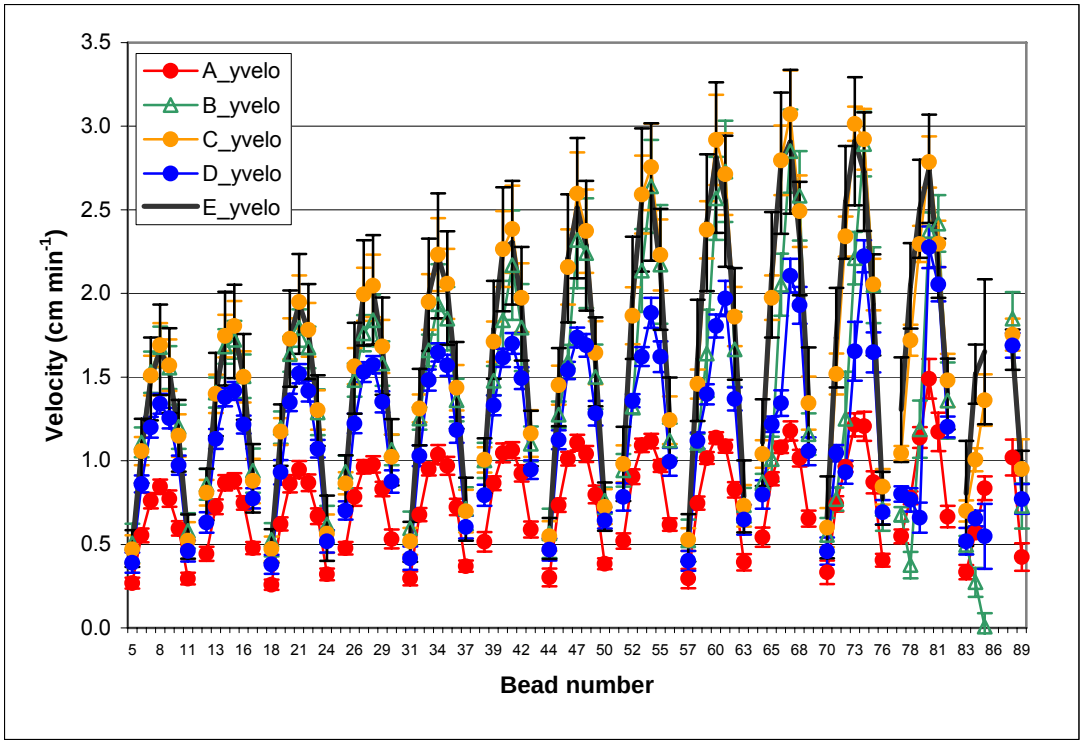

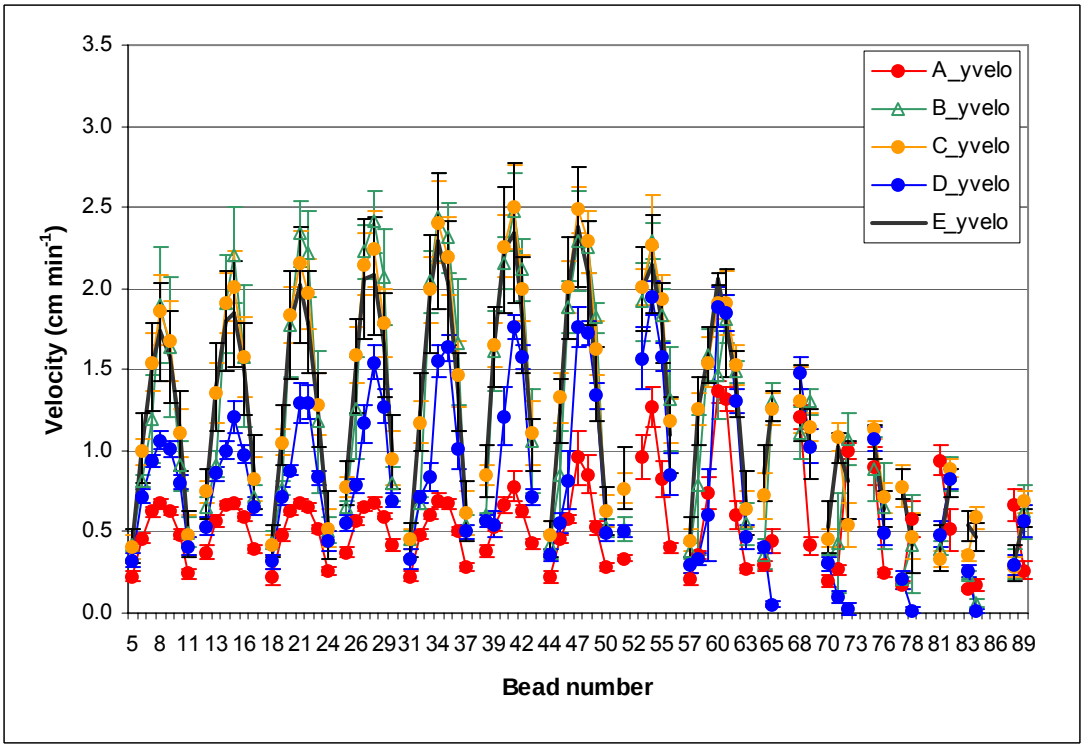

Fig 4.29 – Mean longitudinal velocity for each of the five blockage experiments in frames 024 (A) and 057 (B). Each parabola corresponds with a transect in the surface strain grid and each ID number is a unique marker point.

The mean velocity graphs display several key elements of the results of these blockage experiments.

1. The angled blockage (A) consistently has the lowest longitudinal velocities of the five trials implying that this obstruction is the most effective at blocking flow in the valley. The D blockage has the next lowest mean longitudinal velocity while the remaining blockages (B, C and E) are quite similar.
2. The plotted lateral velocity means indicate the point in the strain grid where each individual marker bead contacts the blockage. Unlike the longitudinal velocity, the lateral velocity plots both magnitude and direction of flow and thus indicates the time at which certain beads are moving around the blockage. In frame 024 the upper plotted transect's diagonal lines with positive values left of the centreline and negative values right of the centre line indicate that beads are moving towards the centreline as the material flows. As the beads encounter the blockage they return spikes in the lateral velocity, indicating their sudden lateral displacement as they flow around the obstructions.
3. These spikes in lateral velocity also indicate the distance up valley from the blockage that is affected by the obstruction. In frame 024 (Fig 4.30A) this lateral adjustment occurs lower in the strain grid in blockage B than in the other trials. The top 3 rows in Trial B appear unaffected, but the 5^{th} row has high positive values, indicating a fast right lateral movement around the blockage. Likewise, the B trials also have the highest left lateral velocities (-), indicating fast left lateral flow below the blockage.

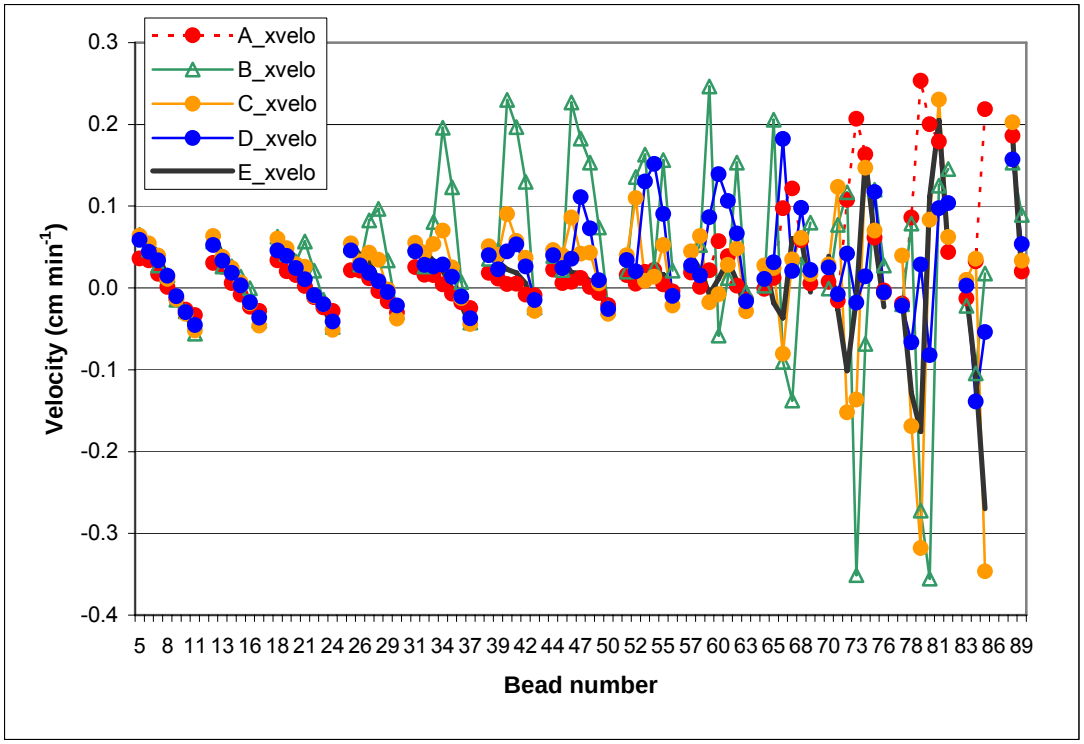

A

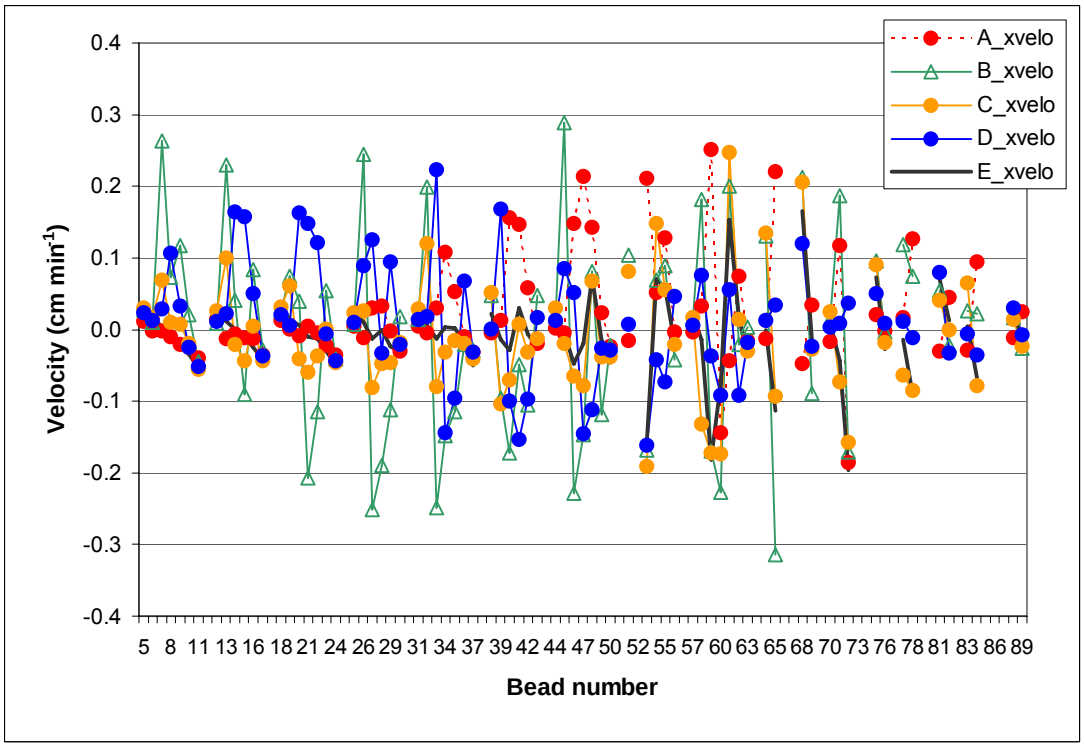

B

Fig 4.30 – Mean lateral velocity for each of the five blockage experiments in frames 024 (A) and 057 (B). Breaks in the line divide the transects in the surface strain grid and each ID number is a unique marker point.

The overall means and standard deviations for the 10 runs of the total velocity of each of the five blockages (A - E), can be seen in Table 4.2. The A blockage has the lowest total velocity throughout the trial, followed by D with a slightly higher velocity. Blockages B, D and unblocked trial E are very similar, but the B blockage has the lowest total velocity in frame 024, 0.20 cm min^{-1} lower than blockage C and the unblocked E. However, in frames 057 and 090 the difference in total velocity rates between trials B, C and E decreases substantially to only 0.07 cm min^{-1}. The differences in flow velocity between the B, D and E trials are smaller than the standard deviation indicating that the overall velocities are statistically similar.

Table 4.2 – Mean and Standard Deviations for total velocity found in the five blockage trials

Total Velocity (cm min^{-1})						
	Frame 24		Frame 57		Frame 90	
TRIAL	mean	stdev	mean	stdev	mean	Stdev
A	0.7681	0.2832	0.5539	0.2777	0.5850	0.2471
B	1.4122	0.6580	1.2208	0.7142	1.1820	0.6672
C	1.6186	0.7058	1.2958	0.6466	1.2905	0.6724
D	1.1800	0.4778	0.8459	0.5104	0.8219	0.5001
E	1.6254	0.6756	1.2568	0.5956	1.1003	0.5472

Visual interpretation of the mean velocity graphs and interpretation of the data in Table 4.2 suggest that Trial A has the lowest overall velocities, followed by Trial D, and that there are no significant differences between the mean velocities of Trials B, C and E. In order to statistically test these suggested differences using an analysis of variance test (ANOVA), the mean longitudinal and lateral velocity data (lines plotted in Figures 4.29 and 4.30) were initially tested for normality through a Kolmogorov-Smirnov normality test, P-P plots and histograms. Statistically significant normal distribution was found only in the longitudinal velocity data for the trials in frame 024, however, plots of the remaining longitudinal velocity data did not return results that necessitate the downgrading of the data and the use of the non-parametric Kruskal-Wallis test (McGrew

and Monroe, 2000), though this K-W test was nevertheless run as a comparison for and a companion to the ANOVA results (Table 4.3). Further, Levene's test of homogeneity of variance indicates that all variances are homogeneous, and it appears that ANOVA is quite robust, even for non-normally distributed data (e.g. Sokal and Rohlf, 1995). The ANOVA test statistics indicate that for time 024 (24_xvelo) there are no statistically significant differences between the lateral velocities of the trials (at α=0.05), but there are for the longitudinal velocities. Table 4.3 shows a highly significantly (sign=0.000) larger mean square of variance between the groups than within the groups, and F values that are higher than the critical F. In frames 057 and 090 the results are similar to those seen in frame 024; there is little variation in lateral velocity between the different blockages but the variation in longitudinal velocity is significant.

In order to unravel which of the trials is significantly different from the others, a Tukey Post Hoc test (Appendix IV) was also carried out using these data. The results of this Post Hoc analysis indicate that the A blockage was significantly different from the other blockages results in frames 024 and 057. It also indicates that the D blockage was significantly different from all blockages except B for the same frames. Nonparametric Kruskal-Wallis tests were done on the same datasets, and returned the same statistically significant differences, suggesting that the ANOVA test results are indeed robust, even though the data were not all completely normally distributed. The results from these statistical tests correspond with the groupings of trials as visually interpreted from figures 4.29 and 4.30.

TABLE 4.3 – Results from ANOVA test of lateral and longitudinal velocity for each of the five blockages in frames 024, 057 and 090.

		Sum of Squares	df	Mean Square	F	Sig.
24_xvelo	Between Groups	.037	4	.009	1.633	.165
	Within Groups	2.353	410	.006		
	Total	2.390	414			
24_yvelo	Between Groups	42.721	4	10.680	31.495	.000
	Within Groups	139.036	410	.339		
	Total	181.757	414			

		Sum of Squares	df	Mean Square	F	Sig.
57_xvelo	Between Groups	.058	4	.015	1.926	.105
	Within Groups	2.806	370	.008		
	Total	2.864	374			
57_yvelo	Between Groups	31.399	4	7.850	24.185	.000
	Within Groups	120.090	370	.325		
	Total	151.489	374			

		Sum of Squares	df	Mean Square	F	Sig.
90_xvelo	Between Groups	.072	4	.018	2.107	.080
	Within Groups	2.608	305	.009		
	Total	2.680	309			
90_yvelo	Between Groups	13.781	4	3.445	12.329	.000
	Within Groups	85.233	305	.279		
	Total	99.014	309			

4.4 – Errors and Problems

Problems encountered in the execution of this experiment are discussed in this section, as are the errors and discrepancies that were accounted for or acknowledged.

4.4.1 – Weight Discrepancies

As stated in Chapter 3, the material was weighed before and after each trial. This practice revealed a reduction in the weight of material with each trial run, with an average of about 16 grams or 0.5% of the original weight (Appendix II)**.** In order to attempt to isolate the cause of this loss a small amount of the material was placed in a separate,

unsealed container and left over night in the storage container with the rest of the material. There was no recordable change in the weight of the isolated material. It was assumed that the loss seen during the trial runs was a result of dehydration of the material during its exposure in each trial. As a result of this loss of water, the flow properties of the material may not remain consistent. It was believed that the amount of mass lost was small enough to not significantly affect the outcome of the experiments. Since the standard deviations shown in figures 4.29 and 4.30 are quite small, this weight loss is not expected to have had a significant effect on the overall viscosity or rheological properties of the material. Some discrepancy in pre- and post-trial weight may also be attributed to the post-trial weighing process. The exact error in this aspect is not known, but the scale itself is limited to an accuracy of 1 g. A simple test of the scale was carried out in order to eliminate it as the source of the weight discrepancy. The amount of material used in an average trial was weighed in 500 g increments to a total of 3500 g as it was when filling the reservoir in each of the experiments. The same 3500 g of material was then immediately weighed as a total mass. This indicated no variation in weight leading to the acceptance of the loss as a result of air exposure of the material during the trials rather than a cumulative error occurring as a result of measuring the material in increments of 500 g.

4.4.2 - Accuracy in Recreating Glacial Flow

Unlike a real glacier, where the accumulation of snow regularly replenishes the ‘natural glacier reservoir’, the ice analogue material used in the experiment tends to thin out as it flows. However, an addition of material would result in a ‘kinematic wave’ type flow rather than a recreation of regular surface accumulation (Stearns and Osterberg,

2003). A further major discrepancy between real glaciers and the model is that the analogue material flows completely coupled to the base and so there is no basal sliding or till deformation and the material tends to fold over itself as it 'flows' down the trough. This is easily seen in any sequence of frames from any of the trials. A similar problem was noted in experiments run by Shoemaker (1981) who used viscous malt (see section 2.3). Though the analogue material used was different, it was also subject to basal coupling and to folding under itself even when the base of the model was lubricated (Shoemaker, 1981).

4.4.3 - Inadequate Lab Conditions

Two issues can be included under this heading; both were a minor source of problems in this series of experiments.

a. Inadequate lab space: The experiment was not set to ideal specifications because of the rigid boundaries associated with lab bench space. Several changes had to be made to create a space large enough to set up the model. With the removal of several shelves and the addition of a section of lab bench the space issue was somewhat resolved though still limited. Ideally, access would have been from both sides of the model, with the camera mounted directly above the apparatus. This limitation did not appear to have affected the outcome of the experiments though may have introduced errors as a result of extra adjustments allowing for the camera angle.

b. Ventilation and Temperature Control: Because an outside group from a different department controls access to the thermostat, continuous temperature regulation is nearly impossible. The small space and the poor design of the lab resulted in

one of two AC/heating ventilation fans being placed directly above the experiment set up. This fan was covered and the draught reduced, but not eliminated, as the second fan was located approximately 1.5 m away and could not be blocked. These ventilation fans may be partially responsible for the loss of mass over the course of the trial at an average approximate rate of 0.3 grams per minute.

4.4.4 - Errors in the Digitization Process

Occasionally some images that corresponded with one of the ten selected frames would be out of focus. This was attributed to an unknown issue with the camera, as it appeared to be somewhat random and was not a result of any physical contact with the camera, tri-pod or lab bench. In the event of this occurring, the nearest clear frame was used. In trial B20 there are no data for frames 002 and 013 as these were found to be out of focus to an extent that rendered them unusable. Instead, data were collected from frames 003 and 014 respectively. This resulted in a time difference between the second and third frames of 30 seconds less than in other trails. This should result in no noticeable variation in the results, as the velocity calculations incorporate this time difference. In one instance several adjacent frames were also out of focus, and data for one frame in that trial was skipped entirely. This loss of frame data occurred only once: in trial A04 frame 035. This was not, however, an issue because this entire A04 trial had to be removed from the analysis entirely due to a separate problem with the camera.

Errors in manual digitization may have been added as a result of the high resolution of the digital images. Care was taken to digitize the points at the same location in each image. Each bead was considered a solid point and digitized by placing the cross of the

point tool directly in the centre of the bead, regardless of its orientation, for all frames. Unfortunately, the shape of the beads did not lend itself well to attempts at digitizing the same pixel on individual beads. The time lapse between frames that were digitized means that the amount of movement of each bead was almost always substantially greater than the size of the bead itself. However, this was not always the case in all points, as some beads, such as those located in the top right and left corners, had a tendency to move very little in the lateral direction after the initial phase of rapid flow and subsequent extension (see Chapter 4.1). This was particularly noticeable in flow trials with substantial blockages such as Blockages A and B.

In some of the blockage experiments there was very little movement of beads behind the blockages themselves. This was most noticeable in Blockage D, that which filled half the valley width and half the valley depth. Here, beads had a tendency to remain relatively stationary in locations both directly above and directly below the blockage. These bead markers returned unsound data (i.e. the lateral strain rates and shear strain rates equations had zeros in the denominator) and these were removed before analysis.

Finally, the digitization process is subject to human error. In the review of the data several instances were found where the same point had been erroneously digitized twice and in one case 59 of 89 points were missing entirely. These missing or repeating data were checked against original images and re-digitized and the corresponding XY coordinates entered manually in the analysis coding when possible.

4.5 - Error Analysis

From a repeat exercise in which two top rows of the strain grid in an image were digitized 5 times over, and the range of x and y positions were calculated, it transpired that the average human error in the digitizing process amounts to about 3 pixels in the x and y directions. Further, a limitation of the algorithm calculating the grid rotation adjustment in the data analysis spreadsheet (see section 3.4.2) results in a maximum error of 2.7 pixels in the x direction, and 0.4 pixels in the y direction (for a bead travelling from the far left or far right to the centre). The sum of these errors, using normal error analysis techniques whereby the total error is the square root of the sum of each of the error components squared (Squires, 1976), is 4.04 pixels in the x direction and 3.03 pixels in the y direction. Since the frames are digitized every 5.5 minutes, this error can be expressed as 0.73 pixels min^{-1} in the x direction, and 0.55 pixels min^{-1} for the y direction. Since y displacements are always much larger (mostly at least ten times larger) than this error, no unusual results will be the output of strain rate calculations (which have the ∂y and ∂x in their denominator). However, displacement in the x direction falls more often within this error margin. Therefore, all pixels having displacements in the x direction of less than 0.73 pixel min^{-1} were omitted from the shear strain rate maps. However, these data points were not omitted from the lateral strain rate maps, as, even though these points have large errors, it was deemed important to still show the general patterns. However, detailed treatment of these points with potential large errors was not given, as only general patterns were described.

4.6 - Summary of the Model Results

Each blockage was subject to ten experimental trials in the model valley. A single trial was selected to represent the behaviour of the analogue material in the experiments for each blockage and the results from each of these five distinct trials presented in this chapter.

Analysis of the analogue model flow patterns indicates that:

1) Longitudinal velocity above the blockages indicates an undisrupted surface velocity pattern of parabolic flow where the maximum velocity is found in the centre of the valley and substantially lower velocities are found near the margins. Longitudinal velocity on the blocked side of the valley was reduced in all trials though the magnitude varied substantially.

2) Lateral velocity in the unblocked valley was uniformly low throughout the trial. Analogue material subjected to blocked flow experienced high rates of directional lateral velocity directly above and directly below the blockages. The A, B and to a lesser extent C trials experience a similar pattern of lateral velocity. Above the blockage the material was subjected to high rates (>0.2 cm min^{-1}) of right lateral movement and below the blockage it experienced a high rate of left lateral velocity of a similar magnitude. High right lateral velocities were recorded in the D trials but the design of the blockage did not allow for the sudden left lateral flow of material below the blockage.

3) A, B and D blockages experience high longitudinal compression on the blockage side, and extension as the material flows through the constriction. The C blockage has a pattern of longitudinal strain rate similar to that in the unblocked trials.

4) In frames 024 and 057, perpendicular obstructions that block half the valley width (A, B and D) experience a 'banding' of lateral compression occurring ~ 2 cm above the constriction. Extension occurs as marker beads approach the constriction, they are then subject to a region of compression as they begin to move through the opening. After the beads have moved through the constriction they again experience extension as they flow into the lower valley.

5) Lateral strain rates are low in all blockage trials in frame 090.

6) Shear strain rates were always higher early in the trial (frame 024). There were few distinct differences in shear strain rates between the trials, rates were mostly lower in the E and C trials than in either the A or B trials. No distinct shear strain zones can be seen in these experiments; this is discussed in section 5.2.

Chapter 5 - Discussion

5.1 - Inventory Analysis

Analysis of the glacier inventories was carried out to provide a basis for the construction of the model glacier valley and blockages. The discussion of the results of those inventory analyses will be limited as they are manifest both in the design of the model itself and in the results of the flow experiments. That being said it should be noted that the inventory analysis revealed interesting characteristics about tributary-trunk confluences in the study regions. Most notably the predominance of confluence angles between 45° and 90° in these systems. For the region of the St. Elias Range in Yukon Territory, Canada, as well as for other regions that experience large scale faulting, these angles may very well reflect the pre-glaciation dendritic river systems with right-angle offsets caused by extensive faulting in the tectonically active region (see Chapter 2.5.1) (Gregory and Walling, 1973).

5.2 – Modelling Experiments

The analogue material is subject to both extension and compression as it flows through the model valley, which can occur in both the longitudinal and lateral directions. In glaciology it is common to interpret flow variations along the flow-line by analysing patterns in longitudinal strain. Longitudinal strain rates are usually greater than lateral strain rates and are controlled by various factors including valley constriction and thinning of the ice (Paterson, 1994). An examination of the combined velocity and strain data for the flow trials reveals a picture of what is occurring on the surface of the material during the flow trials. The flow of the analogue material in the valley glacier approximated the flow regime of valley glaciers suggested by Harbor (1992). In all trials,

regardless of the blockage, the centre flow line consistently had the highest longitudinal velocities. Results differ based on the geometry and orientation of the obstruction.

As suggested in Nye (1952) the longitudinal compressive and extensional strain rates can be stress responses to both a narrowing of the glacial valley and widening of the valley, respectively. Compression is recorded during flow in the constrictions in blockage trials A, B and D as the analogue material moves through the narrow unblocked valley. Extension was recorded below the blockage in those trials that blocked the valley to the full depth (A and B). Extensional strain rates did not occur below the blockage in the D trials because there was no 'widening' of the valley because material was allowed to flow under the blockage and fill the valley below.

E Trials – Unblocked Flow

Experimental trials in an unblocked valley were carried out to create a baseline dataset for comparison to the results collected from flow in blocked valleys. The E trials indicated parabolic longitudinal flow with higher velocities occurring in the centre of the valley and lower velocities found near the margins of the valley. Lateral velocities indicated that little directional movement was occurring during a flow trial of an unblocked valley which allows for the conclusion that transverse directional movement found in blocked valleys is directly related to the analogue material interacting with the blockage. Flow in an unblocked valley is also associated with low longitudinal strain rates except in areas that are influenced by drag from the valley walls or bottom.

Shear strain rates were expected to be high near the margins and approach zero in the centre flow-line (Nye, 1952). This did not occur in these experiments, however there is some indication in the unblocked trials that shear strain rates are higher at the valley

walls and the leading edge of the flow than in the centre (Fig 4.8). An increase in velocity of the material through a change of slope may result in the appearance of distinct zones of shear strain. A decrease in temperature and subsequent decrease in velocity may also cause crevasses to appear in areas of the model where high shear strain rates are expected such as at the margins of the model valley.

Unblocked (E) Flow vs. Taku Glacier - Information on the research conducted on the Taku Glacier is discussed in detail in section 2.1.2. The Taku Glacier is a tidewater valley glacier located in the Juneau icefield, Alaska and accumulates mass from a complex system of tributaries (Daellenbach and Welsh, 1993); however the location of the field studies is in an area relatively free of tributary influence (Wu and Christensen, 1964; Daellenbach and Welsh, 1993).

In a strictly observational and superficial comparison between the two it appears that unblocked flow of the ice analogue model conforms to the observed flow behaviour of the Taku Glacier in that flow velocity is highest in the centre of the valley. The model glacier consistently indicated parabolic flow as a result of the high levels of shear stress at the model valley walls.

A Trials – ½ Width, Full Depth, 45°

Blockage A was designed to mimic the blocking potential of a convergence between a tributary and a trunk glacier at an angle of 45°. An angle of 45° was determined to occur frequently in the regions of study (Svalbard, Yukon, East Greenland, Arctic Canada) (see Chapter 4.2.1). Of the 50 trial experiments run, blockage A consistently had the lowest values of total velocity at and above the blockage; however, one must be

careful in attributing this to the effective flow obstructing power of an angled blockage. There are two other possible explanations for the low velocities in this blockage:

1. The increase of exposed surface area of the angled blockage increased drag as more of the material was coupled to the surface rather than an initial coating material that allowed other material to flow by with less drag. If this is the case shear strain rates on the left side of valley during the A trials should be substantially higher at the blockage than other trials. If this in fact what is occurring in the A trials then the velocity rates would decrease during the early trial as the material initially encounters the blockage but would experience a subsequent increase in velocity once the blockage is coated with the material and it is in essence sliding on itself. However, this appears to not be the case, as the shear strain rates do not appear to be higher along the blockage.
2. The material used in this series of experiments was used in several trial runs prior to the actual recorded trials. These blockage experiments should be retried with new material to see if there is an increase in over all velocity. If the values remain low when re-tried then the age of the material can be discarded as a possible cause of the low rates of velocity associated with this blockage.

Angled (A) Blockage vs. Kaskawulsh Glacier - The angled blockage results indicate a reduction of velocity for the left side of the valley and a subsequent increase below the blockage as the slowed material catches up with the marker beads on the right (unobstructed) side of the valley. This is essentially what happens at the confluence of the North and South arms of the Kaskawulsh Glacier, each with a different flow regime, as

they experience a reduction in velocity as they enter the confluence (Anderton, 1973) (see Chapter 2.4).

B Trials – ½ Width, Full Depth

When average lateral velocities from mid-trial (frame 057, Fig 4.19) are mapped it becomes apparent that the B blockage had a significant blocking effect and subsequently upon the longitudinal and lateral movement of the analogue material. It seems logical that the greater the width of the blockage equals a higher blockage potential, however, the angled (A) blockage also obstructs half the valley but did not experience deformation of the strain grid as high in the valley as those seen in the perpendicular, half width B trials. The angled blockage appears to have the effect of 'funnelling' the analogue material towards the constriction while the perpendicular blockage fully retards the flow of the material on the left side of the valley until it more or less 'overflows' into the constriction.

Perpendicular (B) Blockage vs. Rusty / Backe Glaciers - The 'piling up' of the material behind the B blockage is suggested to be a potential trigger mechanism for surging behaviour in tributary effected glacier systems. A confluence involving a bulging tributary (Ra >>1) and trunk, such as that of the Backe and Rusty Glaciers indicated a thickening of the trunk glacier up-ice from the confluence (Collins, 1972 and Kargel *et al*., 2005). All details regarding the Backe and Rusty glaciers are from Collins (1972), however, few details were known about the Backe glacier at the time of that publication. The assumption of Rusty/Backe Glacier being a Type IV convergence (overriding) is based on the acceptance that the flow behaviour of the Backe glacier is indicative of surge-type flow (see section 2.4.2). Despite the lack of quantitative evidence the

assumption is made that the extensive crevasses at the tongue of Backe Glacier are the result of rapid extensional flow and thus; 'a questionable or borderline example of a surge' (Collins, 1972). The bulging tongue of the Backe Glacier converges with the Rusty Glacier at nearly 90°, approximately 1000 m above the Rusty Glacier terminus. Velocity and strain rates on the Rusty glacier were extremely slow at 0.4 m/year and $< 8 \times 10^{-3}$ $year^{-1}$, respectively, and the lower area of the glacier that is affected by the intrusion of the Backe Glacier tongue is nearly stagnant. However, one of the regions with the highest recorded longitudinal compression was directly above the Backe Glacier tributary. It should be noted, though, that a second tributary located further up ice from the Backe Glacier bulge also directly affects this region. The area between these two tributaries has greater ice thickness than was expected and revealed an unusual flow line pattern. The flow line that usually was found parallel to the bed along the length of the glacier was observed to be altered so the flow line emerged at a higher angle than was predicted. This was attributed to a damming effect by the stagnant ice of the Rusty Glacier snout (Nielson and Stockton, 1956; Nielson, 1968 and 1969). However, the results of the B blockage trials suggest that this pattern may in fact be a result of the damming effect of the rapidly advancing Backe Glacier tributary. The noted increase in ice thickness and the change in mean flow direction that were noted on Rusty Glacier near the emerging snout of the Backe glacier correspond with two of the three processes occurring at the confluence of temperate glaciers as suggested by Gudmundsson *et al*. (1997) (see Chapter 2, section 4.2). The increased ice thickness noted above the tributary could be similar to the behaviour seen in the analogue material in the B blockage trials (Fig 5.1).

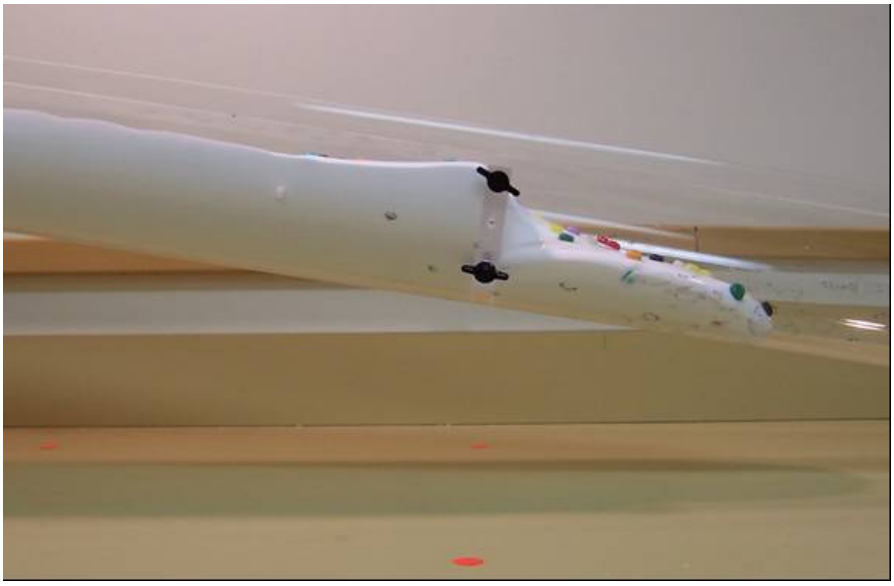

Fig 5.1 – Thickening of the analogue material behind blockage B at mid-trial. Some of the analogue material has flown past the obstruction and into the lower valley but there is a noticeable thickening of material directly upstream of the blockage.

C Trials – ¼ Width, Full Depth

The overall velocity and strain rate patterns recorded in the blockage C trials are similar in magnitude to those recorded for the unblocked trials (E). This is likely because the blockage is small enough that it does not cause substantial disruption of the marker beads in the strain grid. Deformation of the surface strain grid occurs later in the trial than with the B blockage because the material does not encounter the smaller obstruction until the centre bead of the lower transect is parallel to it. This occurs because the material flows faster in the centre of the valley than at the margins, which means that the leading edge of the material is not subjected to a reduction in velocity until a later time interval. The parabolas created in the initially parallel lines of the strain grid can easily be followed even after the material has begun to flow past the blockage.

D Trials – ½ Width, ½ Depth

The strain grid on the surface of the analogue material was blocked and piled up behind the blockage. This blockage essentially 'scraped' the surface as the material flowed beneath it (Appendix I: Blockage D, Frame 090). A number of beads on the left side of the strain grid became buried behind the blockage resulting in the disappearance of some beads as early as frame 013. The effect that this had on the strain grid was to effectively simulate a blockage in the strain grid without the presence of a full obstruction. Despite this blockage being the same width (½ valley width) as the B trial blockage, the material was still able to flow under it and subsequently there was no void below the blockage that the material rapidly flowed into once past the obstruction. Results from this trial are difficult to interpret, as the strain grid is removed from the surface of the material as it flows under the blockage.

5.3 – Summary

The analogue model was constructed and these experiments carried out for the eventual comparison between the analogue and its real world counterparts. Blockage A, the angled blockage, can be compared to the Kaskawulsh confluence, despite the fact that the North and South arms of the Kaskawulsh confluence converge at an angle less than 45°. The perpendicular blockage (B) is compared to the Type IV tributary confluence (see Kargel *et al*., 2005 and Chapter 3) represented by the convergence of the Backe Glacier with the Rusty Glacier. Unblocked flow in the analogue model can be compared to flow in the Taku Glacier.

Chapter 6 - Conclusions

6.1 – Conclusions

1. Analogue models are an effective tool in the study of glacial flow and can be successfully used to simulate glacial flow in a lab setting. The simulation of pure creep behaviour through the use of the ice analogue material is a simple, inexpensive and safe way to collect velocity data on the flow mechanics of valley glaciers. Lateral and longitudinal velocity and strain data were useful in determining the effect of geometrically different obstructions in a model valley glacier based on rheology discussed in Nye (1952). Shear strain data is inconclusive as no distinct zones of shear are visible in the results.
2. The flow dynamics of a valley glacier flowing within an ideal glacial valley can be substantially disrupted by contact with an obstruction. The size and orientation of the obstruction significantly influences the magnitude of disruption within the confluence region and down ice from the confluence. An effective flow blocking structure will initially retard the flow of the material down-valley before causing it to experience lateral movement as it is then forced around the blockage. It will then experience lateral displacement in the opposite direction as it flows around and behind the blockage before resuming its 'normal' down valley movement.
3. Tributary confluence angles of 45° - 90° are most commonly occurring in the regions of Svalbard, East Greenland, Yukon Territory and the Thompson Glacier system. However, a wide range of entrance angles occur in nature, ranging from those that enter the trunk glacier and flow parallel to it to those that enter at an angle as wide as 120° and move against the flow direction of the trunk glacier.

Also common in these glaciated regions is the occurrence of trunk / tributary width ratios less than 4, meaning that the trunk is generally ≤ 4 times the width of the tributary. Data from the Svalbard inventories is proportionally similar to those data from the Yukon Territory and East Greenland which means that it can be assumed that average width can be used effectively when more localized measurements are unavailable.

4. It is suggested that the blockage of the trunk glacier and subsequent storage of energy up ice from the tributary confluence could result in the triggering of a surge in the trunk glacier when the Ra (kargel et al., 2005) of the tributary glacier is reduced either through a phase change to its quiescent flow phase or through detachment of the tributary as a result of threshold stress or large-scale glacial recession. The piling of material behind the B blockage is suggested to be a potential trigger mechanism in a surge-type glacier system with tributary-trunk interactions of 90°. Adjustments in the methodology of the experiments need to be made before this can be said for sure. The lack of a consistently replenished reservoir could be prohibitive to effective modelling of surge behaviour, as is the fully coupled basal flow of the ice analogue material.

6.2 – Further Research

This experiment was intended as a structural and design preliminary to more complex analogue model experiments. It was designed to mimic potential constrictions and obstructions in an otherwise uniform glacial valley. The next logical step in the analogue modelling of ice obstructions would be the design and construction of a model glacier tributary system that includes a tributary filled with actively flowing analogue material

and a strain grid that includes the area immediately above and below the confluence on both the tributary and trunk glaciers. The results from the glacier inventory analysis conducted in this thesis should be useful in the design and construction of such a tributary model. However, prior to designing a more complicated model, the exact properties of the ice analogue material should be thoroughly tested using a loaded strain devise similar to that used by e.g. Glen (1952), in a controlled environment, so that its strain response can be quantitatively compared to that of glacier ice over a range of stresses.

Another potential avenue of research would be to experiment with changes in the basal texture or topography of the model valley and addition of fluid to the base to mimic slip rather than pure creep over more realistic basal structures. An oil-based lubricant would have to be used for experiments with basal slip, as any addition of water would dilute the material and change its flow properties. This model also ignores the effect of subglacial sediment on the flow of the valley glacier. Experiments such as those conducted in this thesis could be recreated with changes in the basal texture through the addition of a lining of coarse material to examine how changes in basal texture affect the flow dynamics.

List of References

Acocella, V., F. Cifelli and R. Funiciello. 2001. Formation of nonintersecting nested calderas: insights from analogue models. *Terra Nova*. 13(1), 58-63.

Adomaitis, V. Unknown. Mt. Kaskawulsh. Digital Image http://www.jovial.on.ca/vica/ Accessed March 2006.

Alley, R.B., D.E. Lawson, E.B. Larson and G.S.Baker. 2003. Stabilizing feedbacks in glacier-bed erosion. Letters to Nature. *Nature*. 424(11), 758-760

Anderton, P.W. 1973. Structural glaciology of a glacier confluence, Kaskawulsh Glacier, Yukon Territory, Canada. Institute of Polar Studies, Report # 26. 108pp.

Atkinson, P., H. Jiskoot, R. Massari and T. Murray. 1998. Generalized linear modelling in geomorphology. *Earth Surface Processes and Landforms*. 23, 1185-1195.

Benn, D.I. and D.J. Evans. 2002. *Glaciers and Glaciology,* 2nd ed. Oxford University Press, New York. 734 pp.

Boulton, G.S.1986. A paradigm shift in glaciology? News and Views. *Nature*. 322, 18.

Boulton, G.S. and C.A Hindmarsh. 1987. Sediment deformation beneath glaciers: rheology and geological Consequences. *Journal of Geophysical Research.* 92(B9), 9095-9082.

Clark, P.U. 1994. Unstable behaviour of the Laurentide Ice Sheet over deforming sediment and its implications for climate change. *Quaternary Research*. 41(1), 19-25.

Clark, P.U. 1997. Sediment deformation beneath the Laurentide Ice Sheet: in Martini, IP (ed.), *Late glacial and postglacial environmental changes: Quaternary, Carboniferous – Permian and Proterozoic*. Oxford University Press, New York. 343 pp.

Clarke, G.K.C., S.G. Collins and D.E Thompson. 1984. Flow, thermal structure, and subglacial conditions of a surge-type glacier. *Canadian Journal of Earth Sciences*. 21(2), 232-240.

Clarke, G.K.C. 1987. Subglacial till: A physical framework for its properties and processes. *Journal of Geophysical Research*. 92(B9), 9023-9036

Clarke, G.K.C. 1991. Length, width and slope influences on glacier surging. *Journal of Glaciology*. 37 (126), 236-246.

Clarke, G.K.C. 2005. Subglacial processes. *Annual Review of Earth and Planetary Sciences*. 33, 247-76.

Clarke, G.K.C., J.P Schmok, S.L. Ommanney and S.G. Collins, S.G. 1986. Characteristics of surge-type glaciers. *Journal of Geophysical Research.* 91(B7), 7165-7180.

Collins, I.F. 1970. A slip-line field analysis of deformation at the confluence of two glacier streams. *Journal of Glaciology*. 9(56), 169-193.

Collins, S.G. 1972. Survey of the Rusty Glacier area, Yukon Territory, Canada, 1967-1970. *Journal of Glaciology*. 11(62), 235-250.

Daellenbach, K.K. and W.M. Welsh. 1993. Determination of surface velocities, strain and mass flow rates on the Taku Glacier, Juneau Icefield, Alaska. *Zeitschrift fur Gletscherkunde und Glazialgeologie*. 26(2) 169-177.

Echelmeyer, K., R. Butterfield and D. Cuillard. 1987. Some observations on a recent surge of Peters Glacier, Alaska, U.S.A. *Journal of Glaciology*. 33(115), 341-445.

Eyles, N. 1993. Earth's glacial record and its tectonic setting. *Earth-Science Reviews*. 35(1-2), 1-248.

Eyles, N and R.J. Rogerson. 1977. Glacier movement, ice structures, and medial moraine form at a glacier confluence, Berendon Glacier, British Columbia, Canada. *Canadian Journal of Earth Sciences*. 14(12) 2807-2816.

Fleisher P. J. and J.K. Sales. 1972. Laboratory models of glacier dynamics. *Geological Society of America Bulletin*. 93, 905-910.

Gerbi, C. 2003. Kitchen Table Rheology. http://www.geology.um.maine.edu/geodynamics/analogwebsite/Projects2003/Gerbi_2003/index.html Accessed September 2004

Glen, J.W. 1952. Experiments on the deformation of ice. *Journal of Glaciology*. 2(12), 111-114.

Glen, J.W. 1955. The creep of polycrystalline ice. *Proceeding of the Royal Society of London. Series A, Mathematical and Physical Sciences.* 228(1175), 519-538.

Gudmundsson, G.H., A. Iken, and M. Funk. 1997. Measurements of ice deformation at the confluence area of Unteraargletscher, Bernese Alps, Switzerland. *Journal of Glaciology*. 43(145), 548-556.

Gregory K.J. and D.E. Walling. 1973. *Drainage Basin Form and Process: a geomorphological approach*. Edward Arnold Ltd. London. 456 pp.

Goldsby, D.L. and D.L. Kohlstedt. 2001. Superplastic deformation of ice: Experimental observations. *Journal of Geophysical Research*. 106(B6), 11,017-11,030.

Hagen, J.O., O. Liestøl, E. Roland and T. Jørgensen. 1993. *Glacier atlas of Svalbard and Jan Mayen*. Meddelelser 129, Norsk Polarinstitutt. 140 pp.

Hamilton, G.S. and J.A. Dowdeswell. 1996. Controls on glacier surging in Svalbard. *Journal of Glaciology*. 42(140), 157-168.

Hansen, J.E. 2007. Scientific reticence and sea level rise. *Environmental Research Letters*, in press.

Harbor, J.M. 1992. Numerical modeling of the development of U-shaped valleys by glacial erosion. *Geological Society of America Bulletin*. 104, 1364-1375.

Hooke, R.L., 2005. *Principles of glacier mechanics*. 2nd Edition. Cambridge University Press, Cambridge, United Kingdom. 448 pp.

IPCC, 2001. Climate Change 2001: The Scientific Basis. Contribution of Working Group I to the Third Assessment Report of the Intergovernmental Panel on Climate Change [Houghton, J.T.,Y. Ding, D.J. Griggs, M. Noguer, P.J. van der Linden, X. Dai, K. Maskell, and C.A. Johnson (eds.)]. Cambridge University Press, Cambridge, United Kingdom and New York, NY, USA. 881 pp.

Jiskoot, H., P. Boyle and T. Murray. 1998. The incidence of glacier surging in Svalbard: evidence from multivariate statistics. *Computers and Geoscience*. 24(4), 387-399.

Jiskoot, H. 1999. *Characteristics of surge-type glaciers*. Unpublished Ph D dissertation, University of Leeds, Leeds, UK.

Jiskoot, H., T. Murray and P Boyle. 2000. Controls on the distribution of surge-type glaciers in Svalbard. *Journal of Glaciology*. 46(154), 412-422.

Jiskoot, H., A.K. Pedersen and T. Murray. 2001. Multi-model photogrammetric analysis of the 1990s surge of Sortebrae, East Greenland. *Journal of Glaciology*. 47(159), 677-687.

Jiskoot, H., T. Murray and A. Luckman. 2003. Surge potential and drainage basin characteristics in East Greenland. *Annals of Glaciology*. 36, 142-148.

Jiskoot, H. 2003 (unpublished). *Effects of the glacier system disintegration on recession*. Poster session presented at the Workshop on Assessing Global Glacier Recession. Boulder, CO, 16-18 March 2003.

Kamb, B. 1987. Glacier surge mechanism based on linked cavity configuration of the basal water conduit system. *Journal of Geophysical Research*. 92(B9), 9083-9100.

Kargel, J.S, M.J. Abrams, M.P. Bishop, A. Bush, G. Hamilton, H. Jiskoot, A. Kääb, H.H. Kieffer, E.M. Lee, F. Paul, F. Rau, B. Raup, J.F. Shroder, D. Soltesz, D. Stainforth, L. Stearns, and R. Wessels. 2005. Multispectral imaging contributions to Global Land Ice Measurements from Space. *Remote Sensing of Environment* 99 (special issue on Terra/ASTER science), 187-219.

Lewis, W.V. and M.M. Miller. 1955. Kaolin model glaciers. *Journal of Glaciology*. 2(18), 533-538.

McCay, K. and T. Dooley. 1995. Analogue models of pull-apart basins. *Geology.* 23(8), 711-714.

Meier, M.F., 1957. *Mode of flow of Saskatchewan Glacier. Alberta, Canada*. Unpublished PhD dissertation, California Institute of Technology, Pasadena California, U.S.A.

Metallurgical Consultants. 1999. Creep and stress rupture. http://www.materialsengineer.com/CA-Creep-Stress-Rupture.htm Updated, 2006. Accessed August 2006

Montgomery, D.R. 2002. Valley formation by fluvial and glacial erosion. *Geology*. 30(11), 1047-1050.

Murray, T. 1997: Assessing the paradigm shift: Deformable glacier beds. *Quaternary Science Reviews*. 16(9), 995-1016.

Murray, T., T. Strozzi, A. Luckman, H. Jiskoot and P. Christakos, 2003. Is there a single surge mechanism? Contrasts in dynamics between glacier surges in Svalbard and other regions. *Journal of Geophysical Research.* 108(B5), 2237, doi:10.1029/2002JB001906.

NSIDC/WDC for Glaciology, Boulder, compiler. 2002, updated 2006. Online glacier photograph database. Boulder, Colorado USA: National Snow and Ice Data Center/World Data Center for Glaciology. Digital media.

NRCan (Natural Resources Canada), 2002. Melting glaciers. http://adaptation.nrcan.gc.ca/posters/pr/pr_04_e.php Accessed Nov 2006.

Nye, J.F. 1952. The mechanics of glacier flow. *Journal of Glaciology*. 2(12), 82-93.

Nye, J.F., 1957. The Distribution of Stress and Velocity in Glaciers and Ice-Sheets. *Proceedings of the Royal Society of London. Series A, Mathematical and Physical Sciences*, 5(41), 113-133.

Ommanney, C.S.L. 1980.The inventory of Canadian glaciers: procedures, techniques, progress and applications. *IAHS-AISH*. 126, 35-44.

Paterson, W.S.B. 1994. *The Physics of Glaciers*, 3rd ed. Elsevier Science Ltd, New York, 480 pp..

Pattyn, F. 2003. A new three-dimensional higher-order thermomechanical ice sheet model: Basic sensitivity, ice stream development, and ice flow across subglacial lakes. *Journal of Geophysical Research.* 108(B8), 2382, doi:10.1029/2002JB002329

Plummer, C.C. and D. McGeary. 1991. *Physical Geology,* 5th ed. Wm C. Brown Publishers, Dubuque, IA, U.S.A. 543 pp.

Post, A. 1969. Distribution of surging glaciers in western North America. *Journal of Glaciology*. 8(53), 229-240.

Price, J.F. 2006 (unpublished). Lagrangian and Eulerian Representations of Fluid Flow: Kinematics and the Equations of Motion. Woods Hole Oceanographic Institution, Woods Hole, MA. http://www.whoi.edu/science/PO/people/jprice (accessed 15 Dec 2006).

Price, N.J. and J.W. Cosgrove. 1994. *Analysis of Geological Structures*, 3rd ed. Cambridge University Press, Cambridge, UK, 502pp..

Randall, B.A.O. 1961. On the relationship of valley and fjord directions to the fracture pattern of Lyngen, Troms N. Norway. *Geografiska Annaler*. 43(3-4), 336-338.

Raymond, C.F. 1969. *Flow in a transverse section of Athabasca Glacier, Alberta, Canada*. Unpublished PhD dissertation, California Institute of Technology, Pasadena, California, U.S.A.

Regard, V., C. Faccenna, J. Martinod, and O. Bellier. 2005. Slab pull and indentation tectonics: insights from 3D laboratory experiments. *Physics of the Earth and Planetary Interiors*. 149(1,2), 99-113.

Roberts, J.L. 1996: *The Macmillan Field Guide to Geological Structures*, Paperback ed. The Macmillan Press. London. 224 pp.

Scott, D. and B. Jones. 2005. Climate Change & Banff National Park: Implications for Tourism and Recreation. Report prepared for the Town of Banff. University of Waterloo, Waterloo, Ontario, Canada.

Shoemaker, E.M. 1981. Creep slump in glacier reservoirs - theory and experiment. *Journal of Glaciology*. 27(97), 393-406.

Sokal, R.R. and F.J. Rohlf. 1995. *Biometry: the principles and practice of statistics in biological research*. 3rd ed. W. H. Freeman and Co., New York. 887 pp.

Spotila, J.A., J.T. Buscher, A.J. Meigs, and P.W. Reiners. 2004. Long-term glacial erosion of active mountain belts: Example of the Chugach - St. Elias Range, Alaska. *Geological Society of America*. 32(6), 501-504.

Squires, G.L., 1976. *Practical Physics.* 2nd ed. McGraw-Hill Book Company (UK) Ltd, 224 pp.

Stearns , L. and E. Osterberg. 2003. Modeling the Malaspina. http://www.geology.um.maine.edu/geodynamics/analogwebsite/Projects2003/Sterns_Osterberg_2003/index.html Accessed September 2004

Sugden D.E. and B.S. John. 1985. *Glaciers and Landscape*. Edward Arnold Ltd. London, 276 pp.

van der Veen, C.J. 1999. *Fundamentals of glacier dynamics*. A.A. Balkema, Rotterdam, Netherlands. 462 pp.

Wilbur, S.C. 1988. *Surging versus nonsurging glaciers: a comparison using morphometry and balance*. Unpublished MSc. thesis, University of Alaska, Fairbanks, Alaska, U.S.A.

Wilson, G. 1961. The tectonic significance of small-scale structures and their importance to the geologist in the field. *Annals of the Geological Society of Belgium*. 84, 423-548.

Wu T.H. and R.W. Christensen, 1964. Measurement of surface strain-rate on Taku Glacier, Alaska. *Journal of Glaciology*. 5(39), 305-313.

APPENDIX I: Tributary-trunk entrance angles and width ratios

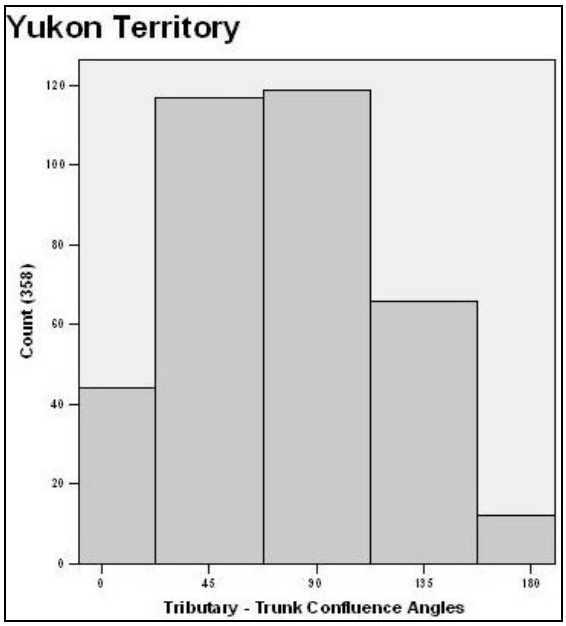

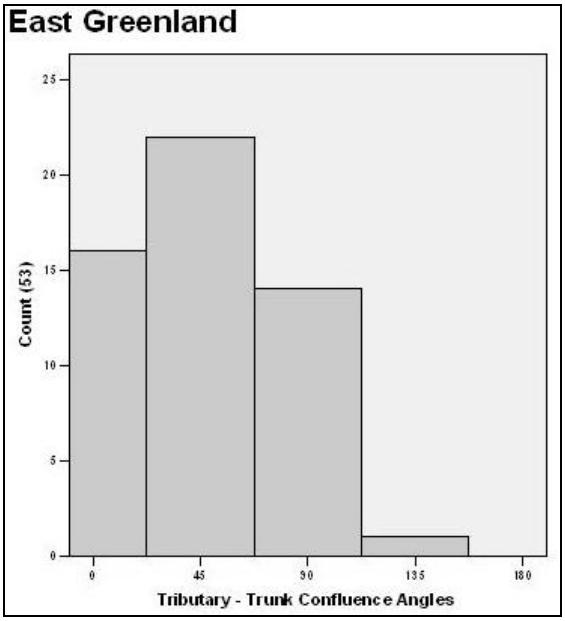

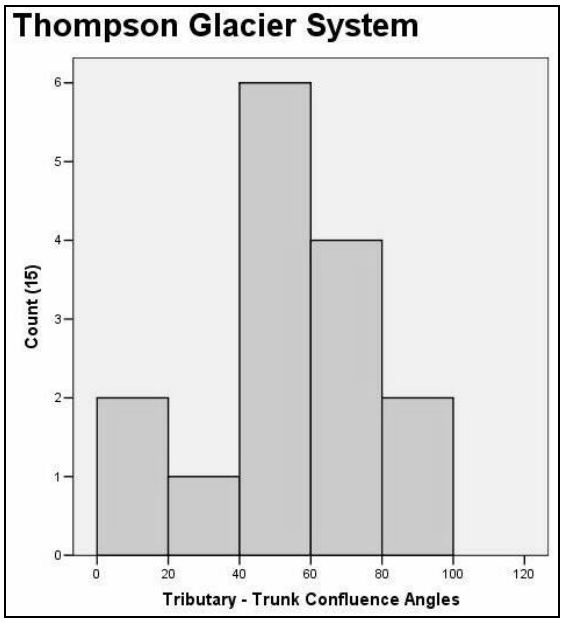

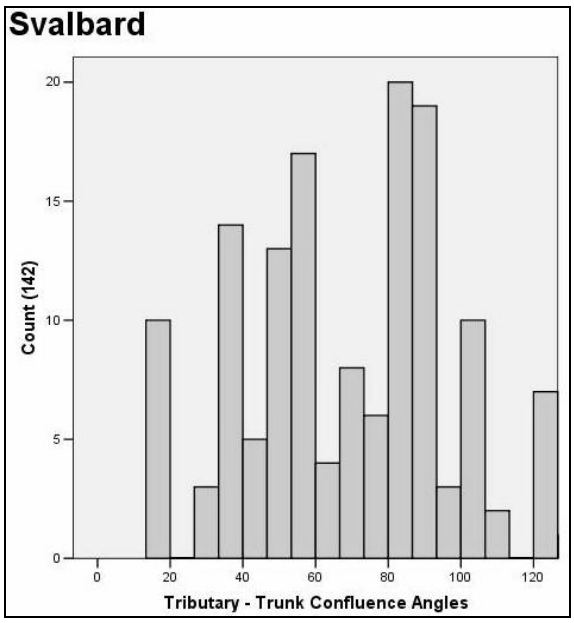

APPENDIX I (con't): Tributary-trunk entrance angles and width ratios

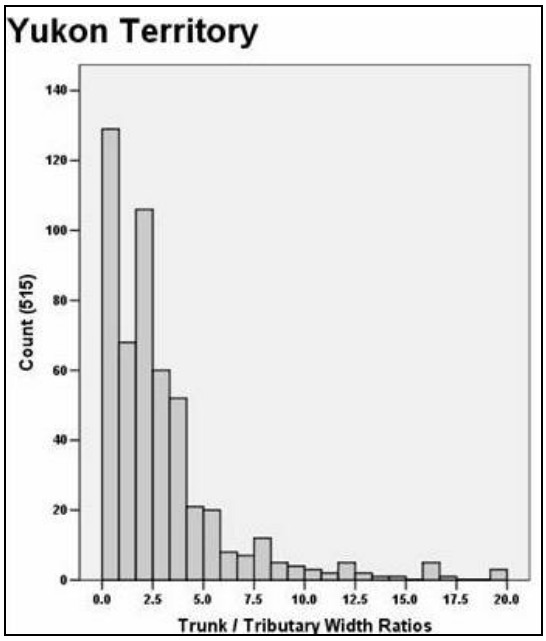

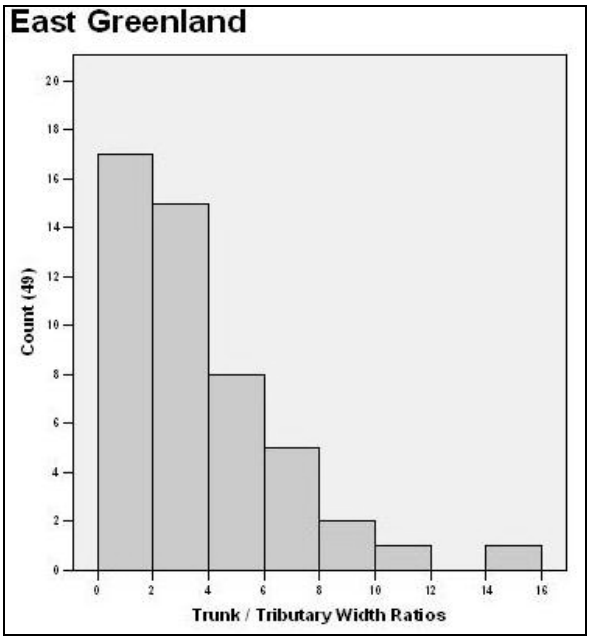

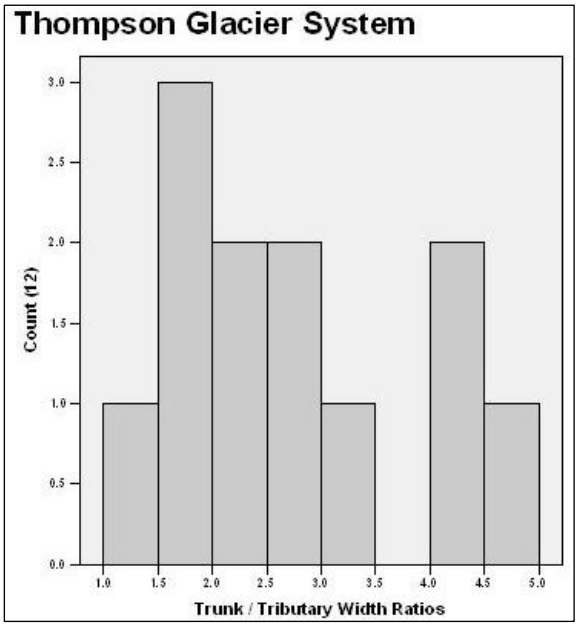

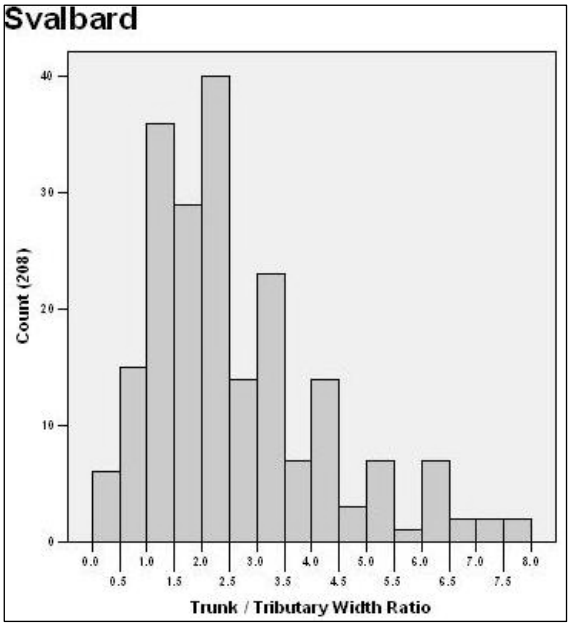

APPENDIX II: Trial weight data

Trial Weight Data						
Blockage	**Date**	**Run#**	**Group ID**	**Start (g)**	**End (g)**	**Loss (g)**
A	04/07/2006	1	1	3500	3487	13
	04/07/2006	2	2	3500	3489	11
	04/07/2006	3	3	3500	3487	13
	04/10/2006	4	4	3500	3492	8
	04/10/2006	5	5	3500	3495	5
	04/10/2006	6	6	3495	3481	14
	04/10/2006	7	7	3500	3489	11
	04/11/2006	8	8	3500	3492	8
	04/11/2006	9	9	3500	3485	15
	04/11/2006	10	10	3485	3470	15
AVG - A				**3498**	**3486.7**	**11.3**
B	04/12/2006	11	1	3500	3484	16
	04/12/2006	12	2	3500	3464	36
	04/18/2006	13	3	3500	3470	30
	04/18/2006	14	4	3500	3480	20
	04/18/2006	15	5	3500	3486	14
	04/19/2006	16	6	3500	3480	20
	04/19/2006	17	7	3500	3487	13
	04/20/2006	18	8	3500	3485	15
	04/20/2006	19	9	3500	3487	13
	04/20/2006	20	10	3500	3484	16
AVG - B				**3500**	**3480.7**	**19.3**
C	04/20/2006	21	1	3500	3483	17
	04/21/2006	22	2	3500	3488	12
	04/21/2006	23	3	3500	3472	28
	04/21/2006	24	4	3500	3489	11
	04/21/2006	25	5	3500	3487	13
	04/25/2006	26	6	3500	3481	19
	04/25/2006	27	7	3500	3482	18
	04/25/2006	28	8	3500	3489	11
	04/25/2006	29	9	3500	3485	15
	04/26/2006	30	10	3500	3479	21
AVG C				**3500**	**3483.5**	**16.5**

Note: Highlighted dates indicate the first trial that was run with a new batch.

APPENDIX II (con't): Trial weight data

Trial Weight Data						
Blockage	**Date**	**Run#**	**Group ID**	**Start (g)**	**End (g)**	**Loss (g)**
D	04/26/2006	31	1	3500	3480	20
	04/26/2006	32	2	3500	3479	21
	04/26/2006	33	3	3500	3481	19
	04/27/2006	34	4	3500	3478	22
	04/27/2006	35	5	3500	3480	20
	04/27/2006	36	6	3500	3489	11
	04/27/2006	37	7	3500	3490	10
	04/27/2006	38	8	3500	3480	20
	04/27/2006	39	9	3500	3490	10
	04/28/2006	40	10	3500	3477	23
AVG D				**3500**	**3482.4**	**17.6**
E	04/28/2006	41	1	3500	3481	19
	04/28/2006	42	2	3500	3477	23
	04/28/2006	43	3	3500	3481	19
	04/29/2006	44	4	3500	3489	11
	04/29/2006	45	5	3500	3493	7
	04/29/2006	46	6	3500	3480	20
	04/30/2006	47	7	3500	3483	17
	04/30/2006	48	8	3500	3486	14
	04/30/2006	49	9	3500	3481	19
	04/30/2006	50	10	3500	3487	13
AVG E				**3500**	**3483.8**	**16.2**

Note: Highlighted dates indicate the first trial that was run with a new batch.

APPENDIX III: Digital Images of Trials

Digital Images of Experimental Trials - Angled (45°) Blockage Trials (A)

Frame 024

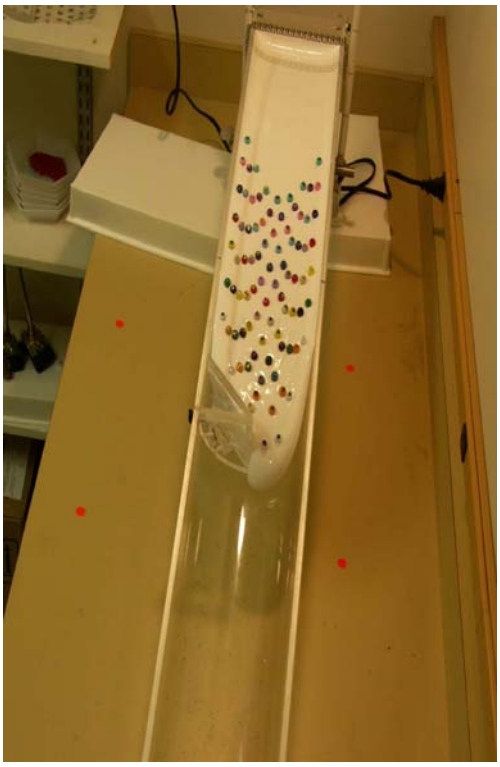

Frame 057

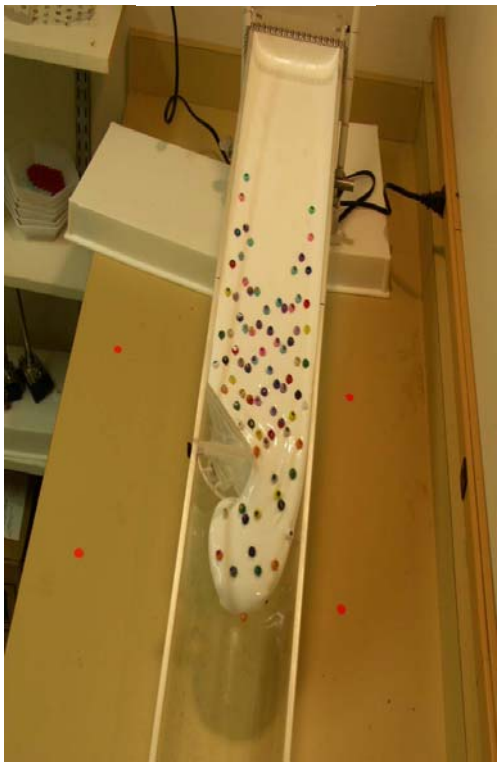

Frame 090

APPENDIX III (con't)
Digital Images of Experimental Trials - Perpendicular Blockage Trials (B)

Frame 024

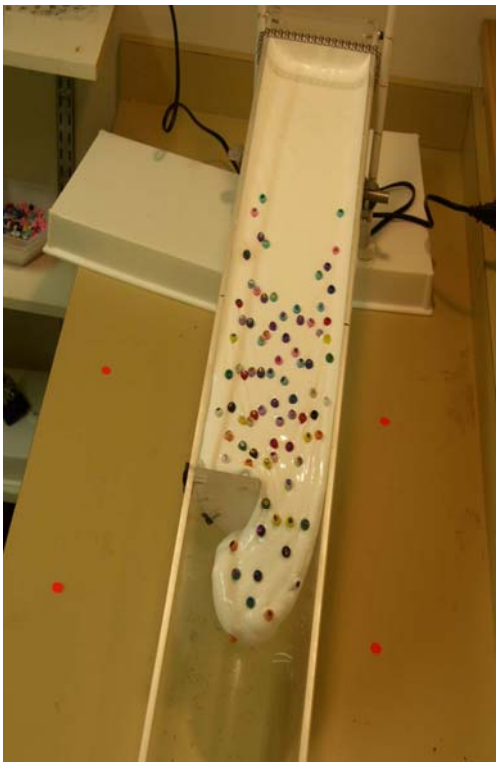

Frame 057

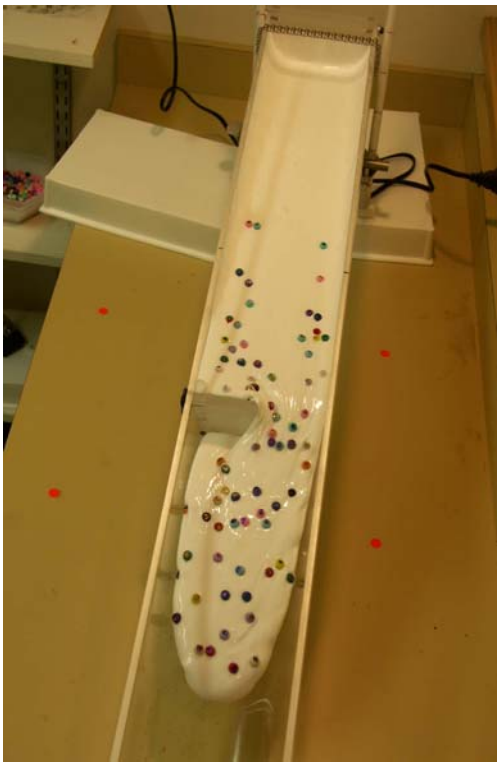

Frame 090

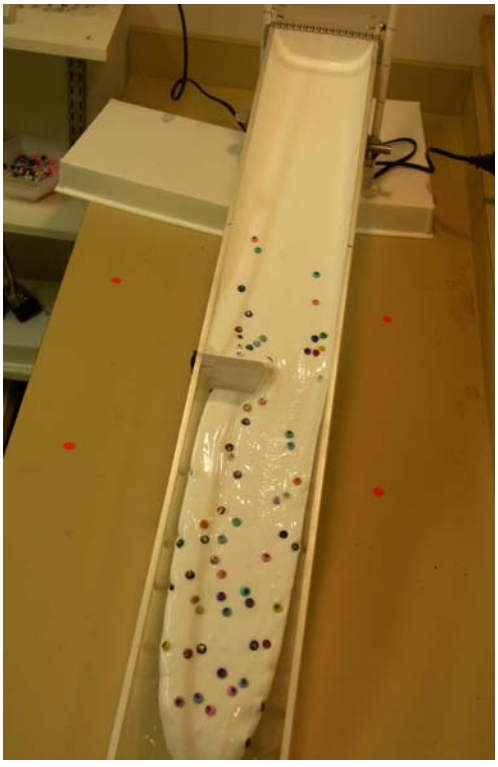

APPENDIX III (con't)

Digital Images of Experimental Trials - Perpendicular Blockage (C) – ¼ width, ½ depth

Frame 024

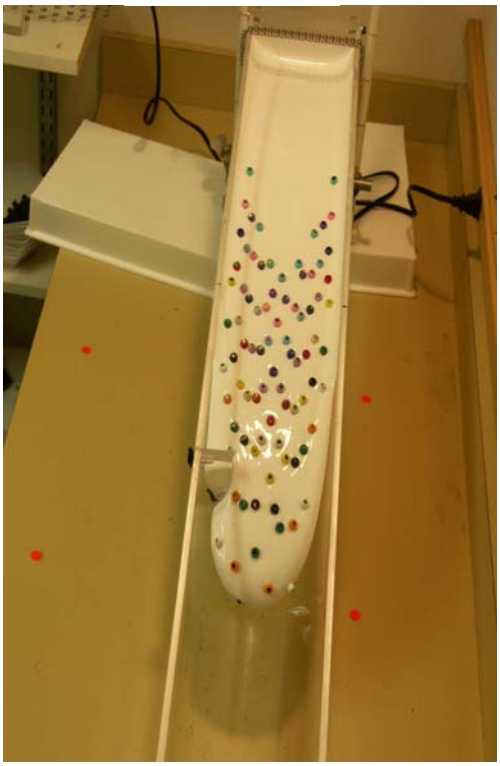

Frame 057

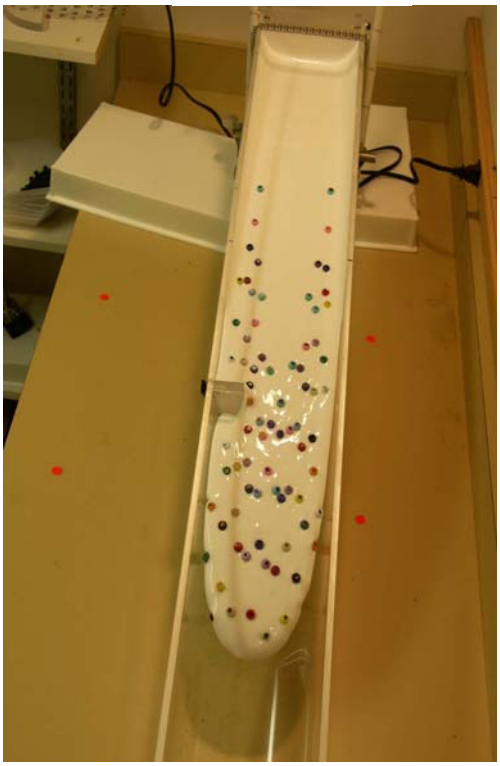

Frame 090

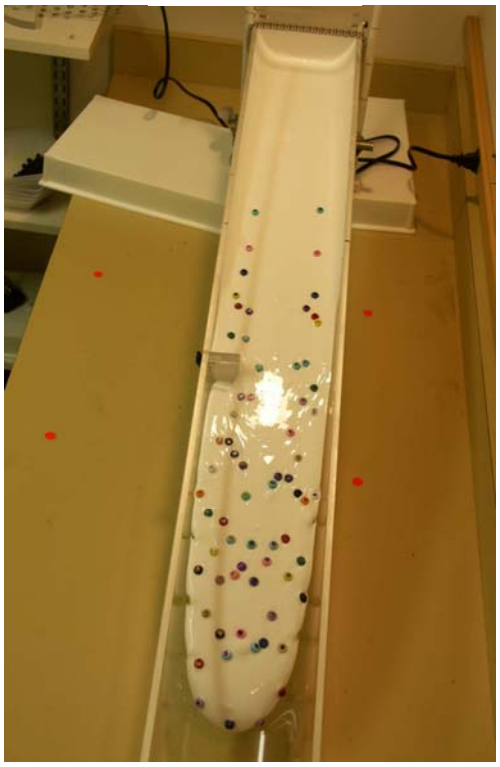

APPENDIX III (con't)

Digital Images of Experimental Trials - Perpendicular Blockage (D) – ½ width, ½ depth

Frame 024

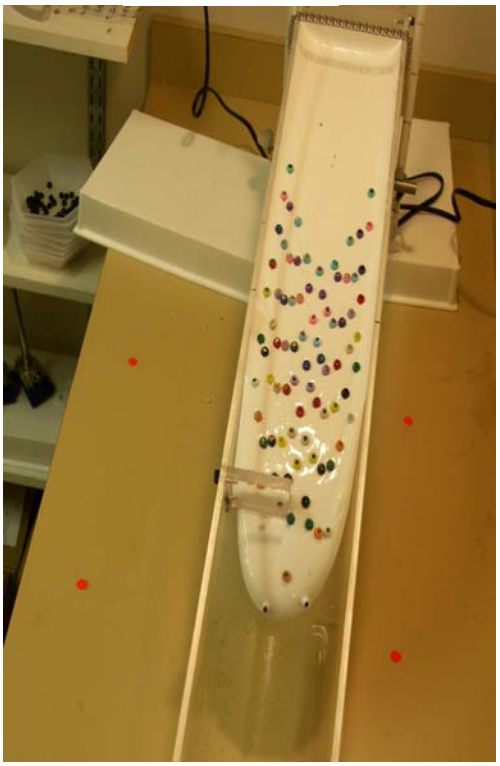

Frame 057

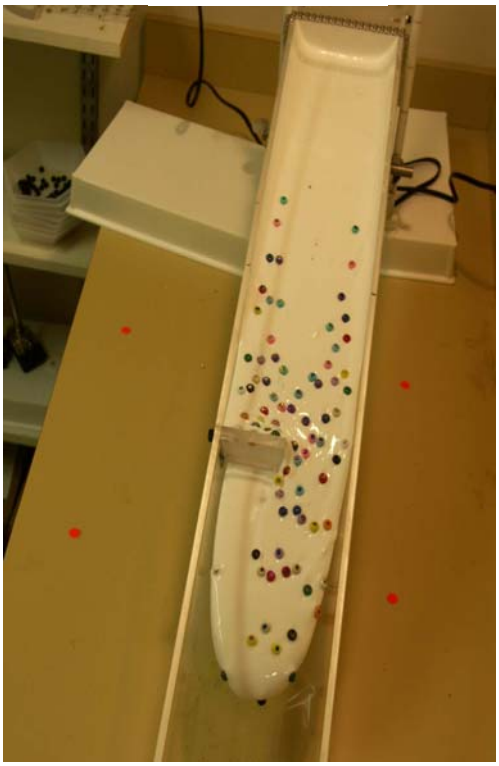

Frame 090

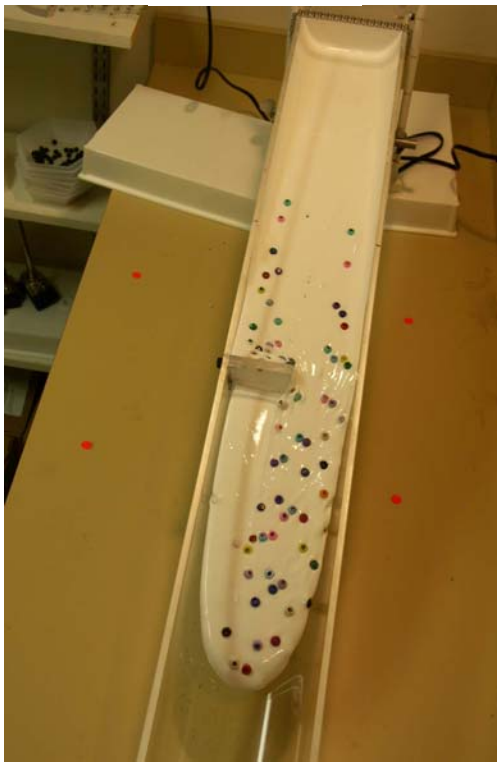

APPENDIX III (con't)
Digital Images of Experimental Trials - Unblocked Trials (E)

Frame 024

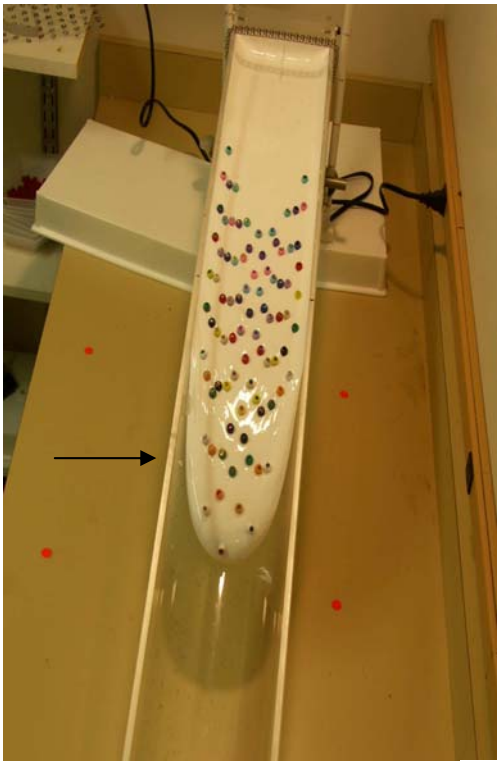

Frame 057

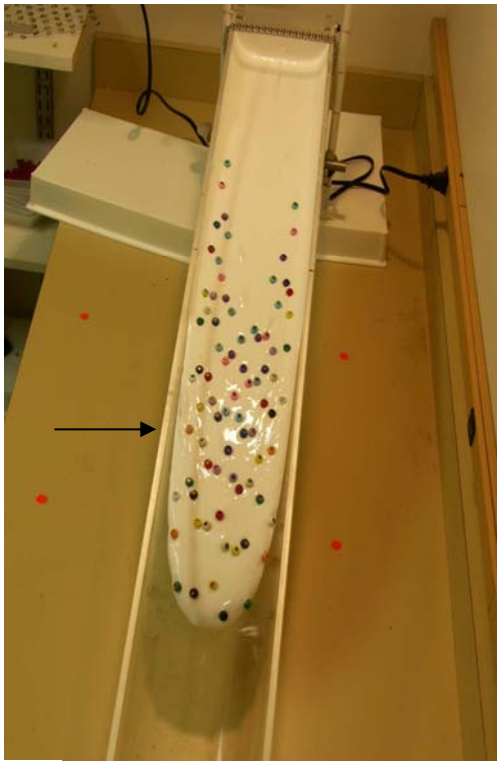

Frame 090

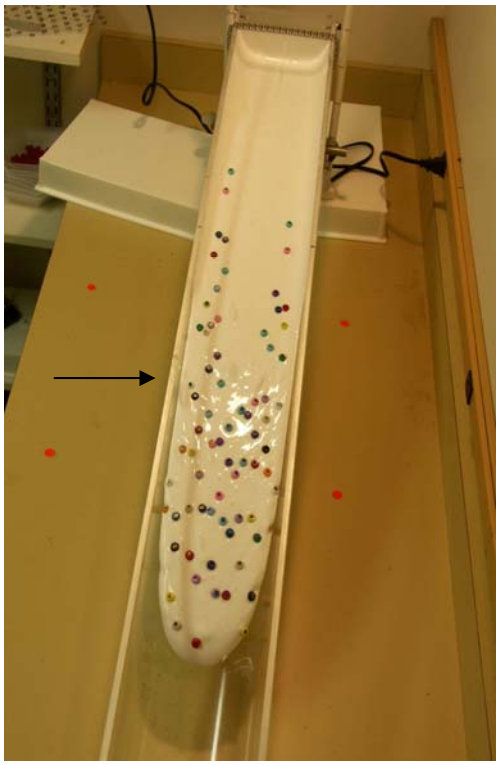

APPENDIX IV

Kruskal-Wallis Tests

	trial#_24	N	Mean Rank
24_xvelo	1	83	188.94
	2	83	237.04
	3	83	217.57
	4	83	212.39
	5	83	184.07
	Total	415	
24_yvelo	1	83	102.92
	2	83	226.55
	3	83	258.98
	4	83	189.43
	5	83	262.12
	Total	415	

	trial#_57	N	Mean Rank
57_xvelo	1	75	209.41
	2	75	190.56
	3	75	166.32
	4	75	201.51
	5	75	172.20
	Total	375	
57_yvelo	1	75	102.73
	2	75	214.08
	3	75	232.43
	4	75	160.95
	5	75	229.81
	Total	375	

APPENDIX IV (con't)
Tukey Post Hoc Test - Time 024

Multiple Comparisons

Tukey HSD

Dependent Variable	(I) trial#_24	(J) trial#_24	Mean Difference (I-J)	Std. Error	Sig.	95% Confidence Interval	
						Lower Bound	Upper Bound
24_xvelo	1	2	-.0096285	.0117586	.925	-.041846	.022590
		3	.0109901	.0117586	.883	-.021228	.043208
		4	.0006621	.0117586	1.000	-.031556	.032880
		5	.0177792	.0117586	.555	-.014439	.049997
	2	1	.0096285	.0117586	.925	-.022590	.041846
		3	.0206186	.0117586	.402	-.011599	.052837
		4	.0102905	.0117586	.906	-.021927	.042509
		5	.0274077	.0117586	.137	-.004810	.059626
	3	1	-.0109901	.0117586	.883	-.043208	.021228
		2	-.0206186	.0117586	.402	-.052837	.011599
		4	-.0103280	.0117586	.905	-.042546	.021890
		5	.0067892	.0117586	.978	-.025429	.039007
	4	1	-.0006621	.0117586	1.000	-.032880	.031556
		2	-.0102905	.0117586	.906	-.042509	.021927
		3	.0103280	.0117586	.905	-.021890	.042546
		5	.0171172	.0117586	.592	-.015101	.049335
	5	1	-.0177792	.0117586	.555	-.049997	.014439
		2	-.0274077	.0117586	.137	-.059626	.004810
		3	-.0067892	.0117586	.978	-.039007	.025429
		4	-.0171172	.0117586	.592	-.049335	.015101
24_yvelo	1	2	-.6407011*	.0903956	.000	-.888381	-.393021
		3	-.8504850*	.0903956	.000	-1.098165	-.602805
		4	-.4126176*	.0903956	.000	-.660298	-.164938
		5	-.8579805*	.0903956	.000	-1.105661	-.610301
	2	1	.6407011*	.0903956	.000	.393021	.888381
		3	-.2097840	.0903956	.140	-.457464	.037896
		4	.2280834	.0903956	.088	-.019597	.475763
		5	-.2172795	.0903956	.116	-.464959	.030401
	3	1	.8504850*	.0903956	.000	.602805	1.098165
		2	.2097840	.0903956	.140	-.037896	.457464
		4	.4378674*	.0903956	.000	.190187	.685547
		5	-.0074955	.0903956	1.000	-.255176	.240184
	4	1	.4126176*	.0903956	.000	.164938	.660298
		2	-.2280834	.0903956	.088	-.475763	.019597
		3	-.4378674*	.0903956	.000	-.685547	-.190187
		5	-.4453629*	.0903956	.000	-.693043	-.197683
	5	1	.8579805*	.0903956	.000	.610301	1.105661
		2	.2172795	.0903956	.116	-.030401	.464959
		3	.0074955	.0903956	1.000	-.240184	.255176
		4	.4453629*	.0903956	.000	.197683	.693043

*. The mean difference is significant at the .05 level.

APPENDIX IV (con't)
Tukey Post Hoc Test - Time 057

Multiple Comparisons

Tukey HSD

Dependent Variable	(I) trial#_57	(J) trial#_57	Mean Difference (I-J)	Std. Error	Sig.	95% Confidence Interval	
						Lower Bound	Upper Bound
57_xvelo	1	2	.0252705	.014220	.389	-.013711	.064252
		3	.0320215	.014220	.163	-.006960	.071003
		4	.0114180	.014220	.930	-.027564	.050400
		5	.0315369	.014220	.175	-.007445	.070519
	2	1	-.0252705	.014220	.389	-.064252	.013711
		3	.0067510	.014220	.990	-.032231	.045733
		4	-.0138525	.014220	.867	-.052834	.025129
		5	.0062664	.014220	.992	-.032716	.045248
	3	1	-.0320215	.014220	.163	-.071003	.006960
		2	-.0067510	.014220	.990	-.045733	.032231
		4	-.0206035	.014220	.596	-.059585	.018378
		5	-.0004846	.014220	1.00	-.039466	.038497
	4	1	-.0114180	.014220	.930	-.050400	.027564
		2	.0138525	.014220	.867	-.025129	.052834
		3	.0206035	.014220	.596	-.018378	.059585
		5	.0201189	.014220	.619	-.018863	.059101
	5	1	-.0315369	.014220	.175	-.070519	.007445
		2	-.0062664	.014220	.992	-.045248	.032716
		3	.0004846	.014220	1.00	-.038497	.039466
		4	-.0201189	.014220	.619	-.059101	.018863
57_yvelo	1	2	-.6605404*	.093033	.000	-.915570	-.405511
		3	-.7438523*	.093033	.000	-.998882	-.488823
		4	-.2931303*	.093033	.015	-.548160	-.038101
		5	-.7060948*	.093033	.000	-.961124	-.451065
	2	1	.6605404*	.093033	.000	.405511	.915570
		3	-.0833119	.093033	.898	-.338342	.171718
		4	.3674101*	.093033	.001	.112380	.622440
		5	-.0455544	.093033	.988	-.300584	.209475
	3	1	.7438523*	.093033	.000	.488823	.998882
		2	.0833119	.093033	.898	-.171718	.338342
		4	.4507220*	.093033	.000	.195692	.705752
		5	.0377575	.093033	.994	-.217272	.292787
	4	1	.2931303*	.093033	.015	.038101	.548160
		2	-.3674101*	.093033	.001	-.622440	-.112380
		3	-.4507220*	.093033	.000	-.705752	-.195692
		5	-.4129645*	.093033	.000	-.667994	-.157935
	5	1	.7060948*	.093033	.000	.451065	.961124
		2	.0455544	.093033	.988	-.209475	.300584
		3	-.0377575	.093033	.994	-.292787	.217272
		4	.4129645*	.093033	.000	.157935	.667994

*. The mean difference is significant at the .05 level.